MULTISCALE CLOUD SYSTEM MODELING

Wei-Kuo Tao[1] and Mitchell W. Moncrieff[2]

Received 11 September 2008; revised 23 January 2009; accepted 22 June 2009; published 26 November 2009.

[1] The central theme of this paper is to describe how cloud system resolving models (CRMs) of grid spacing ~1 km have been applied to various important problems in atmospheric science across a wide range of spatial and temporal scales and how these applications relate to other modeling approaches. A long-standing problem concerns the representation of organized precipitating convective cloud systems in weather and climate models. Since CRMs resolve the mesoscale to large scales of motion (i.e., 10 km to global) they explicitly address the cloud system problem. By explicitly representing organized convection, CRMs bypass restrictive assumptions associated with convective parameterization such as the scale gap between cumulus and large-scale motion. Dynamical models provide insight into the physical mechanisms involved with scale interaction and convective organization. Multiscale CRMs simulate convective cloud systems in computational domains up to global and have been applied in place of contemporary convective parameterizations in global models. Multiscale CRMs pose a new challenge for model validation, which is met in an integrated approach involving CRMs, operational prediction systems, observational measurements, and dynamical models in a new international project: the Year of Tropical Convection, which has an emphasis on organized tropical convection and its global effects.

Citation: Tao, W.-K., and M. W. Moncrieff (2009), Multiscale cloud system modeling, *Rev. Geophys.*, *47*, RG4002, doi:10.1029/2008RG000276.

1. INTRODUCTION

[2] A foremost challenge for weather and climate prediction lies in representing clouds, precipitation, and dynamical interactions in numerical models across a continuum of scales ranging from the microphysical (10^{-3} m to 10^{-1} m, seconds to minutes), to cloud and boundary layer turbulence ($1-10^3$ m, minutes to hours), to mesoscale convective organization (10^4-10^5 m, hours to days), to the global scale (10^7 m, days and beyond). This challenge is being met by utilizing numerical models that can simulate cloud systems of scales larger than ~10 km: cloud system resolving models (CRMs, grid spacing ~1 km). Cloud systems are a manifestation of convective organization and a form of dynamical coherence, which is an important property of moist atmospheric motion. In CRMs, the interactions between mesoscale dynamics and small-scale processes (i.e., microphysics, latent heating (LH) and evaporation, the effect of clouds on radiation, surface exchange, and boundary layer turbulence) are more complete than in global models where they are represented indirectly by parameterizations. This paper describes how CRMs have been applied to various important problems in atmospheric science, with particular attention to the tropics where convection is the dominant transport process.

[3] The tropics are fundamental to the Earth's weather-climate system and are strongly affected, if not driven, by transports and scale interactions involving moist convection (see section 10). Approximately two thirds of the global precipitation occurs in the tropics where mesoscale cloud systems account for a large percentage of the rainfall [*Nesbitt et al.*, 2006]. In the tropics, LH accounts for about three quarters of the total atmospheric heat energy [*Riehl and Simpson*, 1979]. The vertical and horizontal distribution of LH affects tropical variability, such as the 30–60 day intraseasonal oscillation [*Hartmann et al.*, 1984; *Sui and Lau*, 1989] and, in turn, the global circulation. Tropical rainfall provides fresh water that stabilizes the upper ocean and modulates ocean-atmosphere interaction. Large-scale tropical convective heating affects extratropical weather and climate through planetary wave teleconnections [e.g., *Hoskins and Karoly*, 1981] involving the Madden-Julian Oscillation (MJO) [*Madden and Julian*, 1972] among other examples of large-scale convective organization. Convective heating and convective organization also affect the variability of monsoon systems, notably their precipitation characteristics. Shifts in the global atmospheric circulation associated with climate variability such as the El Niño–Southern Oscillation cause prolonged droughts and floods that impact humankind, the biosphere, agriculture, and the global economy. The organization of precipitating convection into multiscale cloud systems is central to the water and energy cycles.

[1]Mesoscale Atmospheric Processes Branch, Laboratory for Atmospheres, NASA Goddard Space Flight Center, Greenbelt, Maryland, USA.
[2]National Center for Atmospheric Research, Boulder, Colorado, USA.

8755-1209/09/2008RG000276
Paper number 2008RG000276

TABLE 1. Highlights of CRM Development Over the Past 4 Decades[a]

	Highlights
1960s	loading, buoyancy, and entrainment
1970s	slab versus axis symmetric models, cloud seeding, supercell dynamics, cloud dynamics and warm rain, and wind shear effect on cloud organization
1980s	ensembles of clouds, cumulus parameterization; cloud interactions and mergers; ice processes; squall lines; convective and stratiform; wind shear and cool pools; gravity waves and density currents; large-scale and cloud-scale interactions; and cloud radiation interaction
1990s	2-D versus 3-D; land and ocean processes; multiscale interactions; cloud chemistry; process modeling, climate variation implications; GCSS; and coupling with microwave radiative transfer models for TRMM

[a]Adapted from *Tao and Moncrieff* [2003] and *Tao* [2003] and modified by *Juang et al.* [2007]. CRM, cloud system resolving model; GEWEX, Global Energy and Water Cycle Experiment; GCSS, GEWEX Cloud System Study; TRMM, Tropical Rainfall Measuring Mission.

[4] The occurrence of convective organization in the $\sim$10–100 km range contradicts a key assumption of contemporary convective parameterization: a scale gap between the cumulus-scale and large-scale motion. In high-resolution short-range weather prediction models, convective organization can be explicitly represented. However, no reliable parameterization has yet been devised that is suitable for climate models. Another challenge for climate modeling is the representation of cloud-radiation interaction. Addressing such formidable challenges was why, in the early 1990s, clouds and radiation became a priority of the Global Change Research Program and why the World Climate Research Program (WRCP) Global Energy and Water Cycle Experiment (GEWEX) set up the GEWEX Cloud System Study (GCSS). The CRM, which is also known as a cloud ensemble model, is a mainstay of the GCSS in acknowledgment of its potential for addressing clouds, radiation, precipitation, surface processes, and multiscale dynamics in a unified way. The intercomparison studies coordinated by the GCSS, as well as the Department of Energy's Atmospheric Radiation Measurement (DOE ARM) program, show that the explicit representation of convection by CRMs is superior to convective parameterizations represented by single-column models [*Browning et al.*, 1993; *Moncrieff et al.*, 1997; *Randall et al.*, 2003a]. Observationally verified CRMs are a basis for improving parameterizations of convection and cloud-radiation interaction for global prediction models and cloud microphysics parameterizations for CRMs.

[5] Global numerical weather prediction (NWP) models and climate models have to represent unresolved physical processes, namely, subgrid-scale (SGS) processes as functions of the resolved scale variables, a procedure called parameterization. Until about the mid-1990s, all moist process had to be parameterized in global models due to the coarse resolution (grid spacing $\sim$ hundreds of kilometers). Partly as a result of computational advances, the state of the art has forever changed. First, operational and global NWP models with 25 km grid spacing in tandem with cumulus parameterization may crudely represent the mesoscale organization of precipitating convection. Second, CRMs with global computational domains have recently been run. And third, the convective parameterizations in global models have been replaced by CRMs as a cloud-resolving convective parameterization (aka superparameterization).

[6] The central theme of this paper is to review how CRMs have been applied to various important problems in atmospheric science and address the long-standing problem of representing precipitating convection in weather and climate models. Sections 2–4 describe the historical background, the components of CRMs, and the parameterization of key physical processes, respectively. Aerosols, surface exchange, cloud-radiation interaction, and the diurnal variation of precipitation are the subjects of sections 5–8, respectively. Satellite applications are described in section 9, and the multiscale organization of convection is described in section 10. The paper concludes in section 11 with examples of improvements needed to further advance multiscale modeling.

2. HISTORICAL BACKGROUND

[7] Table 1 highlights CRM development over 4 decades. The earliest kind of cloud model, the one-dimensional (1-D) entraining plume, simply represents the lateral entrainment and entrainment of environmental air. The entraining plume model was used to guide cloud-seeding research [*Simpson et al.*, 1965, 1967] and is still used as a transport module in convective parameterizations. These were followed by two-dimensional (2-D) cloud models, which were used to examine cloud development and interactions with the near environment [*Ogura and Phillips*, 1962]. The 1970s witnessed the development of 2-D and three-dimensional (3-D) cloud models and the simulation of cumulonimbus, convective storms, and squall lines at $\sim$1 km grid spacing [e.g., *Steiner*, 1973; *Wilhelmson*, 1974; *Miller and Pearce*, 1974; *Moncrieff and Miller*, 1976; *Sommeria*, 1976; *Klemp and Wilhelmson*, 1978a, 1978b; *Wilhelmson and Klemp*, 1978; *Cotton and Tripoli*, 1978; *Schlesinger*, 1978; *Clark*, 1979]. The effects of model geometry (i.e., slab symmetric versus axial symmetric and 2-D versus 3-D) on cloud life cycles were examined extensively [e.g., *Soong and Ogura*, 1973].

[8] Subsequent to the Global Atmospheric Research Program Atlantic Tropical Experiment (GATE), CRMs were used to examine the collective effects of cumulus clouds, their interaction with the environment, and implications for cumulus parameterization [e.g., *Soong and Ogura*, 1980; *Soong and Tao*, 1980; *Tao and Soong*, 1986; *Lipps and Helmer*, 1986; *Tao et al.*, 1987] (the Global Atmospheric Research Programme Atlantic Tropical Experiment that took place in 1974). Figure 1 illustrates the types of problems examined. Other studies included the effects of ice processes and radiative processes on precipitating systems and the effects of wind shear and downdraft out-

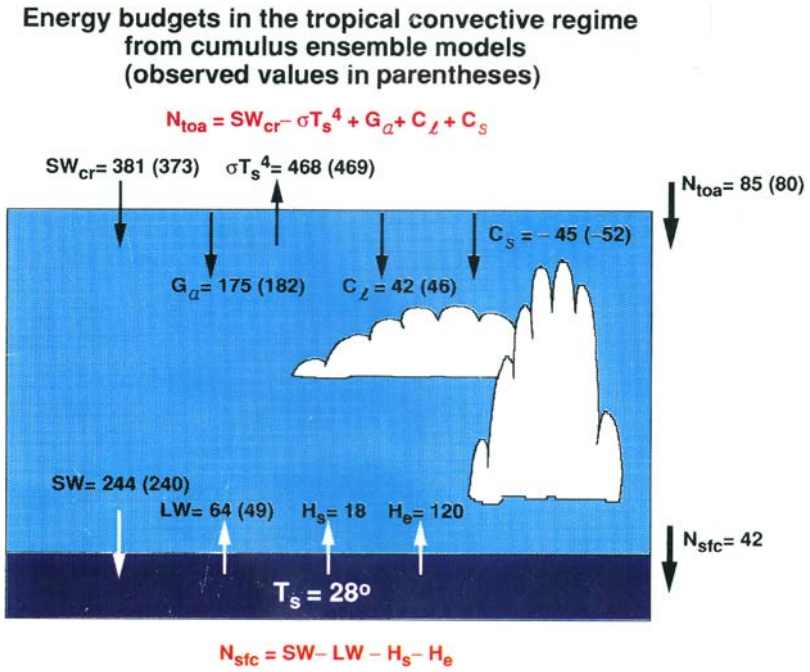

Figure 1. Energy fluxes at the top of the atmosphere and at the ocean-atmosphere interface as computed by the Goddard Cumulus Ensemble (GCE) model. Also included in parentheses are top-of-the-atmosphere fluxes estimated from the Earth Radiation Budget Experiment and surface flux estimates from radiation model for April 1985. The observed values (in parentheses) are averaged over the region from 100 to 180°E, 20°N to 20°S. Subscript "toa" denotes top of the atmosphere, subscript "cr" denotes clear-sky conditions, and subscript "sfc" denotes the surface. SW_{cr} is the net absorbed solar radiation averaged over the clear-sky region. T_s^4 is the longwave radiation emitted by the ocean surface. SW and LW stand for shortwave and longwave radiative heating/cooling, respectively. H_s and H_e stand for surface sensitive and latent heat fluxes, respectively. G_a is the atmospheric greenhouse effect. C_s and C_l are the longwave and shortwave cloud forcing, respectively. Units are in W m^{-2}. T_s is the ocean surface temperature. A reasonable agreement between the modeled and satellite observed budget is found. Adapted from *Lau et al.* [1994].

flows (density currents) on organized precipitating convection [e.g., *Thorpe et al.*, 1980, 1982; *Moncrieff*, 1981; *Redelsperger and Sommeria*, 1986; *Fovell and Ogura*, 1988; *Nakajima and Matsuno*, 1988; *Redelsperger and Lafore*, 1988; *Lafore et al.*, 1988; *Rotunno et al.*, 1988; *Lafore and Moncrieff*, 1989; *Tao and Simpson*, 1989; *Tao et al.*, 1995]. The quest of improving parameterization by utilizing CRMs continues to this day, notably in GCSS.

[9] In the 1990s, advances in computer capability enabled CRMs with computational domains large enough to represent multiscale convective organization [e.g., *Grabowski et al.*, 1998; *Wu et al.*, 1998; *Tripoli and Cotton*, 1989], cloud chemistry interaction (see review by *Thompson et al.* [1997]), idealized climate variability [e.g., *Held et al.*, 1993; *Lau et al.*, 1993, 1994; *Sui et al.*, 1994; *Tao et al.*, 1999] (see also Figure 1), orographic effects on snowfall [e.g., *Saito et al.*, 1996], surface processes [e.g., *Lynn et al.*, 1998; *Golaz et al.*, 2001; *Wang et al.*, 2003; *Zeng et al.*, 2007], and the development of retrieval algorithms for satellite measurements of rainfall (see review by *Simpson et al.* [1996]) and LH (see review by *Tao et al.* [2006]).

[10] Data sets accumulated from radar, instrumented aircraft, satellites, and weather balloon measurements deployed in field campaigns reveal the ubiquity of tropical oceanic mesoscale convective systems (MCSs) consisting of populations of cumulonimbus convection embedded in a mesoscale stratiform region [e.g., *Zipser*, 1969, 1977; *Houze*, 1977, 1989; *Houze et al.*, 1980]. Interactions between precipitating convection, the mesoscale organization of convection, and the larger scales of motion were then examined: first, in a 2-D framework [e.g., *Peng et al.*, 2001; *Grabowski and Moncrieff*, 2001]; then in 3-D on regional scales [e.g., *Grabowski et al.*, 1998; *Yoshizaki et al.*, 2004; *Saito et al.*, 2006]; and eventually in 3-D on a global scale [e.g., *Miura et al.*, 2005; *Satoh et al.*, 2005, 2008]. Over a period of 4 decades, the number of grid points in CRMs has grown from ~1000 to ~1,000,000,000.

[11] The fidelity of "numerical modeling" at all scales of motion depends on (1) the quality of the initial conditions and the boundary conditions at the underlying surface and the lateral boundaries; (2) the accuracy of the parameterization of complex physical processes, notably moist convective processes and land/ocean interaction with the atmosphere; (3) the accuracy of finite difference approximations to the equations of motion, radiation, thermodynamic energy, and water continuity; (4) the evaluation and improvement of the model through comparisons with

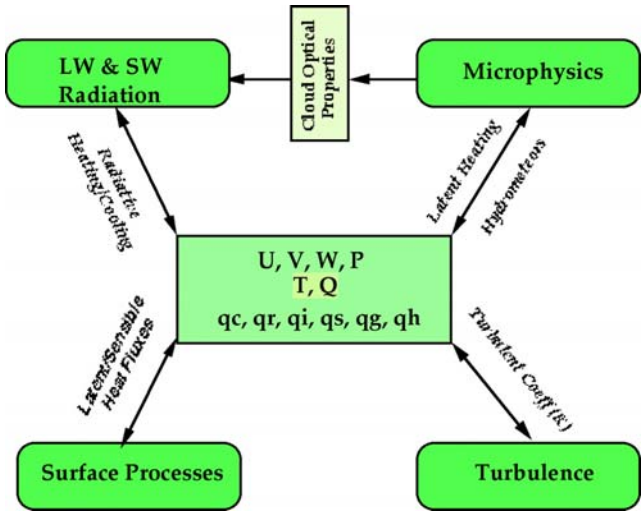

Figure 2. Schema showing the characteristics of cloud-resolving models. Arrows with solid lines indicate a two-way interaction between different physical processes. *U* and *V*, *W*, and *P* stand for the horizontal wind components, vertical wind, and pressure, respectively; *T* and *Q* stand for the atmospheric temperature and water vapor mixing ratio, respectively; qc, qr, qi, qs, qg, and qh stand for the mixing ratio of cloud water, rain, cloud ice, snow, graupel, and hail, respectively; and LW and SW stand for the atmospheric longwave and shortwave radiative cooling and heating, respectively. Adapted from *Tao* [2007].

observations; and (5) understanding the resolution dependence of the parameterized physical processes. Since CRMs represent cloud systems explicitly, the parameterizations of microphysical processes and their interactions with turbulence, radiation, and surface processes impact the simulations more directly than global models where convection is parameterized. The CRM consists of important components described in section 3. However, we defer the specific details, such as the governing equations, numerical approximations, phenomenological and physical descriptions, and technical details to textbooks and reviews [e.g., *Cotton and Anthes*, 1989; *Houze*, 1993; *Emanuel*, 1994; *Gao and Li*, 2008, and references therein].

3. COMPONENTS OF CRMs

[12] The physical resolution of a numerical model is about 6–8 times its grid spacing [*Bryan et al.*, 2003; *Skamarock*, 2004]. It follows that resolving individual cumulus elements in mesoscale cloud systems, the turbulent mixing at cloud boundaries, and the interactions between clouds and the planetary boundary layer requires ultrahigh-resolution CRMs or large-eddy simulation (LES). Conceptually, the large eddies computed by classical LES correspond to the mesoscale circulations simulated by CRMs with an important distinction. In LES, the SGS parameterization is based on self-similar properties within the Kolmogorov inertial subrange. Applied to CRMs on scales outside the inertial subrange where moisture effects are first-order, devising SGS parameterizations is ever more challenging. Advances in computer technology are blurring the distinction between the CRM and LES approaches (see section 11). Importantly, interactions between small-scale processes and resolved dynamics operate at much higher resolution in CRMs than in global models. Cloud microphysical processes (e.g., nucleation, diffusion growth, and collisions between cloud and precipitation particles) are parameterized in CRMs, along with atmospheric turbulence, turbulent exchanges, and radiative transfer (Figure 2).

[13] There are two complementary CRM approaches. First, in cloud process modeling, issues include convective initiation, interaction between physical processes over short periods (hours), and cloud microphysical parameterizations. Examples include the (1) microphysical processes associated with cloud aerosol chemistry interactions, (2) explicit interaction between clouds and radiation, (3) turbulent fluxes associated with convection, and (4) coupling atmospheric-surface models to represent the scale interactions that are key to the atmospheric water and energy cycles. Cloud process simulations can now be run at very high resolution [e.g., *Bryan et al.*, 2003; *Khairoutdinov and Randall*, 2006]. In the second approach, CRMs can be used to examine the collective effects of cumulus and estimate their statistical properties [e.g., *Soong and Ogura*, 1980; *Soong and Tao*, 1980; *Lipps and Helmer*, 1986; *Tao and Soong*, 1986; *Tao et al.*, 1987; *Krueger*, 1988; *Wu and Moncrieff*, 1996, 2001; *Wu et al.*, 1998]. When constrained by specified large-scale advective tendencies for temperature and moisture and environmental shear derived from observations, CRMs can simulate rainfall, temperature, and water vapor distributions with considerable realism [e.g., *Tao*, 2003; *Randall et al.*, 2003a] and provide a wealth of statistical information for parameterization development.

3.1. Dynamical Cores

[14] CRMs are based on the nonhydrostatic equations of motion, which is essential for models with grid spacing finer than about 10 km. CRMs may be anelastic [*Ogura and Phillips*, 1962], an approach whereby sound waves are filtered by neglecting the local time variation of density in the mass continuity equation, or compressible, wherein sound waves are retained. While sound waves are meteorologically unimportant, their fast phase speed ($\sim$300 m s^{-1}) severely limits the time step (e.g., 2 s at 1000 m grid spacing). *Klemp and Wilhelmson* [1978a] improved the computational efficiency by using a semi-implicit time-splitting scheme (the model equations are split into sound wave and gravity wave components). One advantage of the compressible framework is that the set of prognostic equations have a similar (hyperbolic) form, while the anelastic formulation involves a 3-D elliptic equation at each time step, which can be efficiently solved using either direct (e.g., fast Fourier transform) or iterative methods. *Ikawa* [1988] and *Tao and Simpson* [1993] showed that the compressible and anelastic formulations give similar results

compared to the much larger variability associated with applying different cloud microphysics parameterizations.

3.2. Microphysics

[15] In one-moment bulk microphysical schemes [e.g., *Cotton et al.*, 1982; *Lin et al.*, 1983; *Rutledge and Hobbs*, 1984] with two classes of liquid (cloud water and rain) and three classes of ice (cloud ice, snow, and graupel/hail), the shapes of nonprecipitating cloud water and cloud ice are assumed to be monodisperse. (These water substances are generally categorized based on their size and their fall speed. Please see *Houze* [1993] for a definition of these water substances. Graupel has a low density and a high intercept (i.e., high number concentration). In contrast, hail has a high density and a small intercept. The choice of graupel or hail depends on where the clouds or cloud systems developed [*McCumber et al.*, 1991].) The size distributions of the precipitating particles (rain, snow, and graupel/hail) follow a three-parameter gamma distribution function such that $N(D) = N_0 D^{\alpha}\exp(-\lambda D)$, where *No* is the intercept parameter, λ is the slope of the particle size distribution, and α is the shape parameter. (For $\alpha = 0$, the equation reduces to an inverse exponential distribution that was assumed by *Lin et al.* [1983] and *Rutledge and Hobbs* [1984].) Only the substance or hydrometeor mass content, which is proportional to $N(D)$, is predicted. A major uncertainty in the one-moment bulk scheme is its autoconversion formulation. Large hydrometeors such as raindrops are assumed to collect smaller drops and ice by continuous accretion. The autoconversion formulations have been either ad hoc [e.g., *Kessler*, 1969; *Manton and Cotton*, 1977; *Cotton et al.*, 1986] or derived from parcel or grid box detailed explicit (bin microphysics) simulations [e.g., *Berry*, 1967; *Berry and Reinhardt*, 1974; *Beheng*, 1994].

[16] In two-moment bulk schemes [e.g., *Clark*, 1976; *Clark and Hall*, 1983; *Nickerson et al.*, 1986; *Murakami*, 1990; *Ikawa et al.*, 1991; *Ferrier*, 1994; *Meyers et al.*, 1997; *Reisner et al.*, 1998; *Walko et al.*, 2000; *Morrison et al.*, 2005; *Seifert and Beheng*, 2006a], mass content and the total number concentration are predicted. In the multimoment bulk microphysical scheme [*Milbrandt and Yau*, 2005], the value of α varies as a function of the mean mass diameter. An advantage of multimoment schemes is that they predict number concentration and mass mixing ratio (and sometimes higher-order moments), enabling derivation of the broad features of the drop size distribution. Thereby, multimoment schemes improve the representation of growth processes and precipitation formation. For example, the two-moment scheme of *Seifert and Beheng* [2006a, 2006b] predicts the evolution of mass as well as number densities of the five hydrometeor types, cloud droplets, raindrops, cloud ice, snow, and graupel. It also includes new parameterizations for autoconversion, accretion, and self-collection of water drops derived by *Seifert and Beheng* [2001] from the stochastic collection equation. This autoconversion parameterization considers aging of the cloud droplet size distribution with time by relying on dynamic similarity theory. Instead of using continuous accretion approximations, which has been common in cloud parameterizations, full stochastic collection solutions for self-collection among cloud droplets and for rain (drizzle) drop collection of cloud droplets are obtained for realistic collection kernels by using look-up tables [*Feingold et al.*, 1998]. *Saleeby and Cotton* [2008] refined this approach by adding a large cloud droplet mode from 40 to 80 μm in diameter and by predicting the number concentration of cloud droplets through explicit activation of cloud condensation nuclei (CCN) and giant CCN. The large cloud droplet mode provides a better depiction of self-collection of cloud droplets (or autoconversion) and permits simulation of drizzle from fogs and marine stratocumulus clouds. This new scheme has been implemented into the Regional Atmospheric Modeling System [*Pielke et al.*, 1992; *Cotton et al.*, 2003; *Saleeby and Cotton*, 2004] to study the impact of CCN on stratocumulus and deep convective clouds.

[17] Bin microphysical methods were developed for the study of cirrus clouds, stratocumulus, and cloud-aerosol interactions. There are two different approaches. The first is the Lagrangian (or moving mass grid) method, which represents particles at discrete sizes and allows each particle to grow by condensation on a moving mass grid. This approach typically focuses on the initial growth phase from haze to droplet and includes detailed representation of aerosol sizes and composition [*Mordy*, 1959; *Fitzgerald*, 1974; *Facchini et al.*, 1999; *Feingold and Kreidenweis*, 2000; *Feingold and Chuang*, 2002; *Lohmann et al.*, 2004]. The second approach is a Eulerian (in size space) microphysical method that is typically applied in CRMs [e.g., *Telford*, 1980; *Berry*, 1967; *Berry and Reinhardt*, 1974; *Bleck*, 1970; *Clark*, 1973, 1974; *Soong*, 1974; *Takahashi*, 1976; *Tzivion et al.*, 1987; *Hounslow et al.*, 1988; *Bott et al.*, 1990; *Cheng et al.*, 2001; *Khain et al.*, 2004; *Carrió et al.*, 2007]. The advantages, disadvantages, and application of each approach were discussed by *Levin and Cotton* [2008]. The explicit bin microphysical methods are based on the stochastic kinetic equations for the size distribution and are functions of water (i.e., cloud droplets and raindrops) and ice particles of different habits (i.e., columns, plates, dendrites, snowflakes, graupel, and frozen drops). Each type is described in terms of a size distribution function containing over 30 categories (bins). Nucleation (activation) processes are based on the size distribution function for CCN (>30 size categories). This framework is useful for collision-coalescence calculations. For example, *Tzivion et al.* [1987] proposed a two-moment scheme (mass and number density) that solves the stochastic collection accurately and efficiently.

[18] Recent explicit microphysics models [*Tzivion et al.*, 1987; *Hounslow et al.*, 1988; *Chen and Lamb*, 1994] use a multimoment representation of the cloud microphysics in each individual drop category; this significantly reduces numerical diffusion and has the added benefit of conserving more than one moment of the size distribution. This led to development of numerical methods that include a representation of aerosols in each individual hydrometeor size bin [*Bott et al.*, 1990; *Chen and Lamb*, 1994; *Kerkweg et al.*,

2003; *Leroy et al.*, 2006]. Such methods are very accurate since they maintain knowledge of the aerosol particle upon which the drop and/or ice particles form [*Leroy et al.*, 2006]. These detailed microphysics calculations provide a framework for evaluating and improving bulk microphysical schemes. However, the numerous interactions involved in bin microphysical schemes necessitate small domains and short simulations. Simpler methods that track dissolved aerosols within each hydrometeor bin are more commonly used [*Flossmann et al.*, 1985; *Toon et al.*, 1988; *Respondek et al.*, 1995; *Feingold et al.*, 1996; *Yin et al.*, 2005]. A review of various aspects of bin microphysical modeling for both warm and cold cloud processes is given by *Khain et al.* [2000].

[19] Modeling of the dynamical equation for cloud substance requires "positive definiteness" for mass conservation [e.g., *Ferrier et al.*, 1995; *Johnson et al.*, 2002]. Numerical diffusion on the spatial grid also has to be considered along with numerical diffusion on the mass grid. An appropriate balance is desirable [*Clark*, 1973, 1974]. Additional discussions on the different microphysical processes/schemes are given by *Levin and Cotton* [2008].

3.3. Turbulence

[20] SGS turbulent processes must be parameterized in all geophysical models. Typically, a simple *k*-type (*k* is the turbulence coefficient) turbulence closure is used to diagnose the *k* coefficient (first-order), or it may be obtained from the turbulent kinetic energy (TKE) equation (one-and-a-half-order). In the prognostic TKE method, thermodynamic stability, deformation, shear stability, diffusion, dissipation, moist processes, and transport of subgrid energy are represented. In the diagnostic method, deformation and stability are used to compute the *k* coefficient. The most complex turbulence parameterization used in CRMs is third-order closure [*Krueger*, 1988] for simulating shallow cumuli and boundary layer cumulus [e.g., *Cheng and Xu*, 2006; *Cheng et al.*, 2004]. However, for deep convective systems, the performance of third-order turbulence closure is similar to the one-and-a-half-order TKE approach.

[21] The fidelity of a 2-D model for representing shallow 3-D convection in the planetary boundary layer (PBL) was discussed by *Moeng et al.* [2004]. However, the performance of 2-D CRMs in representing complex interactions associated with deep moist convection remains an open question that is highly pertinent for long simulations where nonlinear feedbacks associated with the phase changes of water are poorly understood.

3.4. Radiation

[22] Emission and absorption by water vapor and cloud droplets are represented by a two-stream approximation (one for upward fluxes and one for downward fluxes) for longwave radiative transfer. Broadband methods for longwave radiation include the interactions between gaseous absorption and scattering by clouds, aerosols, air molecules (Rayleigh scattering), and the surface. The treatment of shortwave radiation is also based on broadband approximations. Explicit microphysics and fine horizontal resolution provide relatively realistic cloud optical properties that are crucial for determining the radiation budgets and diurnal variation of precipitation processes. (The parameterization of cloud optical properties (optical thickness), especially in the presence of the ice phase, is still a key issue. Only limited observations are available upon which to base parameterizations for ice clouds.) With high spatial resolution, each atmospheric layer is considered either completely cloudy (overcast) or clear. Partial cloudiness is not assumed. See *Tao* [2003] for a review of mechanisms of cloud-radiation interaction and comparisons among CRMs.

3.5. Ocean Surface Processes

[23] Surface fluxes are complex in the neighborhood of precipitating convection over ocean and land. Two types of surface flux schemes are typically used. The first is a simple surface flux formula where the transfer coefficients for momentum, sensible heat, and latent heat fluxes are functions of wind speed only. The more complex bulk approach is based on the Monin-Obukhov similarity theory [*Fairall et al.*, 1996]. The exchange coefficients in these two flux algorithms differ. In the simple bulk aerodynamic formula they increase linearly with wind speed. At wind speeds less than 5 m s^{-1}, the exchange coefficients in the second algorithm increase with decreasing wind, then decrease when the wind speed exceeds 5 m s^{-1}. In CRMs, the first algorithm predicts much larger surface fluxes of heat and moisture (hence surface rainfall) than those obtained using the second more complex algorithm. The boundary layer structure and convective available potential energy (CAPE) in clear and cloudy areas are also sensitive to the flux algorithms. Fine vertical resolution is required to properly represent interaction between the ocean and convection [*Wang et al.*, 1996].

3.6. Land Surface Processes

[24] Modeling coupled surface-atmospheric processes is particularly important at climate time scales. Detailed interactive land surface models of the heterogeneous land surface (soil, vegetation, and land cover/land use) and adjacent near-surface atmosphere coupled to CRMs can be used to study the effect of soil moisture distribution and surface fluxes on clouds and rainfall. A land surface model usually has three elements: (1) a soil module that calculates water and heat transfer into at least four water reservoirs (i.e., surface material, a topsoil root layer, and a subsoil root layer and at least two deeper layers that regulate seasonal and interannual variability of soil hydrology); (2) a surface slab of vegetation, litter, and other loose material that shades the soil and acts as the source for latent heat flux via transpiration and root water update, intercepts precipitation and dew, and may include plant internal storage; and (3) the atmospheric surface layer (up to the lowest grid level of the atmospheric model), where the fluxes of sensible heat and water vapor are calculated.

[25] High-resolution coupled CRM–land surface models have investigated how land surface conditions affect mesoscale circulations [*Lynn et al.*, 2001; *Golaz et al.*, 2001],

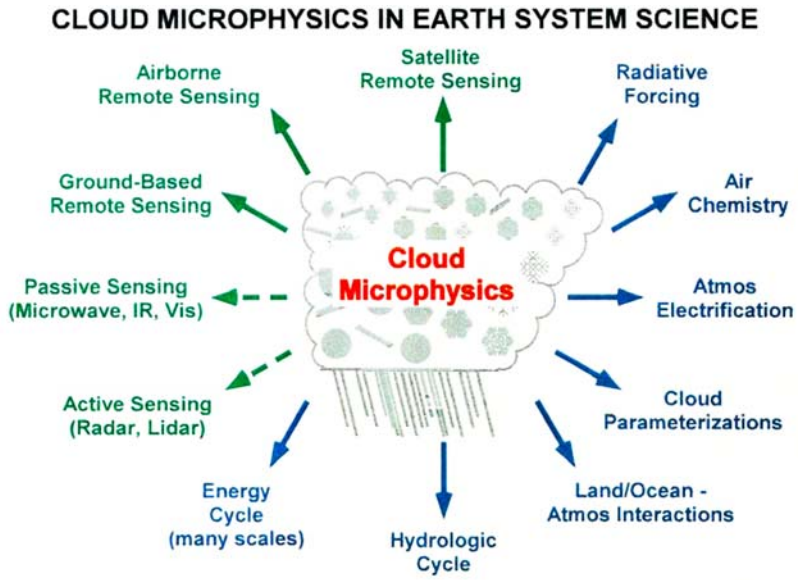

Figure 3. Schematic diagram showing the interactions between microphysics and other Earth system science.

cloud and precipitation processes within organized convective lines [*Baker et al.*, 2001; *Mohr et al.*, 2003; *Alonge et al.*, 2007], and transient convective clouds [*Lynn et al.*, 1998; *Zeng et al.*, 2007]. Quantification of the effects of anthropogenic and natural land cover and land use change motivated a new generation of land surface models that include human-induced land use change (e.g., irrigation, urbanization, and agriculture). Vegetation phenology and biogeochemical cycles of carbon and nitrogen that control photosynthesis and transpiration are included in the newest land surface models.

3.7. Data Assimilation for CRMs

[26] Historically, there has been little effort to assimilate observational data into CRMs as compared to operational NWP models. With the advent of higher-resolution prediction models, data assimilation on the convective scale is a growing area. The assimilation of radar data into CRMs has received attention, mainly in the context of the simulation of midlatitude convective storms. A pioneering work on the convective-scale assimilation of radar data was performed by *Sun and Crook* [1998] with recent contributions by *Xiao and Sun* [2007] and *Hu and Xue* [2007]. The Kalman filter approach to radar data assimilation was examined by *Dowell et al.* [2004] and *Aksoy et al.* [2009]. The reader is referred to the review by *Sun* [2005]. Having identified the components of CRMs, certain key elements (i.e., parameterization of precipitation processes, aerosols, and surface exchange) are now described in more detail in sections 4–6.

4. PARAMETERIZATION OF PRECIPITATION PROCESSES

[27] Figure 3 illustrates the scope of cloud microphysical interactions in Earth system science. Latent heat is released or absorbed by the atmosphere as a result of phase changes in water (e.g., condensation or evaporation of cloud droplets and raindrops, freezing of raindrops, melting of snow and graupel/hail, and the deposition or sublimation of ice particles). Cloud microphysics affects the vertical distribution of cloud substances (or hydrometeors) and size distributions (i.e., from small cloud water droplets and ice particles, to medium-sized snow, to large precipitating raindrops and graupel/hail), aspects of which affect active (i.e., radar reflectivity) and passive (i.e., brightness temperature) remote sensing measurements. Since precipitation can be in the form of light rainfall, heavy rainfall, snow, or mixed phase, it influences surface properties (i.e., soil moisture, runoff, albedo, and emissivity) and the energy and water cycles. Convective transport affects the vertical redistribution of chemical species and, in turn, radiative forcing and atmospheric electrification (see a review by *Cotton et al.* [1995]). CRMs represent the interaction between clouds and radiation with greater fidelity than global models since the spatial and temporal distributions of water substances (vapor, liquid, and ice) are explicitly coupled to the atmosphere circulation at cloud system scale.

[28] Figure 4 depicts the widely used two-class liquid (small cloud liquid water droplets and large precipitating liquid raindrops) and three-class ice (small cloud ice crystals, snow aggregates, and graupel/hail) microphysics schemes. Warm-cloud (ice-free) microphysics assumes a bimodal population of water particles consisting of small cloud water droplets whose terminal velocity is negligible compared to the vertical air velocity and large raindrops that have certain size distributions. Condensation, evaporation, and autoconversion/collection processes are parameterized. Ice microphysics typically assumes three types of particles: small cloud ice whose terminal velocity is negligible, snow whose terminal velocity is $\sim$1–3 m s^{-1}, and large graupel or hail with faster terminal velocities. Graupel has a low

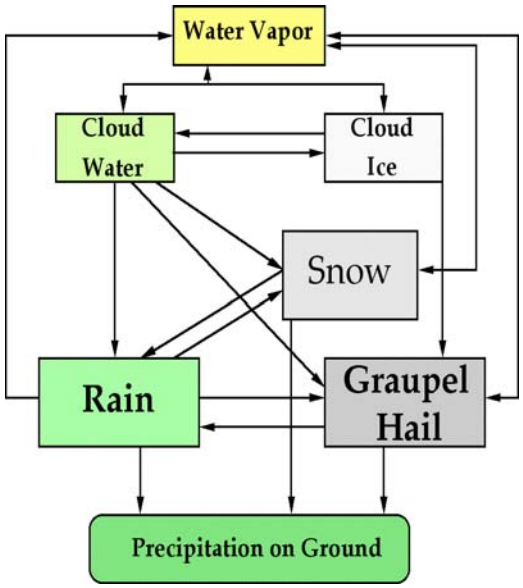

Figure 4. Representation of the three-class ice scheme used in the cloud model. Adapted from *Tao and Moncrieff* [2003].

density and high intercept (high number concentration), while hail has a high density and small intercept. Only large raindrops, snow, graupel, and hail reach the ground. Graupel is characteristic of tropical oceanic convection, and hail is characteristic of midlatitude storms [*McCumber et al.*, 1991]. More than 25 different transfer processes occur between water vapor, liquid, and ice particles such as: the growth of ice crystals by riming, the aggregation of ice crystals, the formation of graupel and hail, the growth of graupel and hail by the collection of supercooled raindrops, the shedding of water drops from hail, the rapid growth of ice crystals in the presence of supercooled water, the melting of all forms of ice, and the deposition and sublimation of ice.

[29] Figure 5 summarizes the microphysical and kinematic aspects of precipitation processes in the convective and stratiform regions of MCSs [*Houze*, 1982, 1989]. Ice is generated once growing drops are lofted through the 0°C level in convective updrafts. Thereafter, the ice particles grow by riming as they accrete supercooled cloud drops forming in the updraft at middle to upper levels. Larger particles fall out rapidly as convective rain, and smaller particles, which fall more slowly ($\sim$1 m s^{-1}), are advected into the stratiform region. The detrainment of snow from the convective cells transports precipitating particles into the stratiform region. The most intense radar bright band and the heaviest stratiform rain at the surface occur where the convectively generated snow particles reach the 0°C level, after passing through the stratiform cloud. In this environment of widespread moderate vertical motion, snow particles precipitate and grow by vapor deposition. In the layer between 0° and −12°C, the particles aggregate into snowflakes and grow by riming. The influx of snow into the stratiform region from convective cells and the growth of snow passing through the mesoscale updraft contribute to stratiform precipitation. See the reviews by *Houze* [2004] and *Tao* [2003] for more explanation.

[30] Figure 6 illustrates the microphysical properties of MCSs obtained from simulations of observed systems from the midlatitude continental Preliminary Regional Experiment for Stormscale Operational and Research Meteorology (STORM)-central (PRESTORM) and tropical oceanic Tropical Ocean Global Atmosphere Coupled Ocean Atmosphere Response Experiment (TOGA COARE) field campaigns. (PRESTORM took place in Kansas and Oklahoma during May and June of 1985 [*Cunning*, 1986].) Evident are

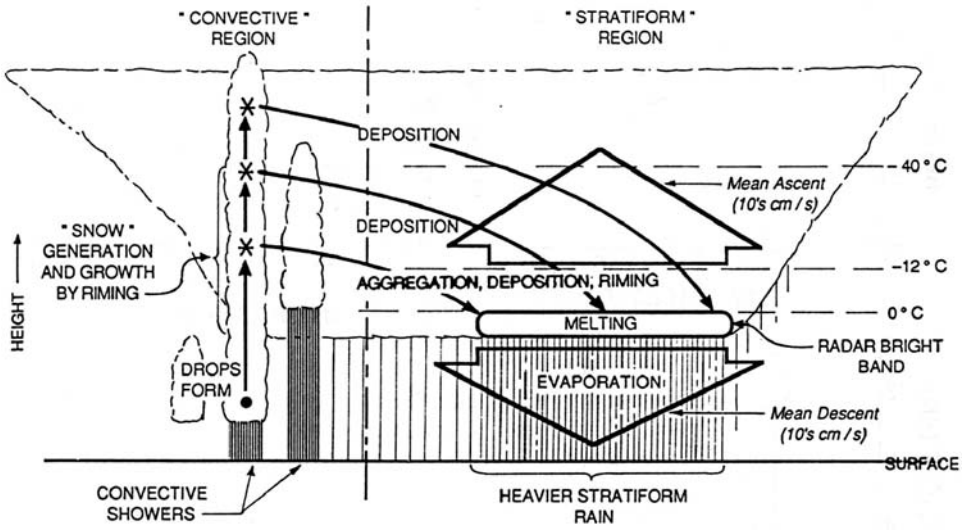

Figure 5. Schematic diagram of precipitation mechanisms for deep convective cells and the associated stratiform region for a mature tropical convective system. Straight solid arrows indicate convective updrafts; wide, open arrows indicate mesoscale ascent and subsidence in the stratiform region where vapor deposition and evaporation occur. Curved solid arrows indicate particle trajectories. Adapted from *Houze* [1989].

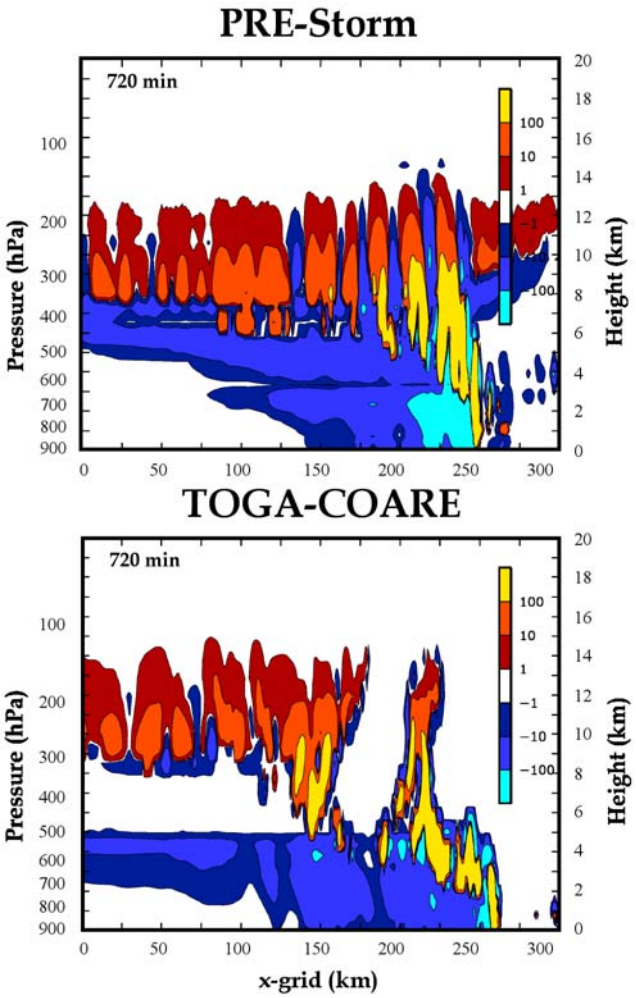

Figure 6. Height-length cross sections of GCE-generated latent heating (°C d^{-1}) consisting of the sum of heating by condensation, freezing, and deposition and cooling by evaporation, melting, and sublimation associated with a (top) midlatitude continental (Preliminary Regional Experiment for Stormscale Operational and Research Meteorology (STORM)-central (PRESTORM)) squall line and (bottom) tropical oceanic (Tropical Ocean Global Atmosphere Coupled Ocean Atmosphere Response Experiment (TOGA COARE)) mesoscale convective system (MCS). Simulations are discussed by *Tao et al.* [1993a, 1995, 1996], *Wang et al.* [1996], and *Lang et al.* [2003]. Adapted from *Tao et al.* [2006].

(1) condensation heating in the lower to middle troposphere of the convective leading edge of the cloud systems, (2) deposition heating in the upper parts of the convective and stratiform regions, (3) cooling in low-level stratiform regions due to the evaporation of rain, (4) cooling due to melting of precipitation near the freezing level (550–600 hPa), and (5) sublimation cooling adjacent to depositional heating in the stratiform regions. The alternating LH and cooling at upper levels in Figure 6 is caused by convectively generated gravity waves, which are of higher amplitude in midlatitudes because of the stronger convective updrafts. Cooling within the stratiform region is larger and deeper in midlatitudes due to the drier environment. The simulated structures are consistent with observed cloud systems.

4.1. Ice Phase

[31] *Tao and Simpson* [1989] showed that the introduction of ice phase microphysics does not significantly affect the propagation speed, life cycle, and total precipitation of a simulated MCS (see Table 2) nor does the total evaporative cooling in the stratiform and convective regions [*Yoshizaki*, 1986; *Nicholls*, 1987; *Fovell and Ogura*, 1988; *Chen*, 1991]. This is consistent with section 10 herein: dynamical interactions between environmental shear, vorticity generated by horizontal gradients of LH, and the hydraulic properties of mesoscale downdrafts control MCS-type convective organization. The main difference lies in the precipitation statistics. Light rain (<10 mm h^{-1}) accounts for only about 26.5% of the total rain but covers 90% of the total rain area when the ice phase is included. By contrast, heavy precipitation (>30 mm h^{-1}) accounts for a large portion of the total rain but occupies a very small portion of the total rain area. Without ice phase microphysics, heavy precipitation increases significantly, and only 12% of the rain is stratiform. The depth of the stratiform cloud is reduced without ice microphysics. These results were confirmed by GATE observations [see *Tao and Simpson*, 1989, Table 2].

[32] A four-class microphysical scheme (4ICE, consisting of cloud ice, snow, graupel, and frozen drops/hail) combines the features of three-class ice (3ICE, consists of cloud ice, snow, and graupel or hail) schemes by calculating the mixing ratios for both graupel and frozen drops/hail [*Ferrier*, 1994; *Ferrier et al.*, 1995]. Additional variables/features include (1) the number concentrations of all ice particles (small ice crystals, snow, graupel, and frozen drops); (2) the mixing ratios of liquid water on each of the precipitation ice substances during wet growth and melting for purposes of accurate active and passive radiometric calculations; (3) more accurate calculation of accretion processes, including partitioning the freezing of raindrops as sources of snow, graupel, or frozen drops/hail; (4) consideration of rime densities and riming rates in converting between ice substances due to rapid cloud water riming; (5) incorporation of new parameterizations for ice nucleation processes, the rime splintering mechanism using laboratory data, and aircraft observations of high ice

TABLE 2. Estimated Surface Rainfall and Rainfall Area at the Surface[a]

	Total Rain (mm/12 h)	Stratiform Portion	Total Rain Area (%)	Stratiform Rain Area (%)
Ice run	24.9	32.7%	22.3	86.8
Ice-free	23.4	11.5%	8.1	66.1

[a]Rain is given in relative units (millimeters per grid point accumulated over a 12 h period). The total rain area is given as a percentage of the total domain area. Stratiform portion and stratiform rain area are given as a percentage of total rain and total rain area, respectively. Adapted from *Tao and Simpson* [1993].

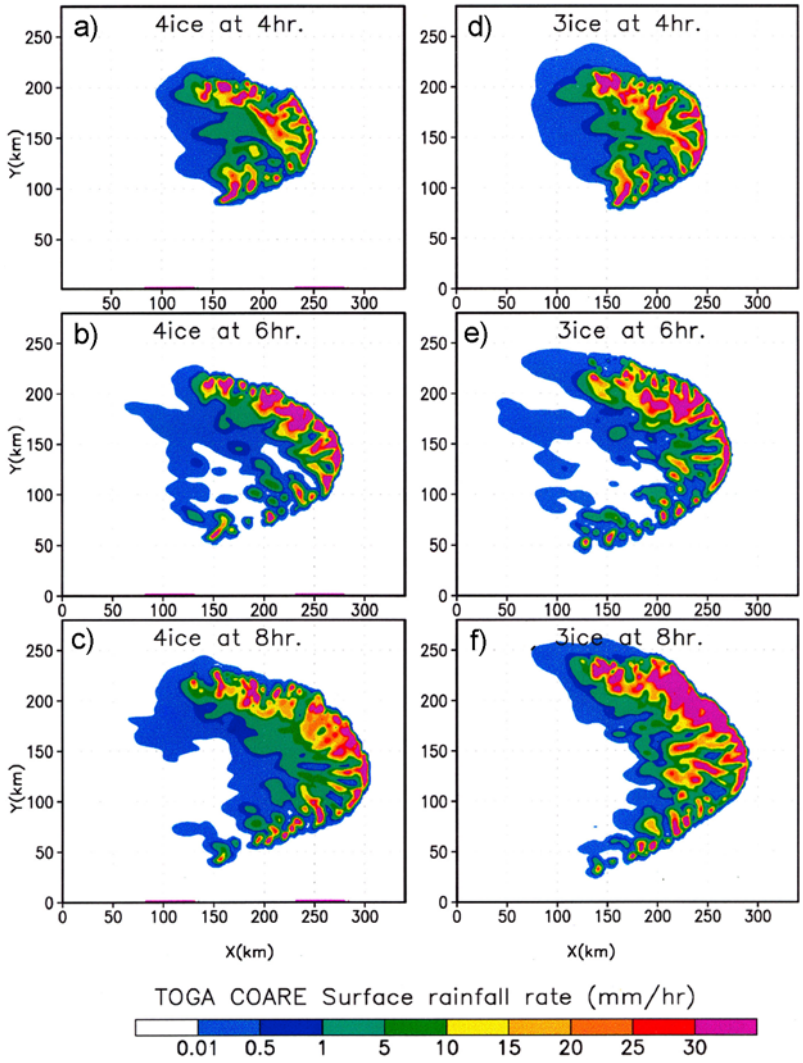

Figure 7. Surface rainfall rate (mm/h) simulated by a 3-D cloud system resolving model (CRM) for a TOGA COARE squall system. The 4ICE scheme at (a) 4, (b) 6, and (c) 8 h into the model simulation. (d–f) The same as Figures 7a–7c except for the 3ICE scheme. The model domain consisted of 172 × 142 grid points in the horizontal x and y directions, and the lateral boundaries were open. The horizontal grid resolution was 2 km. The vertical direction had 34 grid points up to 23.9 km stretched from 42.5 m at the lowest grid point to 1196 m at the top grid. Adapted from *Tao et al.* [2003].

particle concentrations; (6) shedding of liquid water from melting ice and excessive amounts of water accumulated on supercooled frozen drops/hail; (7) preventing unrealistically large glaciation rates immediately above the freezing level by explicitly calculating freezing rates of raindrops and freezing rates of liquid water accreted onto supercooled ice; (8) fall speeds and size distributions for small ice crystals; (9) calculating radar reflectivity of particles with variable size distributions and liquid water coatings from Rayleigh theory; and (10) conversion based on particle number concentrations between hydrometeors while preserving spectral characteristics of particle distributions rather than conserving their number concentrations (important). A detailed description of these parameterized processes is given by *Ferrier* [1994].

[33] The 4ICE scheme does not significantly affect convective organization (Figure 7). For example, the arc shape agrees with the observations for this case [*Jorgensen et al.*, 1997], and the propagation speed of the squall system is also similar to that for 3ICE (14 m s^{-1}), which is ~2 m s^{-1} faster than was observed. However, ice microphysical parameterizations can affect the amount of surface precipitation with 4ICE generally ~30% less than 3ICE (Table 3). The evolution of stratiform rain also differs. The 3ICE scheme produces more/less stratiform rain early/later in the simulation because of the different hydrometeor profiles. In 4ICE, small ice particles (cloud ice and snow) with slow fall speeds (1–3 m s^{-1}) are dominant. The 3ICE scheme produces more and larger graupel particles (with 2–5 m s^{-1} fall speeds) in the convective towers.

TABLE 3. Surface Rainfall Amounts Accumulated Over 9 h for a CRM-Simulated TOGA COARE Squall System Using the 3ICE and 4ICE Schemes[a]

	3ICE	4ICE
Rainfall (mm)	13.38	10.06
Stratiform percentage (%)	35%	35%

[a]The percentage of rainfall that was stratiform is also given. Adapted from *Tao et al.* [2003]. TOGA COARE, Tropical Ocean Global Atmosphere Coupled Ocean Atmosphere Response Experiment.

4.2. Explicit Ice Microphysics

[34] Spectral bin microphysical processes represented in CRMs quantify cloud-aerosol-chemistry interactions that are difficult to directly observe. In addition, the explicit (bin microphysical) approach provides a framework for evaluating and improving the approximations assumed in the bulk microphysical schemes (see the discussion in section 3.2). Explicit schemes have also been used to study the impact of atmospheric aerosols on cirrus and deep convective precipitation [*Khain et al.*, 2004] (see also the review by *Levin and Cotton* [2008]).

[35] Figure 8 shows vertical cross sections of simulated and observed radar reflectivity for a mature squall line (see *Li et al.* [2009] for more detail). Large differences exist between the radar reflectivity structure simulated by the bulk and bin schemes, especially in the stratiform region. Both the size of the stratiform area and its rain fraction are much larger in the bin simulation (see Table 4). The stratiform region simulated by the bin scheme is homogeneous (no signs of convective cells). On the other hand, cellular convective structures occur in the form of high radar reflectivity cores, which are the remnants of previous convective cells that traveled rearward as they decayed, in

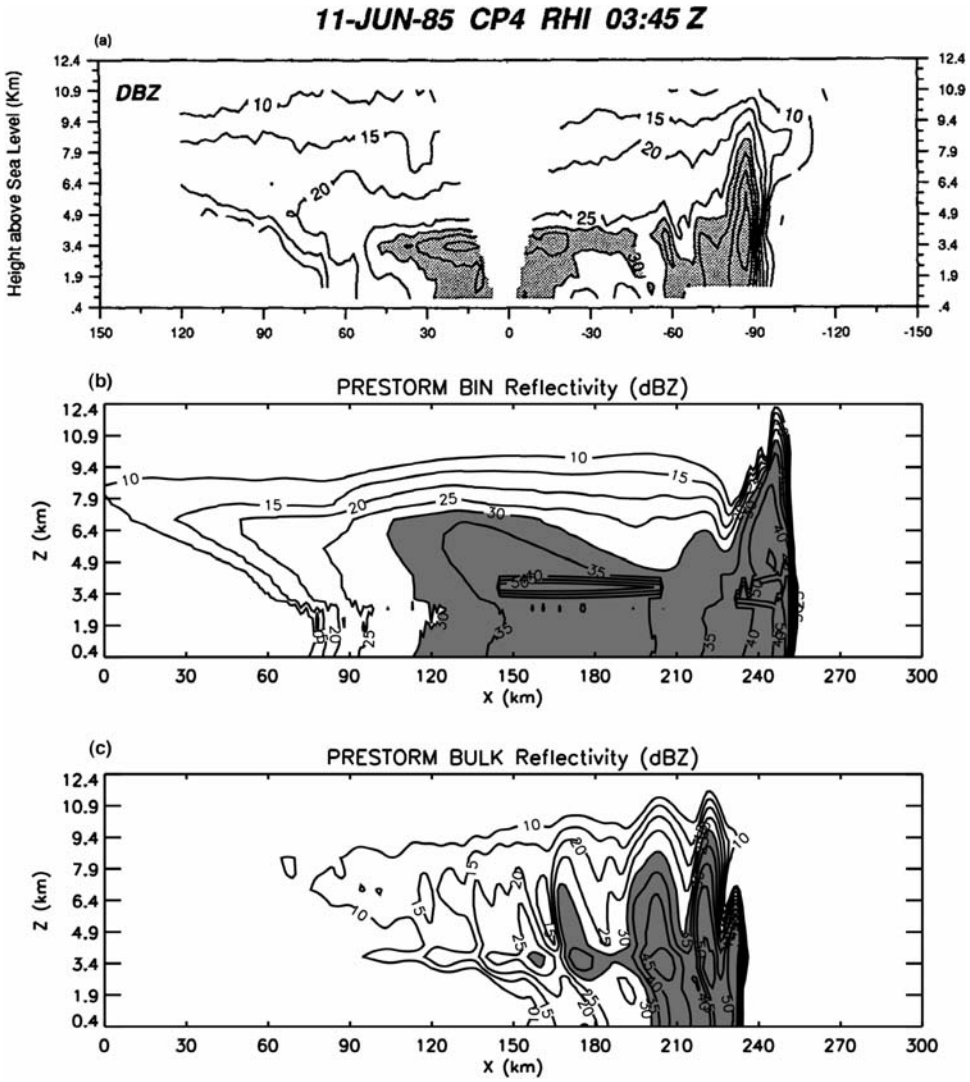

Figure 8. (a) The observed radar reflectivity at 0345 UTC, 11 June 1985, during the mature stage of the PRESTORM squall [*Rutledge et al.*, 1988]. CRM-simulated radar reflectivity using (b) traditional one-moment 3ICE bulk and (c) explicit spectral bin microphysics schemes. Radar reflectivity in the bulk model is calculated using fixed, exponential particle size distributions and densities, whereas the simulated particle size distributions are used in the bin model. The spatial scales and contour levels are matched in all three plots. Adapted from *Li et al.* [2009].

TABLE 4. Surface Rainfall Amounts Accumulated Over 12 h for a CRM-Simulated PRESTORM Squall System Using the 3ICE Bulk and Spectral Bin Microphysical Schemes[a]

	Bulk 3ICE Microphysical Scheme	Spectral Bin Microphysical Scheme
Rainfall (mm)	64.5	56.9
Stratiform (%)	6.6%	19.6%

[a]The percentage of rainfall that was stratiform is also given. Adapted from *Li et al.* [2009]. PRESTORM, Preliminary Regional Experiment for Stormscale Operational and Research Meteorology (STORM)-central.

the bulk scheme. Radar reflectivity observations from the PRESTORM squall are widely reported [e.g., *Smull and Houze*, 1987a, 1987b; *Rutledge and MacGorman*, 1988; *Biggerstaff and Houze*, 1993]. The bin scheme is able to produce a much more extensive and homogeneous stratiform region, which compares better with radar observations.

5. AEROSOLS

[36] The effect of aerosols on clouds is a climate system and hydrological cycle issue [*Ramanathan et al.*, 2001], but the processes and mechanisms involved are poorly understood. A recent report published by the National Academy of Science states [*National Research Council*, 2005, p. 208] "The greatest uncertainty about the aerosol climate forcing - indeed, the largest of all the uncertainties about global climate forcing - is probably the indirect effect of aerosols on clouds." In addition, *Levin and Cotton* [2008] presented a review on the impact of aerosol pollution on precipitation. Aerosols can influence cloud properties in ways such as increasing their optical thickness and albedo [e.g., *Twomey*, 1977] and reducing their coverage/fraction and lifetime [e.g., *Ackerman et al.*, 2000]. Enhanced aerosol concentrations can also suppress warm-rain processes by producing a narrow droplet spectrum that inhibits collision and coalescence processes [e.g., *Squires and Twomey*, 1961; *Warner and Twomey*, 1967; *Warner*, 1968; *Rosenfeld*, 1999].

[37] The aerosol effect on precipitation processes [e.g., *Albrecht*, 1989] is more complex, especially for mixed phase convective clouds. Table 5 summarizes the observations of cloud systems in high-aerosol continental environments. Aerosol concentrations can influence cloud droplet size distributions, warm-rain processes, cold-rain processes, cloud top height, the depth of the mixed phase region, and the occurrence of lightning. Hypotheses have been developed to explain the effect of urban regions on convection and precipitation [*van den Heever and Cotton*, 2007; *Shepherd*, 2005]. See *Tao et al.* [2007] and *Levin and Cotton* [2008] for more on the effects of aerosols on precipitation.

[38] CRMs have quantified the effects of aerosols. Figure 9 shows that rain is suppressed for high CCN concentrations (i.e., dirty environment) but only during the first hour of simulation. Rain reaches the ground early in all the clean cases, in agreement with observations [e.g., *Rosenfeld*, 1999, 2000]. During the mature stage, the effect of increasing the CCN concentration ranges from rain suppression in PRESTORM, to little effect in Cirrus Regional Study of Tropical Anvils and Cirrus Layers–Florida Area Cirrus Experiment (CRYSTAL-FACE), to rain enhancement in TOGA COARE. This suggests that simulations of the entire life cycle of convective systems are needed to assess the impact of aerosols on precipitation processes associated with MCSs and thunderstorms. This also shows the complexity of aerosol-cloud-precipitation interaction within deep convection.

[39] Table 6 shows the domain-averaged surface rainfall amounts, stratiform percentages, precipitation efficiencies, and ice water path ratios (ice water path divided by the sum of the liquid and ice water paths) under clean and dirty conditions. The precipitation is divided into convective and stratiform components [*Tao et al.*, 1993a; *Lang et al.*, 2003]. The convective region includes areas with strong vertical velocities (over 3–5 m s^{-1}) and/or heavy surface rainfall. The stratiform region is nonconvective. It is expected that a high CCN concentration allows for the formation of more small cloud droplets and ice particles. The lower collection

TABLE 5. Key Observational Studies Identifying the Differences in the Microphysical Properties, Cloud Characteristics, Thermodynamics, and Dynamics Associated With Clouds and Cloud Systems That Developed in Dirty and Clean Environments[a]

Properties	High CCN (Dirty)	Low CCN (Clean)	References (Observations)
Cloud droplet size distribution	narrower	broader	*Rosenfeld and Lensky* [1998], *Rosenfeld* [1999, 2000], *Rosenfeld et al.* [2001], *Rosenfeld and Woodley* [2000], *Andreae et al.* [2004], and *Koren et al.* [2005]
Warm-rain process	suppressed	enhanced	*Rosenfeld* [1999, 2000], *Rosenfeld and Woodley* [2000], *Rosenfeld and Ulbrich* [2003], *Andreae et al.* [2004], and *J. C. Lin et al.* [2006]
Cold-rain process	enhanced	suppressed	*Rosenfeld and Woodley* [2000], *Orville et al.* [2001], *Williams et al.* [2002], *Andreae et al.* [2004], *J. C. Lin et al.* [2006], and *Bell et al.* [2008]
Mixed phase region	deeper	shallower	*Rosenfeld and Lensky* [1998], *Williams et al.* [2002], and *J. C. Lin et al.* [2006]
Cloud top height	higher	lower	*Andreae et al.* [2004], *Koren et al.* [2005], and *J. C. Lin et al.* [2006]
Lightning	enhanced (downwind side)/ higher maximum flash	less and lower maximum flash	*Williams et al.* [2002] and *Orville et al.* [2001]

[a]Adapted from *Tao et al.* [2007]. CCN, cloud condensation nuclei.

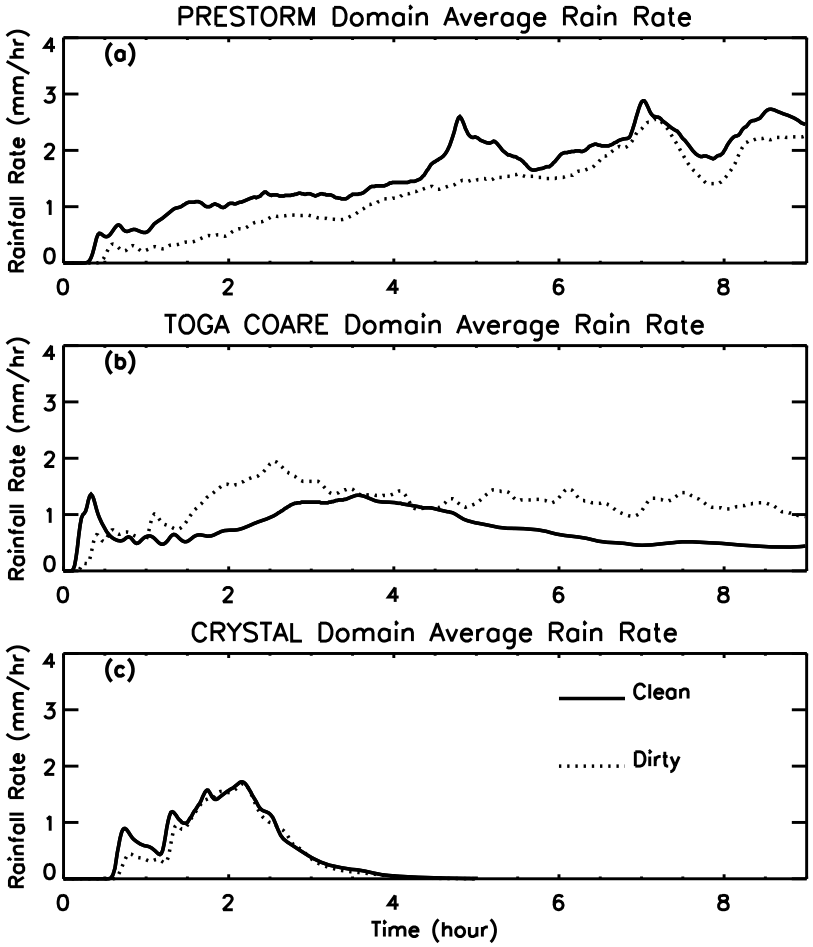

Figure 9. Time series of GCE model-estimated domain mean surface rainfall rate (mm h^{-1}) for the (a) PRESTORM, (b) TOGA COARE, and (c) Cirrus Regional Study of Tropical Anvils and Cirrus Layers–Florida Area Cirrus Experiment (CRYSTAL-FACE) case. The solid/dashed line represents clean/dirty conditions. Adapted from *Tao et al.* [2007].

coefficient for smaller cloud and ice particles allows for a larger amount of ice phase particles to be transported into the trailing stratiform region, producing a higher stratiform rain percentage in the dirty case. Aerosols do not have much impact on the stratiform percentage for the CRYSTAL-FACE case because of its short life span. For further information, the reader is referred to the following publications that illustrate the complexity of aerosol interactions with convection: *Twomey et al.* [1984], *Albrecht* [1989], *Rosenfeld* [1999, 2000], *Khain et al.* [2004, 2005, 2008], *Cheng et al.* [2007], *Lynn et al.* [2005], *Wang* [2005], *van den Heever et al.* [2006], *Teller and Levin* [2006], *van den Heever and Cotton* [2007], *Tao et al.* [2007], and *Levin and Cotton* [2008].

6. SURFACE EXCHANGE

[40] The surface and atmosphere are strongly coupled. Solar energy, mostly absorbed at the land and ocean surfaces, is transmitted to the atmosphere through boundary layer turbulence, shallow nonprecipitating convection, and deep precipitating convection. In global models, atmo-

TABLE 6. Domain-Averaged Surface Rainfall Amount and Stratiform Percentage for the TOGA COARE, PRESTORM, and CRYSTAL-FACE Cases Under Dirty and Clean Conditions[a]

	TOGA COARE Clean	TOGA COARE Dirty	PRESTORM Clean	PRESTORM Dirty	CRYSTAL-FACE Clean	CRYSTAL-FACE Dirty
Averaged rain (mm d^{-1} $grid^{-1}$)	18.0	28.4	38.3	29.1	12.6	11.0
Stratiform (%)	50	17	43	70	43	40

[a]Note there are 9 h in the PRESTORM and TOGA COARE simulations and 5 h in the CRYSTAL-FACE simulation. Adapted from *Tao et al.* [2007]. CRYSTAL-FACE, Cirrus Regional Study of Tropical Anvils and Cirrus Layers–Florida Area Cirrus Experiment.

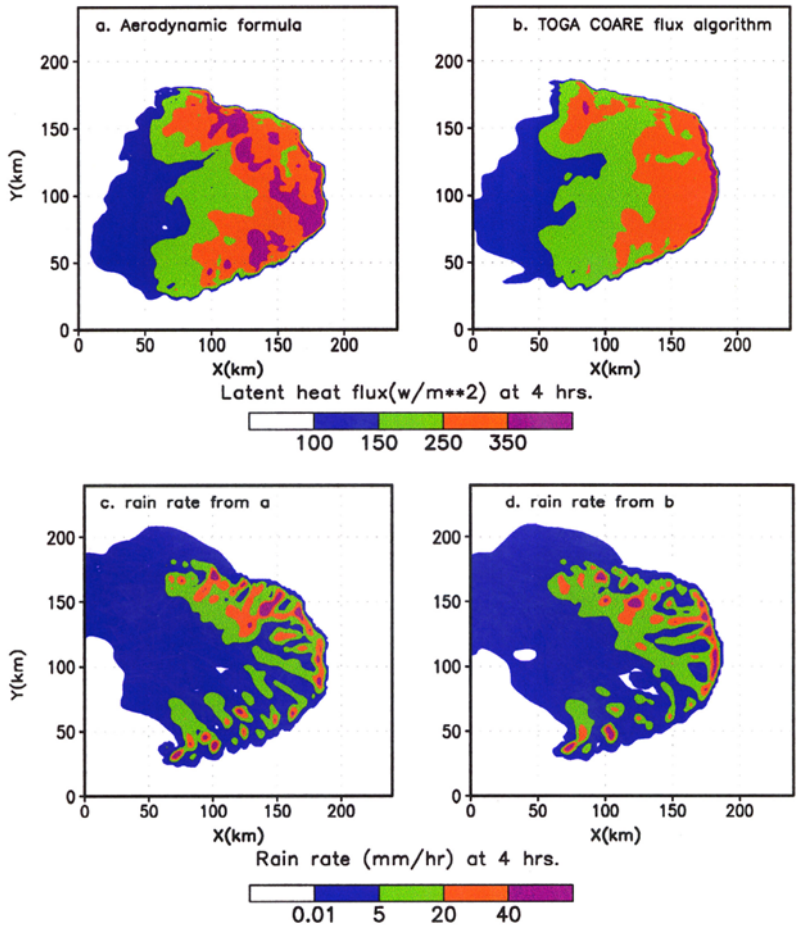

Figure 10. Surface latent heat flux at 6 h into the simulation using (a) a simple bulk aerodynamic method and (b) the TOGA COARE flux algorithm. (c and d) The same as Figures 10a and 10b except showing the surface rain rate. Adapted from *Tao et al.* [2003].

sphere-surface coupling occurs entirely through parameterizations. In CRMs, key processes are explicit. Notably, gustiness associated with cool convective downdrafts can affect large areas as a result of propagating density currents, which can travel hundreds of kilometers from their origin. Simulations of organized mesoscale cold pools generated by the evaporation of rain have long been recognized as an important trigger for precipitating convection [e.g., *Thorpe et al.*, 1980] and the development of multiscale convective organization [e.g., *Liu and Moncrieff*, 1998; *Tulich et al.*, 2007]. However, density currents are not yet fully represented as trigger functions in convective parameterizations, although shear-dependent trigger functions have been formulated [*Moncrieff and Liu*, 1999].

[41] Over land, the surface fluxes are coupled to the surface net radiation, the vegetation state, and the profiles of temperature and water below the surface and through the atmospheric planetary boundary layer. These processes are strongly influenced by topography and the heterogeneous character of the land surface layer. The fluxes of heat and moisture across the interface vary on spatial scales ranging from meters to thousands of kilometers. On the other hand, the western Pacific warm pool is a region of enhanced atmospheric sensitivity to small changes in the ocean temperature [*Webster and Lukas*, 1992]. Modeling these coupled surface-atmospheric processes is crucial to the understanding and simulation of climate system interactions.

6.1. Ocean Surface Fluxes

[42] Observations in the western Pacific warm pool region [*Bradley et al.*, 1991; *Young et al.*, 1992; *Fairall et al.*, 1996] show that surface heat and momentum fluxes peak at the convective leading edge due to strong convective gusty winds and cool downdrafts. The surface fluxes in the cloud clear area are much smaller and more uniform. Figure 10 shows the rainfall and surface latent heat flux values using the TOGA COARE flux algorithm and the simple bulk aerodynamic method. (The TOGA COARE bulk flux algorithm was developed and calibrated with the TOGA COARE surface flux data set. Simple bulk aerodynamic methods have been used frequently in CRMs as well as in hurricane models.) The different flux algorithms do not affect the organization of the squall system. There are large peaks in latent heat flux at the leading edge of the convection, $\sim$4–5 times the value in the clear area. The rainfall total simulated with the TOGA COARE flux algorithm is $\sim$73% of the rainfall amount using the bulk aerodynamic method. Larger surface fluxes cause more rainfall (or

TABLE 7. Estimated Surface Rainfall for Simulations Using Different Surface Flux Formations[a]

	Surface Rainfall (mm)	Sensible Heat: Disturbed	Fluxes: Undisturbed	Latent Heat: Disturbed	Fluxes: Undisturbed
COARE flux	3.4	20.9	8.4	142.2	81.7
Aerodynamic	4.5	31.1	12.9	206.5	127.7
Blackadar	4.2	24.4	10.7	170.8	110.6

[a]Also shown are the ensemble averaged sensible and latent heat fluxes in the disturbed (convective) and undisturbed (nonconvective) regions for simulations using different surface flux formulations. Adapted from *Wang et al.* [1996].

precipitation processes). A sensitivity study by *Wang et al.* [2003] indicated that surface fluxes from the large clear area are more influential to the rainfall amount than the fluxes from the disturbed convective area because the moisture supply is mainly from the clear area ahead of the convective system. The stratiform cloudiness between these two runs is very similar (~35%). Vertical wind shear has a strong effect on convective organization and stratiform rain (see section 10).

[43] Table 7 lists the accumulated domain-normalized surface rainfall amounts as well as horizontally averaged latent and sensible heat fluxes for the disturbed (convective) and undisturbed (cloud-free) areas simulated from three different surface flux formulations: the Blackadar planetary boundary layer, simple bulk aerodynamic method, and TOGA COARE flux algorithm. (The Blackadar PBL has been widely applied in regional modeling studies associated with convective systems.) The surface heat fluxes and the surface rainfall are correlated, but the relationship is not linear. Similar amounts of surface precipitation were simulated using the Blackadar surface fluxes and the bulk aerodynamic method, though the fluxes computed from the bulk aerodynamic method are significantly larger than those from the Blackadar method. Figure 11 shows the latent and sensible heat fluxes in the convective region are much larger than those in the clear region (due to gustiness and drier/cooler air from downdrafts in the convective region). The above results are in agreement with observations [*LeMone et al.*, 1995; *Young et al.*, 1992; *Jorgensen et al.*, 1997].

[44] Surface fluxes affect the integrated potential temperature difference between the moist adiabatic ascent of a surface parcel and the environment, namely, the CAPE [*Moncrieff and Miller*, 1976]. The sensible heat flux is usually small over the ocean compared to the latent heat flux. *Trier et al.* [1996] suggested that the CAPE in clear regions should remain quasi-steady during convection, but only a simulation with the TOGA COARE flux parameterization gives a quasi-steady CAPE [*Wang et al.*, 2003].

6.2. Land Surface Fluxes

[45] Surface convective fluxes are coupled to the surface net radiation flux, the vegetation state, and the profiles of temperature and water below the surface and up through the atmospheric planetary boundary layer. These processes are influenced by topographic features and the heterogeneous character of the land surface layer. The fluxes of heat and moisture across the interface vary on spatial scales ranging from meters to thousands of kilometers.

[46] Cloud data collected at the DOE ARM Southern Great Plains (SGP) site enable the effects of the land surface on clouds to be evaluated using high-resolution CRMs. A 20 day CRM simulation was evaluated using ARM measurements as well as surface fluxes extracted from the NASA land information system (LIS) [see *Kumar et al.*, 2006]. (LIS is capable of resolving mesoscale features, including urban areas, lakes, and agricultural fields, which allows the impact and scaling of such heterogeneity in coupled cloud modeling to be studied.) LIS simulates soil moisture (both liquid and frozen), soil temperature, skin temperature, canopy water content, and the energy and water flux terms in the surface energy and water balance. The land surface parameters were initialized with 1 km data sets for vegetation and land-sea masks [*Hansen et al.*, 2000]. Climatologic data sets were used to initialize other vegetation parameters such as albedo, soil water and temperature profiles, and vegetation fraction. Soil types were set using the 1 km horizontal resolution Soil Geographic Database for State (U.S. Department of Agriculture).

[47] Figure 12 compares observed and modeled (20 day) cloud amounts. The surface relative humidity decreases when the sensible heat flux increases and the latent heat

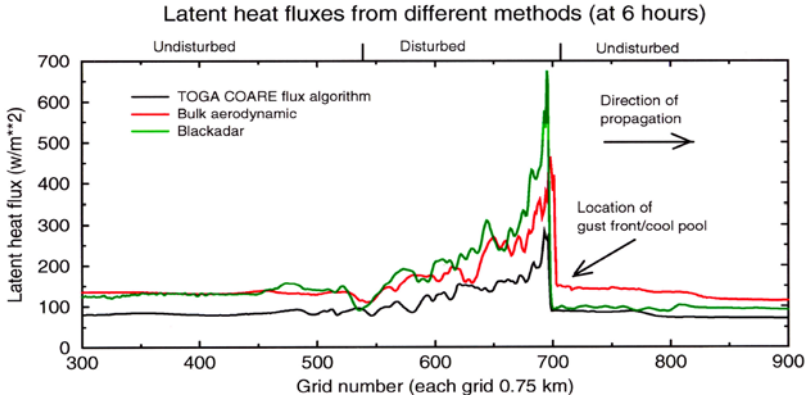

Figure 11. Latent heat fluxes simulated from different surface flux formulations at 6 h. Adapted from *Wang et al.* [1996].

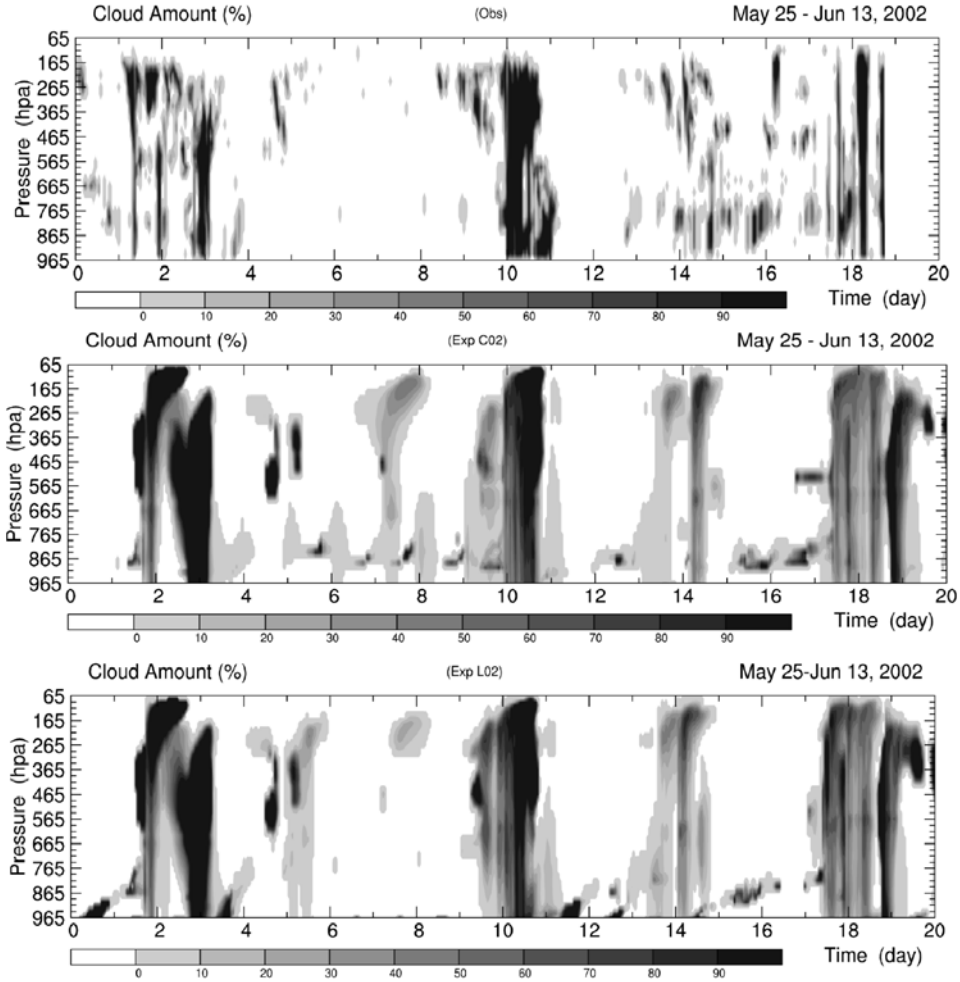

Figure 12. (top) The observed ARM cloud amount corresponding to a 20 day CRM simulation for Oklahoma in 2002. The modeled cloud amount using (middle) ARM and (bottom) land information system (LIS) surface fluxes as input. The results from the numerical experiment with LIS better resolve the observed cloud and precipitation processes, especially for less organized convective clouds. Adapted from *Zeng et al.* [2007].

flux decreases; therefore, the lifting condensation level increases, and, in turn, cloud amount in the lower troposphere decreases. This connection between surface fluxes and the diurnal cycle of clouds in the lower troposphere is consistent with the difference in relative humidity in the planetary boundary layer between the two experiments. It is necessary to properly represent the coupling between clouds and a land surface on an SGS in general circulation models (GCMs).

[48] When coupled to a complex soil-vegetation land model, CRMs simulate moist convection over a heterogeneous landscape and the effects of precipitation on soil moisture. *Lynn et al.* [1998] examined a sea breeze–like front observed during the Convection and Precipitation Electrification Experiment over Florida. Alternating patches of dry and wet soil and various profiles of background wind were used in a total of 28 simulations. The most intense rainfall occurred along sea breeze–like fronts at patch boundaries. While the largest/smallest CAPE occurred over wet/dry patches, the heaviest rainfall did not coincide with the largest CAPE but rather along the sea breeze–like fronts at intermediate values of CAPE. Convection was triggered by the superposition of dynamic frontal forcing with landscape-generated mesoscale circulations. This suggests the need to account for the triggering of moist convection by land surface heterogeneity in atmospheric models.

7. CLOUD-RADIATION INTERACTION

[49] The effect of clouds on radiation is a critical process for climate models. The cloud-radiation interaction problem has been addressed in depth by utilizing CRMs, which represent clouds with more fidelity than global models that parameterize moist convection.

[50] Cloud-radiation interaction is put into perspective by noting that the effects of clouds on climate are ~4 times larger than the effects of doubled carbon dioxide. The coupled cloud-radiation-greenhouse effect is not fully understood in the context of climate change [*Ramanathan and Collins*, 1991]. Hence, a high priority in Earth system

TABLE 8. Summary of Previous CRM Studies[a]

	LW Radiative Processes	Constant LW	LW and SW Radiative Processes	Imposed Mesoscale Lifting	Case
Chen and Cotton [1988]	0%	no	no	no	mid-U. S. MCS
Dudhia [1989]	36%	no	no	no	WMONEX
Tao et al. [1991]	20%	no	no	4 cm s^{-1}, not continuous	TAMEX squall
Churchill and Houze [1991]	0%	no	0%	strong, continuous	GATE MCS
Miller and Frank [1993]	no	34%	18–21%	strong, continuous	tropical (GATE)
Chin [1994]	11%	no	−7%	no	mid-U.S. squall
Xu and Randall [1995]	na	na	na	8–14 cm s^{-1}, not continuous	GATE
Fu et al. [1995]	5%	15%	−1%	8–14 cm s^{-1}, not continuous	GATE
Chin et al. [1995]	15%	no	−18%	no	GATE
Tao et al. [1996]	36%	2%	−7%	7 cm s^{-1}, not continuous	EMEX
Tao et al. [1996]	8%	8%	−6%	no	PRESTORM
Dharssi et al. [1997]	30%	no	no	no	EMEX

[a]The percentage increase or decrease in surface precipitation due to longwave (LW) and shortwave (SW) effects are given along with the mesoscale lifting, if used, for each case. Constant LW indicates no cloud-radiation interaction. The increments in surface precipitation are relative to the run without radiative processes. No means that no experiment is conducted, and na stands for not available. MCS, mesoscale convective system; WMONEX, Winter Monsoon Experiment; TAMEX, the Taiwan Area Mesoscale Experiment; GATE, Global Atmospheric Research Program Atlantic Tropical Experiment; EMEX, the Equatorial Mesoscale Experiment.

science is to understand the coupling between radiation physics and clouds and to satisfactorily represent the coupling in parameterizations. On the one hand, clouds reflect incoming solar and absorb outgoing longwave radiation. The Earth Radiation Budget Experiment estimates of global distributions of cloud-radiative interaction showed that large (stratiform) anvil clouds significantly reflect shortwave radiation [*Ramanathan et al.*, 1989], suggesting that clouds have a cooling effect. On the other hand, *Hartmann et al.* [2001] suggested that individual convective elements can have either a positive or a negative effect on radiation balance depending on their optical depth. Their analyses also showed that the individual positive and negative contributions cancel each other when averaged over a convective cloud system.

[51] Radiation can either enhance or reduce cloud activity. Differential heating between cloudy and clear regions can enhance the cloudy region [*Gray and Jacobson*, 1977]. Longwave radiation cools stratiform cloud tops but warms the associated bases [*Cox and Griffith*, 1979], which can destabilize the stratiform cloud layer. *Webster and Stephens* [1980] suggested that this destabilization was important for the light precipitation region during the Winter Monsoon Experiment. *Kubar et al.* [2007] suggested that clear-sky radiation-driven upper level convergence determines the level at which detrained anvil cloud is maximum. *Stephens* [1983] deduced the effects of radiation on the growth and sublimation rates of ice particles. Particle growth (sublimation) is enhanced (suppressed) in a radiatively cooled (heated) environment. Radiational cooling may also destabilize the large-scale environment [*Dudhia*, 1989]. *Tao et al.* [1996] proposed that an increase in relative humidity by longwave cooling could enhance precipitation in the tropics.

[52] Cloud interactive radiation has important dynamical affects, notably the selection of the scale and morphology of convective organization in the tropics. Comparison of two CRM simulations, one with imposed longwave cooling [*Grabowski and Moncrieff*, 2001] and the other with cloud interactive radiation [*Grabowski and Moncrieff*, 2002], shows that cloud interactive radiation generates a horizontal gradient of heating between the moist and dry regions. This gradient drives a (baroclinic) large-scale circulation in the vertical plane. The two principal regimes of convective organization, the westward propagating MCS-type systems and the eastward propagating large-scale cloud envelope, are affected. With interactive radiation, the MCS-type systems are more persistent than those associated with imposed radiative cooling. In other words, the dynamics and thermodynamics of cloud interactive radiation are coupled in a fundamental way.

[53] CRMs have quantified the effects of cloud-radiation interaction on convective systems (Table 8). For example, *Xu and Randall* [1995], *Miller and Frank* [1993], *Fu et al.* [1995], and *Tao et al.* [1996] indicated that the differential cooling between cloudy and clear regions plays only a secondary role in enhancing precipitation processes. *Xu and Randall* [1995] and *Fu et al.* [1995] also suggested that the cloud top cooling and cloud base warming destabilization mechanism could be important for prolonging the life span of high anvil clouds (around 10 km). However, in the work by *Xu and Randall* [1995] this direct cloud destabilization does not impact surface precipitation. Further modeling studies [*Fu et al.*, 1995; *Miller and Frank*, 1993; *Tao et al.*, 1996] indicated that constant clear-air radiative cooling enhances surface precipitation. On the other hand, *Chin* [1994], *Chin et al.* [1995], *Miller and Frank* [1993], and *Tao et al.* [1996] showed that solar radiation could reduce precipitation. The increase or decrease in surface precipitation varies significantly among the different modeling studies for tropical convective systems but not midlatitude systems. The hypothesis that large-scale forcing (lifting) affects the tropical simulations was tested by imposing adiabatic lifting varying from 2 to 14 cm s^{-1} applied continuously or discontinuously in time (Table 8). *Tao and Simpson* [1989] and *Miller and Frank* [1993] found that the radiative effects on clouds are sensitive to the

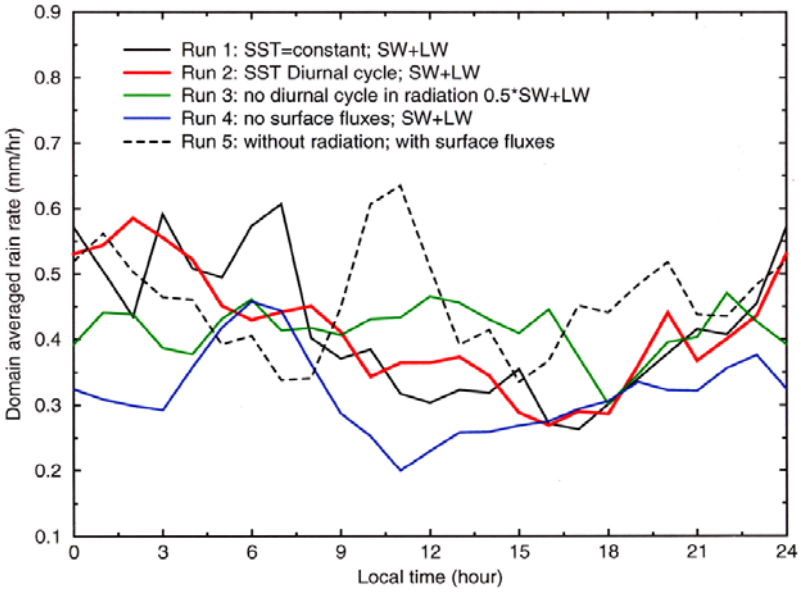

Figure 13. Diurnal composite of CRM domain average daily rain rate (mm h^{-1}). The black solid line denotes the run with constant sea surface temperature (SST, 29.2°C) and explicit/diurnal cloud-radiation interaction. The red line denotes the run with diurnal SST variation (1°C difference between the maximum and minimum) and explicit/diurnal cloud-radiation interaction. The green line is for the run without SST diurnal variation and no diurnal variation in radiation. The blue line denotes the run without SST fluxes but with explicit/diurnal cloud-radiation interaction. The black dashed line denotes the run without radiation but with surface fluxes. The initial thermodynamic conditions are representative of the disturbed periods during the TOGA COARE intensive observation periods (the upper air soundings representing the disturbed periods were averaged). The large-scale vertical velocity for the same disturbed periods was also imposed into the CRM.

imposed lifting. The larger the imposed vertical velocity (9–12 cm s^{-1}), the less the impact of longwave cooling on surface precipitation processes (24 h simulations).

[54] Cloud-radiation interaction is also related to the diurnal variation of precipitation in the tropics. Even though the diurnal variation of precipitation is incompletely understood, it has been quantified by CRM simulations as now shown.

8. DIURNAL VARIATION OF PRECIPITATION

[55] The diurnal cycle of precipitation has been studied using surface rainfall data, radar reflectivity data, and satellite-derived cloudiness and precipitation. Observations indicate a diurnal cycle with a nocturnal–early morning precipitation maximum over tropical oceans and an afternoon-evening maximum over land [e.g., *Kraus*, 1963; *Gray and Jacobson*, 1977; *Randall et al.*, 1991].

[56] Thermodynamic and dynamic mechanisms have been proposed. On one hand, *Kraus* [1963] and *Randall et al.* [1991] suggested that the thermodynamic response of clouds to radiative heating (cloud development is reduced by solar heating and enhanced by IR cooling) is the main mechanism responsible for the diurnal variation of precipitation. On the other hand, *Gray and Jacobson* [1977] indicated that the large-scale dynamic response to the difference in radiative heating between cloudy and clear regions was the main mechanism. *Ramanathan and Collins* [1991] concluded that cooling by cloud activity is more significant than previously estimated and could offset the greenhouse warming induced by human activity.

[57] CRMs have been used to examine the mechanisms associated with the diurnal variation of precipitation processes [*Sui et al.*, 1998]. Figure 13 shows the simulated diurnal variation of surface rainfall from five sensitivity tests. The simulation that did not allow for the diurnal variation of radiative processes (run 3) failed to produce a diurnal variation of rainfall, but the diurnal variation of rainfall was simulated even when the diurnal variation of sea surface temperature was suppressed (run 1). While the diurnal variation of sea surface temperature modulates rainfall processes, it may only play a secondary role in the diurnal variability.

[58] *Sui et al.* [1998] found that the modulation of convection by the diurnal change in available water as a function of temperature was responsible for a maximum in rainfall after midnight. This implies that the increase (decrease) in surface precipitation associated with longwave cooling (solar heating) was due to an increase (decrease) in relative humidity (Figure 14). A similar conclusion had been found by *Tao et al.* [1996]. For more information, see *Sui et al.* [1998, 2008], *Tao et al.* [1996], and *Tao* [2003].

[59] The physical processes affecting the diurnal variation of precipitation can differ among CRMs. *Xu and Randall* [1995] found that nocturnal convection is a direct result of cloud-radiation interactions where solar absorption by

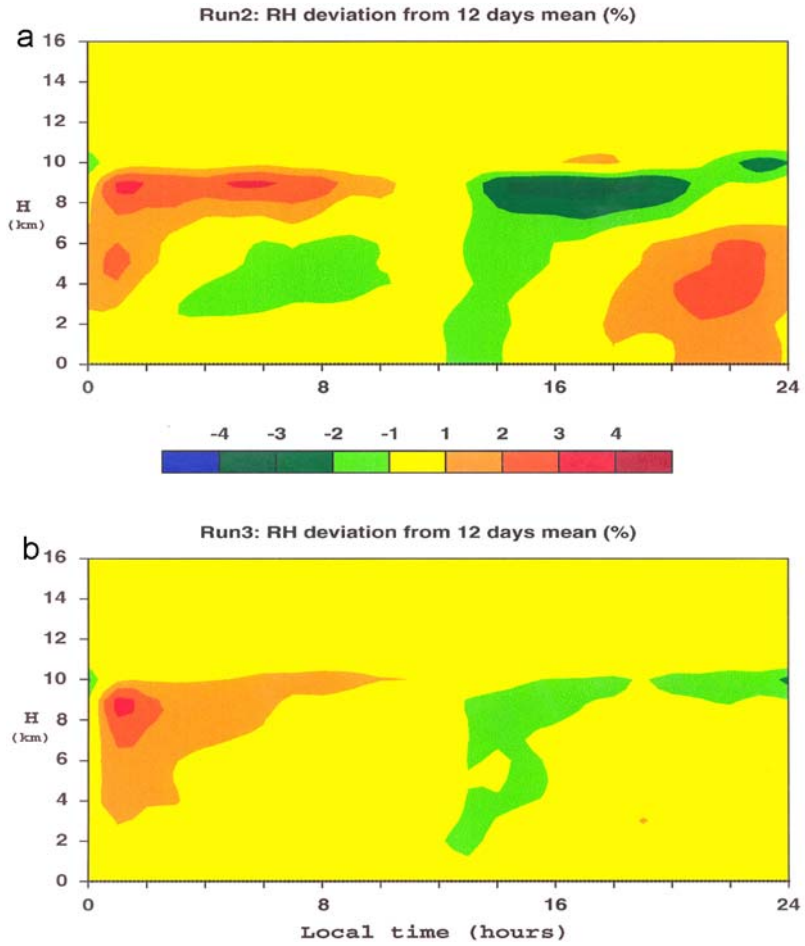

Figure 14. Diurnal composite of horizontal mean relative humidity (%) from the daily mean values obtained from a 12 day simulation. (a) The run that allowed for the diurnal variation of radiative processes and (b) the run did not allow for the diurnal variation of radiative processes. Adapted from *Tao et al.* [2003].

clouds stabilizes the atmosphere. In their CRM study, *Liu and Moncrieff* [1998] showed that the direct interaction of radiation with organized convection determined the diurnal variability of rainfall and that well (less) organized cloud systems can have strong (weak) diurnal variations of rainfall. Some differences can be due to model setup. The model setups of *Sui et al.* [1998] and *Liu and Moncrieff* [1998], for example, were different. In the work by *Liu and Moncrieff* [1998], the horizontal momentum was relaxed to its initial distribution (strong wind shear). On the other hand, the horizontal wind was nudged to time-varying observed values in the work by *Sui et al.* [1998]. Long-lived fast moving squall lines simulated by *Liu and Moncrieff* [1998] occurred throughout the simulation, whereas in the work by *Sui et al.* [1998] the cloud systems had varying sizes and life cycles. A systematic CRM intercomparison as well as high-quality observational data for both initial conditions and model verification are needed.

[60] A systematic relationship exists between solar-heated orography, the diurnal cycle of convective precipitation, and convective organization as identified from satellite measurements [*Laing and Fritsch*, 1997]. In terms of the rainfall distribution, this relationship has been quantified using continental-scale radar networks [*Carbone et al.*, 2002]. CRM investigations by *Moncrieff and Liu* [2006] and *Trier et al.* [2006] showed that downdraft outflows (density currents) from warm-season deep convection over the solar-heated U.S. Continental Divide trigger MCSs. These systems subsequently propagate across the Great Plains and modulate the diurnal cycle of precipitation on the continental scale, in agreement with radar observations. The dynamics of propagating MCSs are described in section 10. The modulation of the diurnal variability of precipitation by MCSs is not at all represented by convective parameterizations in climate models and incompletely represented in global numerical prediction models.

9. SATELLITE APPLICATIONS

[61] The development of sophisticated instruments flown on satellites has expanded enormously in the past 4 decades. Most space-based measurements of atmospheric properties are indirect in the sense that they (e.g., rain rate, moisture distribution, and LH) have to be estimated or retrieved by

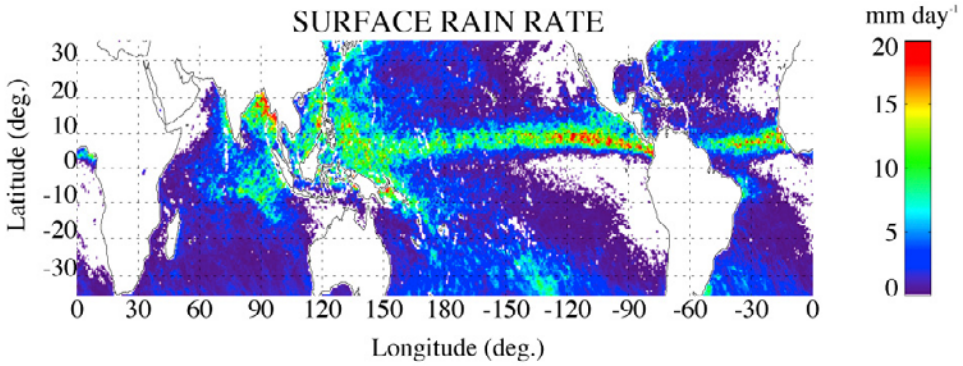

Figure 15. Three month average retrieved surface precipitation rate (June–August 2000) using the Goddard profiling algorithm version 6, which utilized a cloud-resolving model database. The main features correspond to those seen in global climatology [e.g., *Adler et al.*, 2003]. Note the relative minima in convective proportion in the Intertropical Convergence Zone and rainy regions of the western Pacific and Indian Ocean. These relative minima indicate a significant contribution to the total rainfall by organized MCSs as seen in Figure 17 and described by *Rickenbach and Rutledge* [1998] in their analysis of radar observations from the TOGA COARE field campaign. Adapted from *Olson et al.* [2006].

applying complex algorithms. CRMs have played an important part in these retrievals.

[62] Precipitation is highly variable in space and time and incompletely represented by global models. Consequently, LH and its vertical distribution are oversimplified in global models. The Tropical Rainfall Measuring Mission (TRMM), a joint U.S./Japan space agency project, provides unique measurements of rainfall over the global tropics using an inclined low-altitude orbit and a combination of precipitation radar, visible light spectrometer/IR, and microwave radiometers [see *Simpson et al.*, 1988, 1996]. (The TRMM satellite provides fine-resolution views of precipitation systems from the visible/infrared scanner, TRMM Microwave Imager (TMI), and precipitation radar (PR) sensors [*Simpson et al.*, 1996].) A major TRMM objective is to advance knowledge of the global energy and water cycle by providing four-dimensional (4-D) distributions of rainfall and inferred heating over the globe [*Simpson et al.*, 1988]. In order to help meet this objective, CRMs are used to provide 4-D cloud data sets (e.g., frozen and liquid hydrometeor as well as cloud heating structures) as a test bed for satellite remote sensing measurements. Three such applications are presented in sections 9.1–9.3.

9.1. Surface Rain Retrieval

[63] The retrieval of rainfall information from satellite passive microwave observations is linked to the microphysical structure and dynamics of cloud systems. Especially for intense systems, the 4-D relations between surface rainfall, suspended hydrometeors, and the resulting upwelling radiances at various passive microwave frequencies are complex. The problem is compounded because the hydrometeor contents and physical properties of convective systems are difficult to measure continuously over large spatial scales. The vertical structure of the cloud parameters (hydrometeors) drives radiative transfer calculations that determine upwelling radiance at the top of the atmosphere. CRMs can provide synthetic data sets, such as ice-water distributions, for developing surface rainfall retrieval algorithms [*Adler et al.*, 2001; *Smith et al.*, 1992, 1994; *Kummerow et al.*, 1996; *Panegrossi et al.*, 1998; *Olson et al.*, 2006]. Figure 15 illustrates a 3 month average of retrieved surface rainfall.

[64] There are two types of passive microwave rainfall retrievals: the histogram algorithm and the profiling algorithm. The histogram algorithm uses the emission properties of the 10, 19, and 37 GHz channel to obtain monthly rainfall [*Wilheit et al.*, 1991] over ocean areas. The observed emission signal is related to rainfall in each channel via relationships obtained from radiative transfer calculations through modeled rainy atmospheres. Since each microwave frequency has a distinct dynamic range, the algorithms blend the rainfall distributions obtained from each channel into a single distribution, from which rainfall accumulations are inferred. By taking advantage of the known statistical distributions of rainfall rates, this technique compensates for the poor sampling of a polar orbiting radiometer, especially at high rainfall rates.

[65] The profiling algorithm makes use of the fact that weighting functions for various frequencies peak at different levels within a rainy atmosphere in order to determine the vertical structure of hydrometeors. Because the total information to be retrieved far exceeds the number of independent observations, these algorithms use CRMs to provide first-guess profiles [*Simpson et al.*, 1988; *Adler et al.*, 1991; *Smith et al.*, 1992]. For example, a self-consistent iterative technique [*Kummerow et al.*, 1989] has been developed to retrieve hydrometeor distributions from multichannel passive microwave observations. The technique relies on a large set of CRM-simulated distinct cloud structures to simulate the cloud top temperature (T_b). Consistency between observed and simulated values of T_b is then used to select the cloud structure that best fits the rainfall scene in question. For each structure, radiative transfer calculations that account for multiple scattering through the Eddington approximation are used to calculate T_b at different microwave frequencies.

TABLE 9. Summary of the Five LH Algorithms Participating in the First TRMM LH Intercomparison/Validation Project[a]

	TRMM Data Needed	Heating Products	Key References in Algorithm Description	Algorithm Developers
CSH	PR, TMI, PR-TMI	Q_1, LH	*Tao et al.* [1990, 1993b, 2000, 2001]	W.-K. Tao and S. E. Lang
SLH	PR	LH, $Q_1 - Q_R$	*Shige et al.* [2004, 2007]	S. Shige and Y. N. Takayabu
TRAIN	TMI (PR training)	$Q_1 - Q_R$, LH	*Grecu and Olson* [2006] and *Olson et al.* [2006]	M. Grecu and W. Olson
HH	PR-TMI	LH	*Yang and Smith* [1999] and *Yang et al.* [2006]	E. A. Smith and Y. Song
PRH	PR	LH	*Satoh and Noda* [2001]	S. Satoh and A. Noda

[a]See *Tao et al.* [2006] for further details and salient references. Data inputs, retrieved products, and salient references included. The conventional relationship between Q_1 (apparent heating), LH, and Q_R (radiative heating) is expressed by $Q_1 - Q_R$ = LH + EHT, where the final term represents eddy heat transport by clouds (note that vertically integrated EHT is zero; that is, it provides no explicit influence on surface rainfall). LH, latent heating; CSH, convective-stratiform heating; PR, precipitation radar; TMI, TRMM Microwave Imager; SLH, spectral latent heating; TRAIN, trained radiometer algorithm; HH, hydrometeor heating; PRH, precipitation radar heating.

9.2. Latent Heating Retrieval

[66] LH retrievals are calculated for a wide range of surface rainfall rate, surface temperature and emissivity, and vertically integrated cloud water content. A set of linear regression coefficients relating each of these parameters as a function of T_b in each of the microwave channels is determined separately over different rain rate intervals using piecewise linear statistics. Recently, this profile algorithm was improved by using the precipitating profile derived from the TRMM combined radar-radiometer algorithm. Because the observed values of T_b are consistent with those derived from a radiative transfer model embedded in the combined radar-radiometer algorithm, the precipitation-brightness temperature database is considered to be physically consistent.

[67] The TRMM satellite provides measurements of rainfall as well as estimates of the 4-D structure of LH (or diabatic heating) over the global tropics even though it cannot directly measure LH profiles; these must be determined indirectly. The approach is to apply models, ranging in complexity from simple profile shapes to CRMs, to TRMM PR and/or TMI data (see a review by *Tao et al.* [2006]). Five TRMM LH algorithms have been developed, compared, validated, and applied in the past decade, as detailed in Table 9. The convective-stratiform heating (CSH), Goddard profiling, and spectral latent heating algorithms require a full complement of CRM-generated data. A comprehensive intercomparison between the different LH algorithms applied to TRMM data sets emphasized the need to understand the strengths and weaknesses of different methods and their underlying assumptions. Seven separate data sets constitute the intercomparison project: four field experiment cases (South China Sea Monsoon Experiment (SCSMEX), Large Scale Biosphere-Atmosphere Experiment in Amazonia (TRMM-LBA), TRMM Kwajalein Experiment (KWAJEX), and DOE-ARM), two tropical cyclone cases (Atlantic Hurricane Bonnie and Pacific Typhoon Jelewat), and one large-scale regional case. (SCSMEX took place over the South China Sea. TRMM-LBA took place in Rondonia, Brazil. KWAJEX took place around Kwajalein Atoll, Republic of the Marshall Islands. The DOE ARM program supports cloud-radiation experiments in Oklahoma at the SGP Cloud and Radiation Test Bed site.) In the four field experiment cases, a set of quantities involving heating terms diagnostically estimated from sounding networks and retrieved from the satellite algorithms are compared: (1) temporal and horizontal domain-averaged vertical structures of LH, Q_1, and $Q_1 - Q_R$, where Q_1 is the apparent heating and Q_R is the radiative heating; (2) the altitude of maximum heating; (3) vertical convective and stratiform heating structures; (4) the horizontal distribution of LH at different altitudes; and (5) contoured frequency with altitude diagrams [*Yuter and Houze*, 1995] of heating.

[68] Figure 16 illustrates 5 year averaged Q_1 at three different altitudes (2, 5, and 8 km) over the global tropics obtained from the CSH algorithm based upon the PR rainfall product. The horizontal distribution of the estimated Q_1 structure in the middle and upper troposphere mimics the pattern of surface rainfall (i.e., the Intertropical Convergence Zone (ITCZ) in the east and central Pacific and Atlantic oceans, the South Pacific Convergence Zone in the central-southern Pacific Ocean, and broad areas of precipitation events spread over the continental regions). Strong heating in the upper troposphere (5°C d^{-1} and greater) is associated with heavier surface precipitation. Upper tropospheric heating over the Pacific and Indian oceans covers a much broader area than over Africa, South America, and the Atlantic. The differential LH between continents and oceans and within continents and oceans themselves alters the ambient horizontal gradients in the temperature fields that can feed back to the general atmospheric circulation.

[69] An interesting feature in Figure 16 is the relatively weaker heating at the 2 km level (compared to the upper troposphere) throughout the regions of strongest rain rate. There is a more distinct land-sea contrast. Shallow heating occurs almost exclusively over ocean, apart from the maritime continent. The recognized importance of shallow convection in moistening the lower troposphere prior to large-scale organized convective systems is observed.

[70] The LH products provide valuable new data on tropical convection, enabling new insights into convective life cycles, diabatic heating controls and feedbacks of mesosynoptic circulations, and forecasts [e.g., *Schumacher et al.*, 2004]. The distributions of rainfall and inferred heating are used to advance understanding of the global energy and water cycle [*Morita et al.*, 2006]. Presently, three global models, the Florida State University, NASA Goddard Space Flight Center, and NASA Goddard Institute of Space Science, use TRMM LH data sets to improve

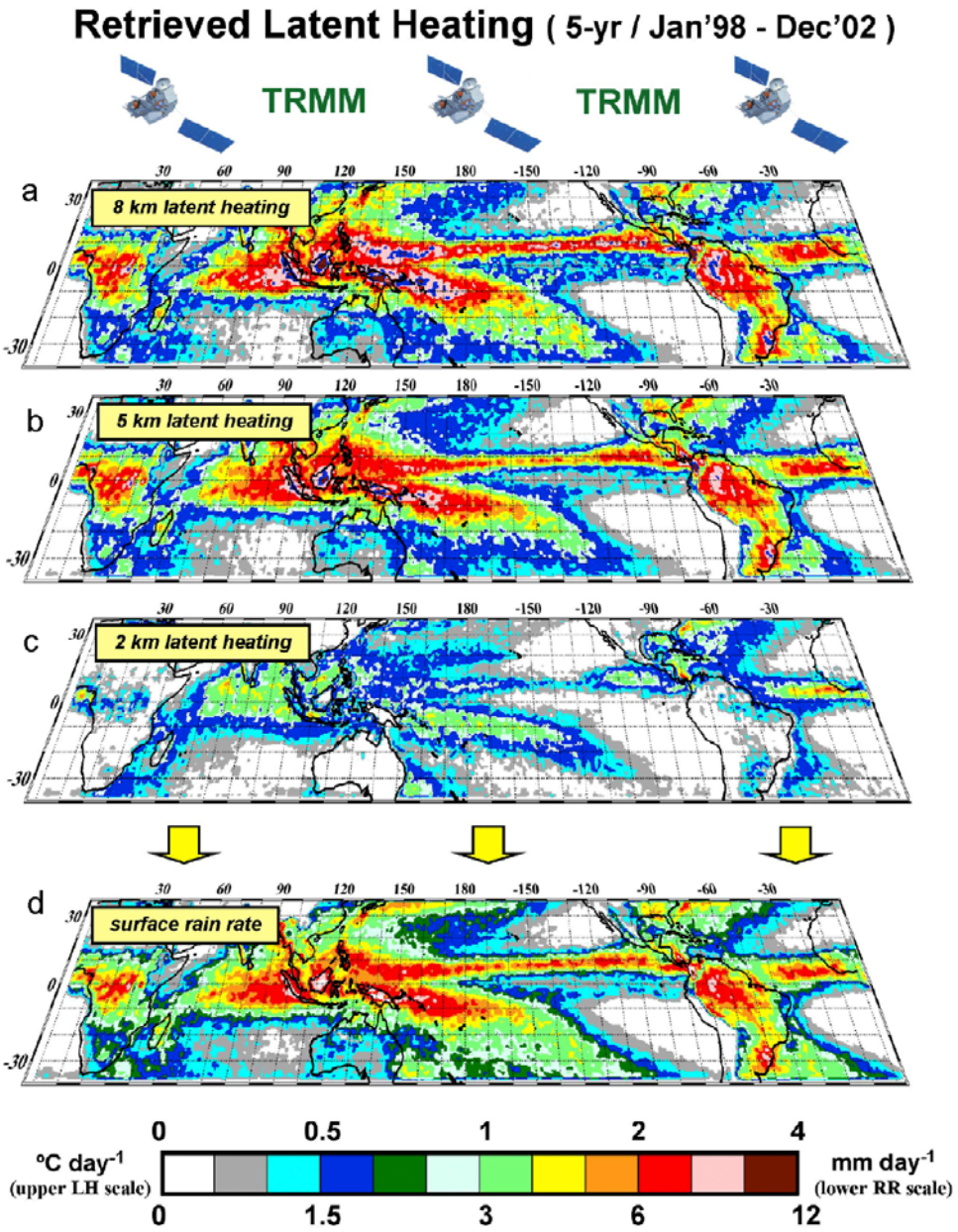

Figure 16. Five year mean Q_1 heating rates at (a) 8, (b) 5, and (c) 2 km above ground level along with (d) surface rain rates over the global tropics obtained from the Goddard Space Flight Center convective-stratiform heating algorithm using 1998–2002 precipitation radar (PR) measurements acquired from the Tropical Rainfall Measuring Mission (TRMM) satellite. Adapted from *Tao et al.* [2006].

cumulus parameterization schemes and address physical shortcomings [e.g., *Rajendran et al.*, 2004; *Chen et al.*, 2007; *Hou and Zhang*, 2007].

9.3. CRMs Coupled to Radar Models

[71] As in the single-wavelength TRMM PR, there are a number of error sources that must be understood before assessing the quality of the information derived from the retrievals [*Iguchi et al.*, 2000]. Because radar signals attenuate, a path attenuation constraint is useful for bounding the errors in the rain rate estimates. Nevertheless, estimates of path attenuation via the surface reference technique are limited in accuracy through the natural variability of the surface scattering properties [*Meneghini et al.*, 2004]. Other factors that affect the accuracy of the retrievals include attenuation effects caused by cloud liquid water and atmospheric gases, uncertainties in the scattering properties of mixed phase hydrometeors, and the effects of surface clutter on near-surface rain rate estimates. Added to these are instrument-related errors such as the variability in the radar return power from a finite number of samples, radar calibration errors, and beam filling effects.

[72] Detailed study of the error sources is possible with a radar simulation program using input data from CRMs. For example, CRM-simulated 4-D synthetic cloud data sets provide insight into the behavior of the snow, rain, and

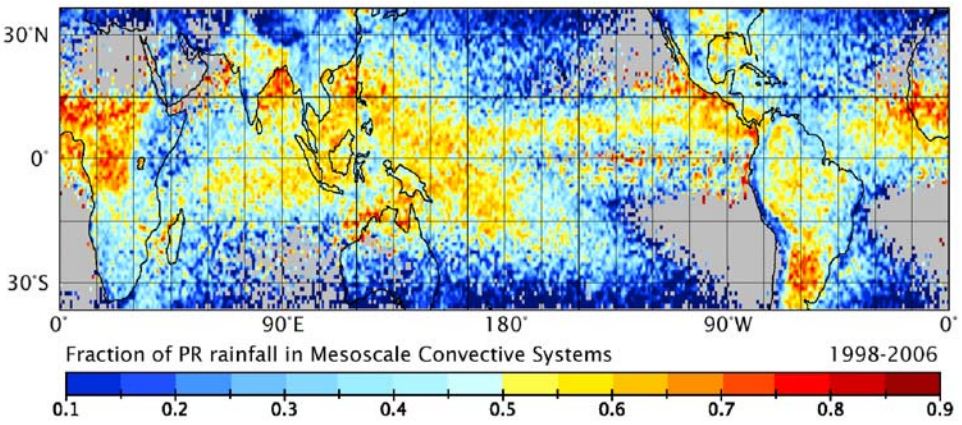

Figure 17. Fraction of estimated rainfall from precipitation features ≥100 km in maximum dimension as measured by the TRMM PR from January 1998 through December 2006. MCSs are shown to be the dominant rainfall producer in most of the heavily raining areas of the tropics and subtropics. Adapted from *Nesbitt et al.* [2006].

surface returns as a function of incidence angle and rain intensity, thereby providing an assessment of the sensitivity and dynamic range of the PR instrument. The results also provide an understanding of the effects of beam filling and attenuation from various atmospheric constituents and their effects on rain rate retrieval accuracy. Apart from the "deterministic" calculations from the storm and surface model, the simulated radar returns were used to test the initial set of PR algorithms. These calculations proved useful in debugging the computer codes, testing the validity of the algorithm assumptions, and comparing the performance of competing algorithms.

[73] Numerical models, and CRMs in particular, are approaching the physical complexity of the natural world, so it is difficult to unambiguously unravel the fundamental mechanisms. Quantification of the basic mechanisms responsible for multiscale convective organization has benefited immensely from theoretical-dynamical modeling, especially when conducted in conjunction with numerical simulation. This constitutes the principal subject of section 10, which is focused on precipitating convection.

10. MULTISCALE ORGANIZATION OF PRECIPITATING CONVECTION

[74] Satellite imagery illustrates that precipitating convection is frequently organized into squall lines, MCSs, convective clusters, and complexes on the mesoscale. Especially in the tropics, precipitating convection is organized into synoptic to large-scale systems on time scales up to seasonal. While organized convective processes are understood from field campaigns, numerical simulations, and dynamical models, convective organization has yet to be successfully represented in parameterizations. The problem is how to take into account important dynamical properties not captured by the oversimplified entraining plume models used in contemporary parameterizations.

10.1. Mesoscale Convective Organization

[75] The statistical significance of organized precipitating convection of the MCS type has been quantified from space based on its correlation with rainfall estimates from TRMM PR and TMI precipitation retrievals. Figure 17 shows MCSs to be the dominant heavy rain producers in the tropics and subtropics, providing more than 50% of the rainfall in most regions. The average annual rainfall from MCSs can exceed 3 mm d^{-1} and contribute up to 90% of the rainfall over certain continental areas (e.g., the La Plata Basin in South America).

[76] Environmental shear has an important organizing effect. Over continents, MCSs are associated with the midlatitude and subtropical jet streams, notably downstream of mountainous regions [e.g., *Laing and Fritsch*, 1997; *Carbone et al.*, 2002]. Over tropical oceans, MCSs are embedded in wave disturbances where the shear is usually larger than the average for the tropics [e.g., *Johnson et al.*, 1999; *Straub and Kiladis*, 2002; *Haertel and Kiladis*, 2004]. The redistribution of horizontal momentum by MCSs affects the large-scale atmospheric circulation. Convective gustiness and evaporative cooling affect the interaction between the atmosphere, land, and ocean. MCSs also transport sensible and latent heat and greenhouse gases (e.g., water vapor and carbon dioxide).

10.2. Mesoscale Dynamics of Convective Organization

[77] MCS-type convective organization has long been observed in the tropics. For example, *Zipser* [1977] conceptualized an MCS in the tropical Pacific in terms of a leading line/trailing stratiform region (Figure 18), in which evaporating precipitation and precipitation loading drove convective and mesoscale downdrafts. The mesoscale updraft and downdraft circulations bypass each other in a 3-D "crossover zone." In the tropical Atlantic, MCSs consist of shallow nonprecipitating cumulus, medium-sized precipitating cumulus, and deep heavily precipitating cumulonimbus

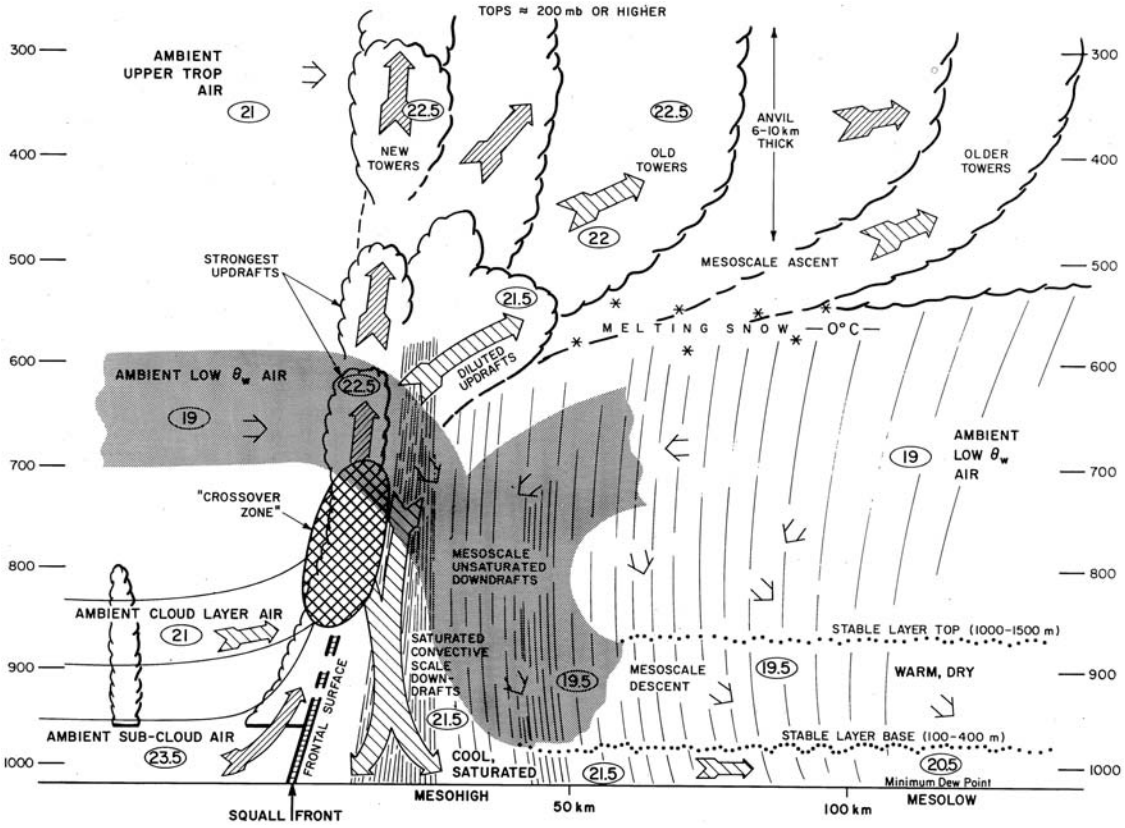

Figure 18. Schematic cross section through a class of MCS. All flow is relative to the convective system, which is moving from right to left. Circled numbers are typical values of potential temperature in °C. The cross section shows that parcels of subcloud boundary layer air rise and form the basic convective updrafts. Ambient cloud layer air is entrained into the updrafts. The updraft parcels rise till they lose their buoyancy by entrainment or by encountering a stable layer in the environment. Entrainment of ambient low equivalent potential temperature air weakens updrafts and forms convective-scale downdrafts, which sink to the surface in the convective precipitation zone. Note that the system has three-dimensionality such that the updraft and downdraft trajectories are not collocated, and the convective region contains a ''crossover zone'' where convective-scale updrafts and downdrafts coexist. Adapted from *Zipser* [1977].

(Figure 19), each featuring a mesoscale updraft and downdraft [*Houze et al.*, 1980]. Please see *Ludlam* [1980], *Cotton and Anthes* [1989], *Houze* [1993], *Smith* [1997], *Houze* [2004], and *Alexander and Cotton* [1998] for more information.

[78] Aided by insights provided by theoretical-dynamical analogs of convective organization, CRMs have played a lead role in quantifying the physics of organized precipitating convection, notably in sheared environments [e.g., *Moncrieff and Miller*, 1976; *Moncrieff*, 1978; *Thorpe et al.*, 1982; *Rotunno et al.*, 1988]. The dynamical coupling between LH, evaporative cooling, and environmental shear is quantified by the 2-D steady model shown in Figure 20 as a propagating, nonlinear system. This system has three tightly coupled branches of airflow: a jump-like updraft, an overturning updraft, and an overturning downdraft [*Moncrieff*, 1981, 1992, 1997; *Thorpe et al.*, 1982]. The backward tilt enables precipitation to fall into the subsaturated environment and drive the downdraft branch through the negative buoyancy due to water loading and evaporative cooling. This type of convective organization is a highly efficient if not the most efficient processor of water, energy, mass, and momentum.

[79] The latent heat released during phase changes of water from vapor to liquid and liquid to ice provides positive buoyancy (CAPE) for the updraft, and the evaporation of precipitation provides negative buoyancy (downdraft CAPE). In regard to convective organization, two additional sources of energy of dynamical origin are important. Strong low-level relative inflow ($\sim$10–20 m s^{-1}) associated with a propagating system supplies kinetic energy (available kinetic energy (AKE) = $1/2(U_0 - c)^2$) that can sustain organized updrafts even if CAPE is zero. The second form of dynamic energy is the energy available from the work done by the cross-system pressure gradient (AWP = $\Delta p/\rho$), which is a hydraulic quantity associated with propagation. These three forms of energy (CAPE, AKE, and AWP) make up two basic scaled quantities that define the general properties of steady propagating systems: the convective Richardson number R = CAPE/AKE

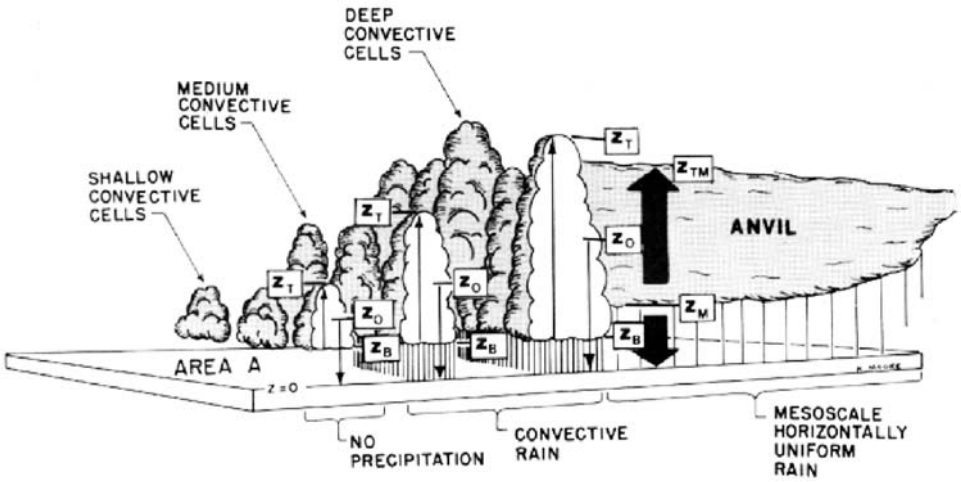

Figure 19. Schematic of a typical population of clouds over a tropical ocean. Thin arrows represent convective-scale updrafts and downdrafts. Wide arrows represent mesoscale updrafts and downdrafts. Z_B and Z_T stand for cloud base and cloud top, respectively; Z_M and Z_{TM} stand for the anvil's cloud base and cloud top, respectively; and Z_o stands for the starting height of the downdrafts. It basically assumes that the cloud population contains convective cells ranging in size from shallow nonprecipitating cells to medium-sized precipitating cells to deep precipitating cells. There is also a convective-scale updraft and a convective-scale downdraft within each convective cell. Furthermore, the system has a widespread anvil cloud, which can deposit large quantities of horizontally uniform rain over a mesoscale region. A mesoscale updraft can occur in the anvil between level Z_M and Z_{TM}. Adapted from *Houze et al.* [1980].

[*Moncrieff and Green*, 1972] and E = AWP/AKE [*Moncrieff and Miller*, 1976].

[80] MCS-type convective organization occurs in specific regions of $\{R, E\}$ space as solutions to the vorticity equation (see Figure 20), which is based on the steady state conservation properties of the Lagrangian equation of motion [*Moncrieff and Green*, 1972] subject to boundary conditions and integral constraints. Solutions of the Moncrieff-Green equation represent distinct regimes of organized 2-D convective overturning [*Moncrieff*, 1981]. Solutions representing MCS-type convective organization occur for small values of R and provide the propagation speed; dynamical structure; and heat, mass, and momentum transports. The Lagrangian formulation enables the transports to be derived directly from the far field without needing the detailed near-field solutions.

[81] The simplest possible (archetypal) model of MCS-type organization is a solution of the far-field Moncrieff-Green equation for $R = 0$ and E in the range $-8/9 \leq E \leq 1$ [*Moncrieff*, 1992]. The archetypal model sketched in Figure 20 (bottom) reveals three regimes. The density current-like regime ($E = -8/9$) is a generalization of the *Benjamin* [1968] density current model that models cold-frontal rainbands that resemble MCS-like dynamics [*Moncrieff and So*, 1989; *Carbone*, 1982; *Moncrieff*, 1989]. The symmetric regime ($E = 0$) is typical of MCSs with respect to a deep mesoscale downdraft and separated upper tropospheric updraft [*Houze et al.*, 1980, Figure 1]. The supercritical hydraulic-jump-like regime ($E = 1$) models tropical squall lines that travel faster than the ambient flow, as in jet-shaped wind profiles [*Betts et al.*, 1976; *Moncrieff and Miller*, 1976].

[82] The backward tilted morphology results in a distinctive convective momentum transport (CMT). The sign of the CMT is opposite of the direction of propagation, and its amplitude attains a maximum value near the midtroposphere (e.g., the eastward propagating system (positive propagation) in Figure 20 generates a westward momentum (negative) flux). The mean flow acceleration is positive/negative in the lower/upper troposphere. The 3-D counterpart of the above 2-D archetypal model featuring the 3-D "crossover zone" of *Zipser* [1977] replaces the 2-D jump updraft by an overturning circulation in the plane transverse to the direction of travel.

[83] The shear dependence of steady state convective organization is upheld by the mature systems in time-dependent CRM simulations and has been verified against field measurements [*LeMone and Moncrieff*, 1994] and 2-D simulations [*Wu and Moncrieff*, 1996]. Three-dimensional simulations further confirm that convective organization depends on CAPE and shear (i.e., R for meteorologically realistic conditions of a field campaign). The snapshots in Figure 21 from the *Grabowski et al.* [1998] simulation of convective organization in tropical easterly waves show three convective regimes: nonsquall cloud cluster, squall cluster, and scattered convection. The squall cluster occurred in moderate CAPE and strong shear (i.e., smallest values of R).

10.3. Large-Scale Convective Organization in the Tropics

[84] The large-scale organization of tropical convection involves interactions between precipitating convection, tropical waves, and the mean state. Inertial gravity waves with low vertical wave number (bore waves), which trans-

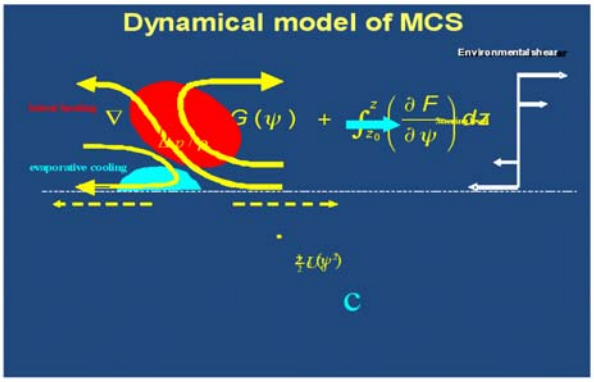

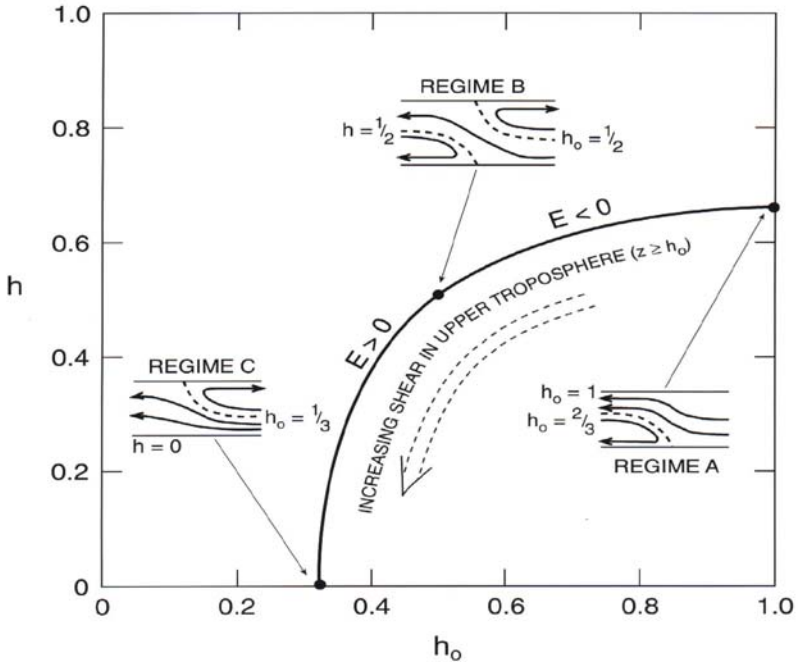

Figure 20. (top) The relative flow for a three-branch steady dynamical model of MCS-type convective organization propagating left to right at speed c. The stream function ψ indicates trajectories in steady flow and is defined by $u = \partial\psi/\partial z$, $w = -\partial\psi/\partial x$; the Laplacian $\nabla^2\psi$ is the vorticity measured along trajectories; $G(\psi)$ is the inflow (environmental) shear; $F(\psi)$ is the buoyancy; and $z_0(\psi)$ is the inflow height of trajectories. (bottom) Specific regimes of organization: propagating (regime A, $E = -8/9$), symmetric (regime B, $E = 0$), and hydraulic jump-like (regime C, $E = 1$). Adapted from *Moncrieff* [1992].

mit the effects of convective heating to the far environment [*Nicholls et al.*, 1991], are essential to cloud cluster formation [e.g., *Mapes*, 1993; *Lane and Reeder*, 2001; *Liu and Moncrieff*, 2004; *Tulich et al.*, 2007]. The first baroclinic vertical mode plays an important role in that it stabilizes the near environment by subsidence that necessarily compensates the vertical mass flux by deep convection. Its influence is limited by the fast phase speed of the first baroclinic mode ($\sim$50 m s^{-1}). The lower tropospheric lifting associated with the second baroclinic mode, which propagates more slowly ($\sim$20 m s^{-1}), destabilizes the near environment. The diminished convective inhibition generates successive generations of convective clusters in the near environment. The inertial effect of the Earth's rotation confines the effects of convectively generated gravity waves within the Rossby radius of deformation so that the largest cloud clusters occur in equatorial regions [*Liu and Moncrieff*, 2004].

[85] The important backward tilted MCS-like systems occur spontaneously in global CRMs. In the work by *Grabowski and Moncrieff* [2001, hereinafter referred to as GM01], backward tilted systems were the preferred mode of convective organization that evolved out of initially motionless, thermodynamically uniform initial conditions. Westward propagating MCSs embedded in large-scale eastward propagating cloud envelopes (Figure 22) redistribute horizontal momentum and generate vertical shear: a positive feedback between shear and convective organization suggested by the above dynamical models. The simulated large-scale cloud envelopes resemble observed eastward propagating convectively coupled Kelvin waves.

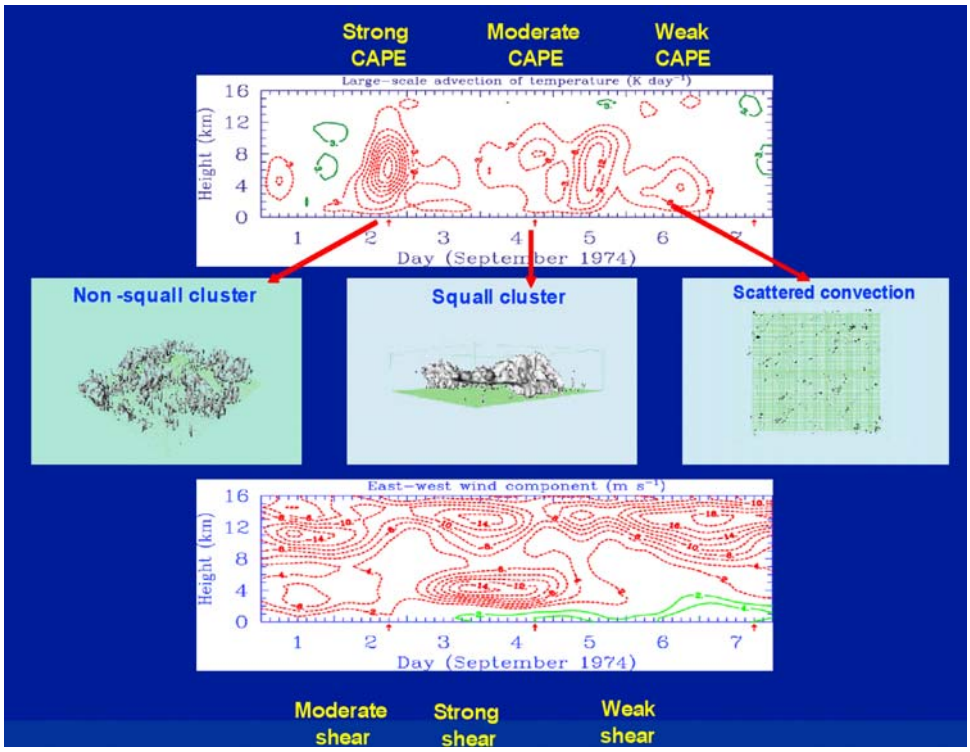

Figure 21. Three regimes of organized precipitating convection simulated by a CRM: (1) nonsquall cluster for strong convective available potential energy (CAPE) and moderate shear, (2) squall cluster for moderate CAPE and strong shear, and (3) scattered convection for weak CAPE and weak shear. The squall cluster has the characteristic backward titled morphology associated with an MCS. Adapted from *Grabowski et al.* [1998].

[86] The MJO is a most remarkable hierarchy of multiscale convective organization consisting of cumulonimbus (∼1–10 km, hour), mesoconvective organization (∼100–500 km, day), synoptic superclusters (∼1000–2000 km, week), and a large-scale cloud envelope (∼10,000 km). Many of the difficulties that global models experience with MJOs are attributed to deficiencies in convective parameterization [e.g., *J.-L. Lin et al.*, 2006; *Moncrieff et al.*, 2007]. Convective organization involving convectively coupled equatorial waves resembles the MJO [*Straub and*

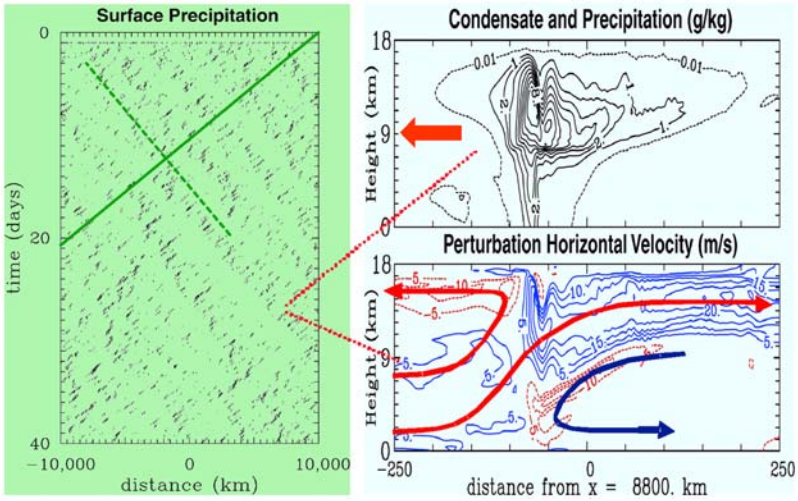

Figure 22. Multiscale convective organization in a 2-D CRM with a 20,000 km domain: westward propagating precipitating systems embedded in eastward propagating cloud cluster envelopes. The vertical section shows the three-branch MCS-type airflow organization typical of the westward moving system. The multiscale organization develops from a randomly perturbed horizontally homogenous motionless state. Adapted from *Grabowski and Moncrieff* [2001].

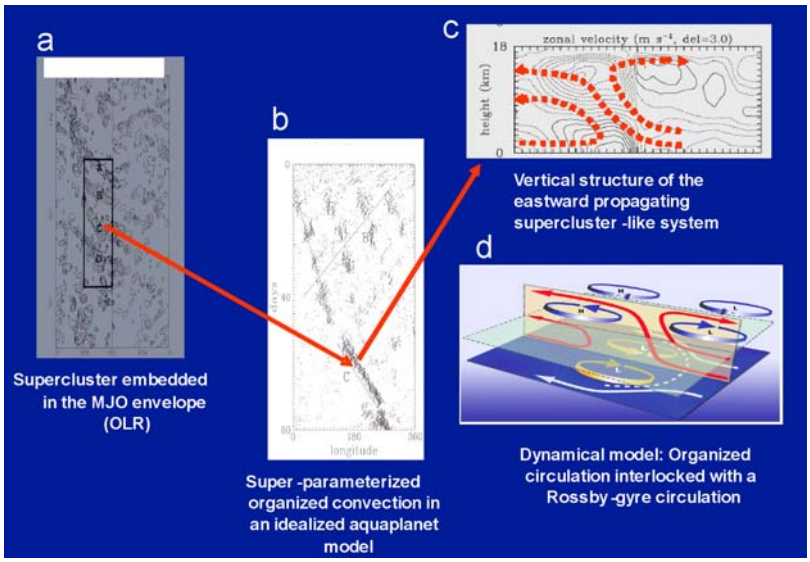

Figure 23. Multiscale convective organization in a Madden-Julian Oscillation (MJO). (a) Eastward propagating superclusters embedded in the MJO envelope [*Nakazawa*, 1988], (b) idealized numerical realization of an MJO-like system in a superparameterization aquaplanet model (during the first 50 days, wave number 4 convective organization occurs followed by a wave number 1 MJO-type convective organization (adapted from *Grabowski* [2001]), (c) cross section of the vertical structure of the MJO-like system, and (d) dynamical model of the MJO-like system representing a scale-invariant vertically titled system interlocked with a Rossby gyre circulation. Adapted from *Moncrieff* [2004].

Kiladis, 2002; *Kiladis et al.*, 2009]. One such example of this large-scale convective organization is the solitary propagating envelope that evolves late in the GM01 simulation. MJO-like systems also occur in simulations that utilize superparameterization (see section 11.1). In the work by *Grabowski* [2001], an MJO-like system evolved spontaneously out of an initially horizontally homogeneous motionless state excited by random perturbations (Figure 23). Paralleling the above analytic models of mesoscale organization, the following analogs of large-scale convective organization provide insight into the physical mechanisms associated with large-scale convective organization.

10.4. Dynamical Models of Large-Scale Convective Organization

[87] *Moncrieff* [2004] derived a scale-invariant equivalence between multiscale convective organization in the vertical plane and Rossby gyres in the horizontal plane. This equivalence explained the momentum transport and accompanying atmospheric superrotation associated with the MJO-like systems simulated by *Grabowski* [2001] summarized in Figure 23. The superrotation mechanism was further quantified by *Biello et al.* [2007]. The multiscale models of *Yano et al.* [1995] and *Khouider and Majda* [2007] are characterized by a passive boundary layer; a dynamically active troposphere; and simple parameterizations of convection, radiation, boundary layer, and surface exchange. These models generate large-scale convective coherence resembling observed and numerically simulated multiscale organization (i.e., eastward traveling convective envelopes and embedded westward traveling synoptic-scale/mesoscale disturbances). *Khouider and Majda* [2007] showed that models containing the second baroclinic wave mode produce more realistic large-scale coherence than those utilizing only the first baroclinic mode.

[88] In section 1, it was alluded to that there are now CRMs with global computational domains available for research and explicit organization occurring in operational global NWP models. Section 11 describes these aspects in more detail.

11. CONCLUDING DISCUSSION

[89] Until about a decade ago, precipitating convection in global models had to be represented by parameterizations. Nowadays, explicit convective organization in multiscale CRMs provides insight into the requirements for future prediction systems. Global NWP systems, climate models, and especially future Earth system models will require convective parameterizations. The application of CRMs to a range of important problems in atmospheric science has been described. The computational domains of modern CRMs are now becoming global and are beginning to quantify the global effects of precipitating convective systems and mesoscale organization. Progress has been made in microphysics and precipitation, clouds and radiation, surface exchange and the planetary boundary layer, and dynamics ranging from the mesoscale to the large scale. The physical interpretation of the mechanisms involved has been assisted by dynamical models.

[90] While global CRMs are the latest development in the context of research, it is too early to comment on their future application to operational prediction. The multiscale

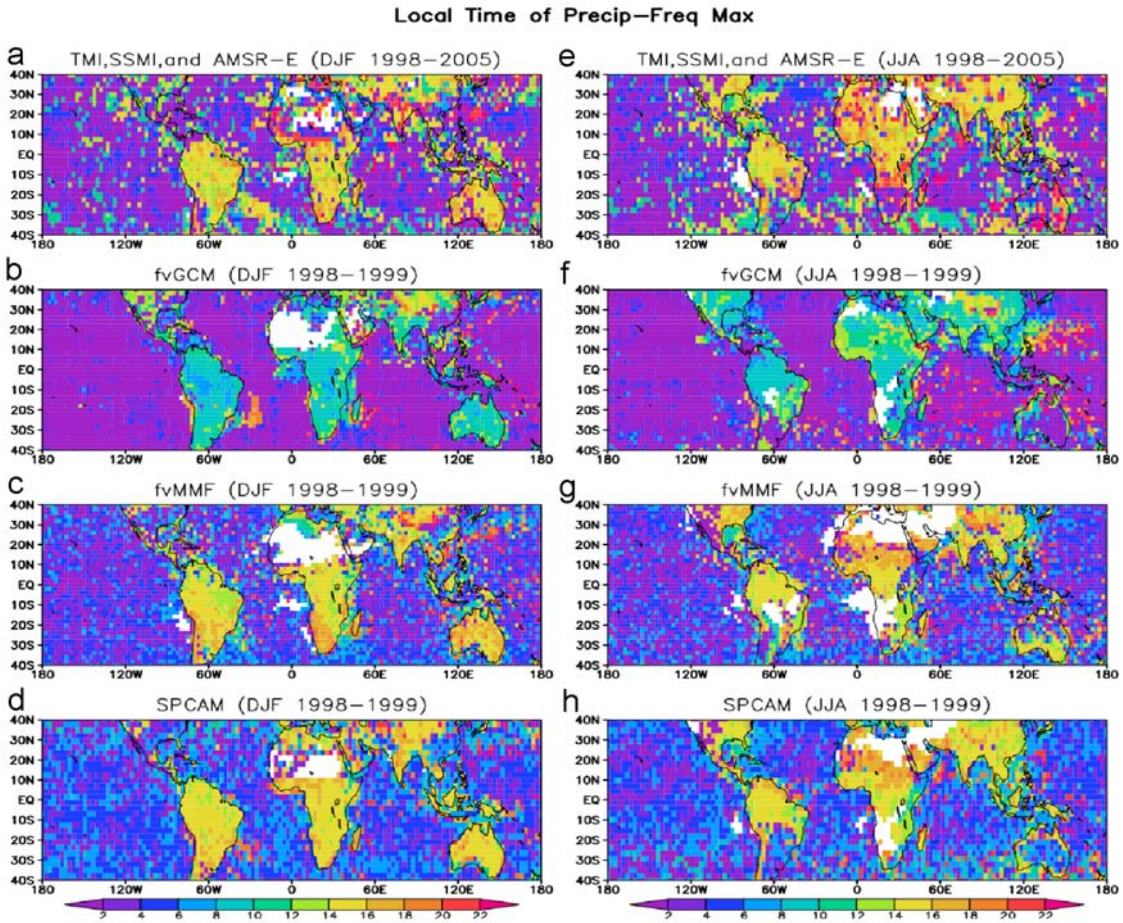

Figure 24. Geographical distribution of the local solar time (LST) for the nondrizzle precipitation frequency maximum in (a–d) winter and (e–h) summer as observed by satellite from 1998 to 2005 (Figures 25a and 25e) and as simulated for 2 years (1998–1999) with the Goddard fvGCM (Figures 25b and 25f), Goddard multiscale modeling framework (MMF) (Figures 25c and 25g), and Colorado State University MMF (Figures 25d and 25h). Blank regions indicate no precipitation. The MMF results are based on detailed 2-D GCE model-simulated hourly rainfall output. Satellite retrieved rainfall is based on a five-satellite constellation including the TRMM Microwave Imager (TMI); the Special Sensor Microwave Imager (SSMI) from the Defense Meteorological Satellite Program F13, F14, and F15; and the Advanced Microwave Scanning Radiometer–Earth Observing System (AMSR-E) on board the Aqua satellite. The MMF-simulated diurnal variation of precipitation shows good agreement with merged microwave observations. For example, the MMF-simulated frequency maximum was in the late afternoon (1400–1800 LST) over land and in the early morning (0500–0700 LST) over the oceans. The fvGCM-simulated frequency maximum was too early for both oceans and land. Adapted from *Tao et al.* [2009].

modeling of cloud systems and its application to the seamless prediction of weather and climate will be a key research element of atmospheric science for a long time to come.

11.1. Multiscale Modeling Framework

[91] The multiscale modeling framework (MMF) bridges the gap between current CRM simulations and nonhydrostatic global cloud system resolving models. The MMF approach is based on superparameterization, which sidesteps traditional convective parameterization by placing a CRM in each grid column of a GCM. The GCM provides global coverage, while the CRM permits more realistic representations of deep convection, cloud overlap, cloud-radiation interaction, and surface fluxes. There is two-way interaction between the CRMs and the parent GCM [*Grabowski and Smolarkiewicz*, 1999; *Grabowski*, 2001, 2004; *Khairoutdinov and Randall*, 2001; *Randall et al.*, 2003b; *Khairoutdinov et al.*, 2005]. Figure 24 shows the geographical distribution of the local solar time of the nondrizzle precipitation frequency maximum in winter and summer for 1998 as simulated by a GCM and two different MMFs based at NASA Goddard and Colorado State University [*Tao et al.*, 2009]. Both MMFs are superior to the standard GCM in regard to the late afternoon and early evening precipitation maximum over land and the early morning precipitation maximum over the oceans. The GCM

produces a dominant morning maximum in rain frequency over continents.

11.2. Interactive Nesting

[92] CRMs have been run extensively with externally specified large-scale advective temperature and water vapor forcing obtained from either sounding networks deployed during field experiments or large-scale models (e.g., GCSS). This one-way interaction cannot address important feedbacks (e.g., the interaction between clouds, radiation, and dynamics with large-scale motion) since the lateral boundary conditions for the CRM are specified from the large-scale model. Interactively nested CRMs (i.e., two-way interaction [see *Clark and Farley*, 1984]) have been used to simulate turbulent mixing in small-scale cumulus [*Grabowski and Clark*, 1991], gravity waves generated by shallow convection [*Clark et al.*, 1986], fields of convection containing mesoscale organization [*Redelsperger and Clark*, 1990], tropical squall lines, and the evolution of the stratiform region [*Lafore and Moncrieff*, 1989; *Alexander and Cotton*, 1998]. Nested regional community models (i.e., the fifth-generation National Center for Atmospheric Research/Penn State University Mesoscale Model (MM5) and the Weather Research and Forecasting Model (WRF)) operate data assimilation of comparable complexity for operational weather prediction. The approach is now being applied in nested regional climate models, although the nesting is usually only one way.

[93] A variant on the nesting approach is the application of superparameterization on a regional scale in a global model, where the CRMs have a higher resolution than in a global superparameterization. *Ziemiański et al.* [2005] applied the regional approach using the Community Atmospheric Model (CAM). The superparameterization applied over the western Pacific warm pool consisted of zonally oriented 2-D CRMs. Compared to the standard CAM, the regional climate was improved in a variety of ways: (1) shallow, midlevel, and deep convection gave more realistic profiles of clouds and water vapor and reduced the midtropospheric dry bias/cold upper troposphere; (2) the ITCZ was improved; (3) the phase and amplitude of the diurnal cycle of precipitation were in agreement with TRMM measurements; and (4) propagating MCSs embedded in superclusters and Rossby gyres were simulated in agreement with the multiscale organization numerically simulated by *Grabowski* [2001] and analytically approximated by *Moncrieff* [2004].

11.3. Tropical Channel Models

[94] Tropical channel models are bounded in the meridional direction and global in the zonal direction. These models can be run at higher resolution than global CRMs for the same amount of computing. Channel models simulate large-scale tropical convection and quantify the role of extratropical excitation [*Ray et al.*, 2009]. Tropical channel models can have interactively nested inner domains.

11.4. Global CRMs

[95] A global nonhydrostatic model with an icosahedral grid configuration has been developed [*Satoh et al.*, 2008] for high-resolution climate simulations incorporating the cloud system resolving approach (i.e., microphysics, radiation, and boundary layer processes). (MMFs can be used to identify the optimal grid size and physical processes (i.e., microphysics and cloud-radiation interaction) needed for future nonhydrostatic global CRMs.) Global CRMs generate large-scale convective organization. For example, an aquaplanet model with grid spacing of 7 or finer (3.5) km can simulate large-scale tropical convective organization [*Tomita et al.*, 2005, *Miura et al.*, 2005; *Nasuno et al.*, 2008]. It is important that these models be analyzed fully to determine the fidelity of the large-scale convective organization, understand any sensitivity to model configuration, and quantify why some global models applying convective parameterization generate more realistic MJOs than others [*Sperber et al.*, 2008].

11.5. Improving and Evaluating Multiscale Models

[96] A few of the many improvements needed to advance multiscale models and to evaluate them are now summarized.

11.5.1. Microphysics Parameterization for CRMs

[97] *Cotton* [2003] discussed the limitations of the microphysical parameterizations applied in CRMs that must be resolved in the coming years: predicting ice particle concentrations and their effect on ice processes, capturing the initial broadening of cloud droplet spectra in warm clouds, detailing hydrometeor spectra evolution, and quantitatively simulating entrainment rates. During the past decade, research and operational NWP models (i.e., MM5, the National Centers for Environmental Prediction Eta, and WRF) have begun using complex microphysical schemes originally developed for CRMs. A report to the U.S. Weather Research Program Science Steering Committee calls for the replacement of cumulus parameterization schemes with explicit bulk microphysical schemes in NWP as part of a community effort to improve quantitative precipitation forecasts [*Fritsch and Carbone*, 2002]. The role CRMs play in the design of algorithms for the retrieval of precipitation and LH from satellite measurements (among other product applications) must not only continue but be extended.

11.5.2. Turbulence Parameterization for CRMs

[98] Improved SGS parameterizations of moist turbulence are essential because CRMs at $\sim$1 km grid spacing do not resolve small-scale cumulus and fine-scale mixing with the environment. This is where the CRM and LES approaches are beginning to converge. For example, M. Khairoutdinov et al. (Large-eddy simulation of maritime deep tropical convection, submitted to *Journal of Advances in Modeling Earth Systems*, 2009) recently completed an LES-type 1 day simulation of tropical deep convection using 100 m horizontal and 50–100 m vertical grid spacing over a 200 km $\times$ 200 km horizontal domain (see Figure 25) using the System for Atmospheric Modeling CRM [*Khairoutdinov and Randall*, 2001]. The time and horizontally averaged statistics converge for horizontal grid spacing smaller than 400 m. The simulated trimodal vertical cloud distribution with the pro-

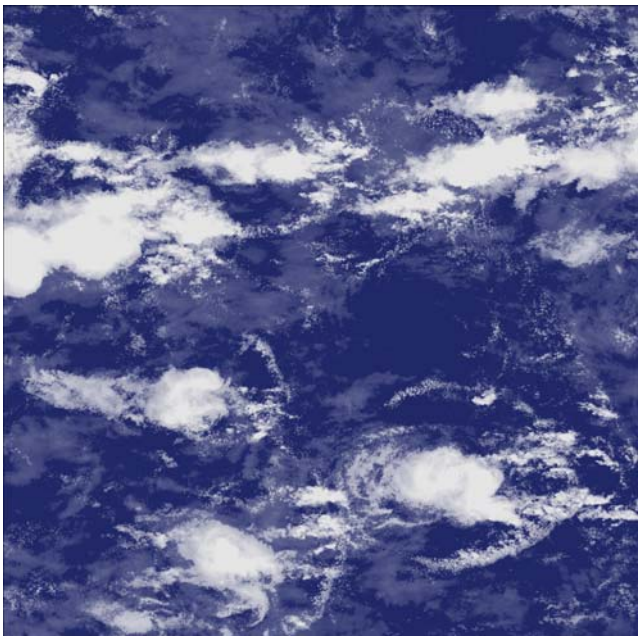

Figure 25. Simulated satellite view of a cloud field from a large-eddy simulation of tropical convection over the ocean with 100 m horizontal grid spacing. The horizontal domain size is about 200 km. From Khairoutdinov et al. (submitted manuscript, 2009).

nounced cumulus congestus maximum observed by *Johnson et al.* [1999] requires high vertical grid spacing of 100 m in the vicinity of the freezing level. It was also shown that downdraft outflows or density currents (see section 10) were important for initiating new cumulus activity. The analysis of simulations of this type is valuable for the evaluation of CRMs with ~1 km grid spacing and for improving the parameterization of moist turbulence in these CRMs.

11.5.3. Cloud-Scale Data Assimilation

[99] Advances in cloud-scale data assimilation for NWP are required in view of the increasingly higher resolution of modern operational prediction systems as summarized in sections 3 and 10 and reviewed by *Sun* [2005].

11.5.4. Parameterizing Moist Convection and Convective Organization for Global Models

[100] While the explicit approach to moist convection and its multiscale organization in global models provides valuable insights, it is an inescapable fact that parameterizations will be required for the foreseeable future, especially for Earth system models and probabilistic models (ensemble models). It follows that much improved convective parameterizations are required. However, the parameterization of convective organization faces a formidable challenge. In sections 9 and 10, it was shown that CRMs simulate organized convection because they can reproduce the salient physics (e.g., LH, evaporative cooling, and cold pools) and, above all, the organized dynamics and convection wave interactions. These salient dynamics cannot be represented by the plume models used for cumulus parameterizations (Figure 26). Efforts to parameterize convective organization are few [*Alexander and Cotton*, 1998; *Moncrieff and Liu*, 2006; *Kuell et al.*, 2007].

[101] The representation of convective organization in global models is at an interesting juncture. Within a few years, global NWP models will have a grid spacing of 10 km, followed in about a decade by climate models. The potential for hybrid parameterization (i.e., cumulus parameterization and explicit grid-scale circulations) at this resolution is interesting. While grid-scale circulations are a primitive convective organization, they are, nevertheless, superior to cumulus parameterization. *Moncrieff and Klinker* [1997] showed that grid-scale circulations in the European Center for Medium-Range Weather Forecasts T213 (grid spacing of about 80 km) represent tropical superclusters within an MJO. The hybrid approach needs to be evaluated in regard to its potential for global operational prediction at 10 km grid spacing.

11.5.5. Stochastic Parameterization

[102] Atmospheric convection is a "fast" process with limited predictability compared to the "slow" evolution of the large-scale state. *Shutts and Palmer* [2007] used CRM simulations to evaluate the extent to which deterministic

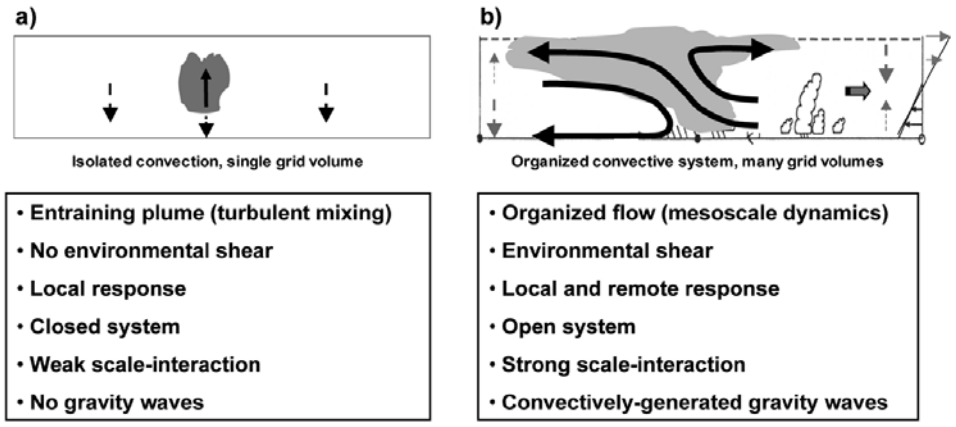

Figure 26. Distinction between (a) ordinary convection and (b) organized convection in terms of morphology, physical, and dynamic processes and interaction with the large-scale environment. Adapted from *Moncrieff and Liu* [2006].

convective parameterizations fail to capture statistical fluctuations and to provide probability distribution functions for stochastic parameterizations. The potential of stochastic parameterization requires further investigation, including the basis of its statistical mechanics [*Craig et al.*, 2005].

11.5.6. Integrated Data Sets for Model Evaluation

[103] CRMs simulate cloud processes at the space and time scales of natural cloud dynamical processes. CRM cloud statistics, including radiance and radar reflectivity/attenuation, need to be evaluated against observational measurements. Not only should such evaluations continue, but they should be extended to a wider range of environments. The TRMM precipitation database is useful in this respect. Earth-observing satellite missions provide global measurements of clouds, radiation, precipitation, aerosols, land characteristics, and other data at fine spatial and temporal scales. Satellite measurement simulators facilitate the evaluation of models against observations as well as the consistency of the microphysical parameterizations [e.g., *Chevallier and Bauer*, 2003]. Dating back to 1983, the International Satellite Cloud Climatology Project provides global cloud characterization at 3 h intervals [*Rossow and Duenas*, 2004].

[104] The large computational domains of tropical channel models, superparameterized models, and regional to global CRMs present new challenges for model evaluation. Integrated data sets involving satellite, in situ, and field campaign data are the ultimate requirement. To address the integrated data issue, the World Climate Research Programme and the World Weather Research Programme are jointly coordinating an observing, modeling, and forecasting project: the Year of Tropical Convection (YOTC). The scientific emphasis for the YOTC project is organized tropical convection and its global interactions. The focus is on time scales up to seasonal in order to advance seamless prediction across the intersection of weather and climate where there occurs a gradual transition from the deterministic approach to the probabilistic approach [*Moncrieff et al.*, 2007; *Waliser and Moncrieff*, 2007, 2008; http://www.wmo.int/pages/prog/arep/wwrp/new/documents/YOTC_Science_Plan.pdf].

[105] **ACKNOWLEDGMENTS.** W.-K. Tao appreciates the inspiring and enthusiastic support by his mentor, Joanne Simpson, over the past 25 years and is grateful to R. Kakar at NASA headquarters for his continuous support of Goddard Cumulus Ensemble model development and applications. This work is mainly supported by the NASA Headquarters Physical Climate Program and the NASA TRMM. He also thanks D. Anderson for support under the NASA Cloud Modeling and Analysis Initiative program and S. Lang for reading and editing the manuscript. The National Center for Atmospheric Research is sponsored by the National Science Foundation. We also thank W. Cotton and two anonymous reviewers for their constructive comments that improved this paper significantly. We also acknowledge Center for Multiscale Modeling of Atmospheric Processes scientists for discussions on future applications of CRMs.

[106] The Editor responsible for this paper was Gerald North. He thanks technical reviewers William Cotton and Robert Houze and one additional anonymous reviewer.

REFERENCES

Ackerman, A. S., O. B. Toon, D. E. Stevens, A. J. Heymsfield, V. Ramanathan, and E. J. Welton (2000), Reduction of tropical cloudiness by soot, *Science*, *288*, 1042–1047, doi:10.1126/science.288.5468.1042.

Adler, R. F., H.-Y. Yeh, N. Prasad, W.-K. Tao, and J. Simpson (1991), Microwave rainfall simulations of a tropical convective system with a three-dimensional cloud model, *J. Appl. Meteorol.*, *30*, 924–953.

Adler, R. F., C. Kidd, G. Petty, M. Morissey, and H. M. Goodman (2001), Intercomparison of global precipitation products: The third precipitation intercomparison project (PIP–3), *Bull. Am. Meteorol. Soc.*, *82*, 1377–1396, doi:10.1175/1520-0477(2001)082<1377:IOGPPT>2.3.CO;2.

Adler, R. F., et al. (2003), The Version-2 Global Precipitation Climatology Project (GPCP) monthly precipitation analysis (1979–present), *J. Hydrometeorol.*, *4*, 1147–1167, doi:10.1175/1525-7541(2003)004<1147:TVGPCP>2.0.CO;2.

Aksoy, A., D. Dowell, and C. Snyder (2009), A multi-case comparative assessment of the ensemble Kalman filter for assimilation of radar observations. Part I: Storm-scale analyses, *Mon. Weather Rev.*, *137*, 1805–1824, doi:10.1175/2008MWR2691.1.

Albrecht, B. A. (1989), Aerosols, cloud microphysics and fractional cloudiness, *Science*, *245*, 1227–1230, doi:10.1126/science.245.4923.1227.

Alexander, G. D., and W. R. Cotton (1998), The use of cloud-resolving simulations of mesoscale convective systems to build a mesoscale parameterization scheme, *J. Atmos. Sci.*, *55*, 2137–2161, doi:10.1175/1520-0469(1998)055<2137:TUOCRS>2.0.CO;2.

Alonge, C. J., K. I. Mohr, and W.-K. Tao (2007), Numerical case studies of wet versus dry regimes in the West African Sahel, *J. Hydrometeorol.*, *8*, 102–116, doi:10.1175/JHM559.1.

Andreae, M. O., D. Rosenfeld, P. Artaxo, A. A. Costa, G. P. Frank, K. M. Longo, and M. A. F. Silva-Dias (2004), Smoking rain clouds over the Amazon, *Science*, *303*, 1337–1342, doi:10.1126/science.1092779.

Baker, R. D., B. H. Lynn, A. Boone, W.-K. Tao, and J. Simpson (2001), The influence of soil moisture, coastline curvature, and the land-breeze circulation on sea-breeze initiated precipitation, *J. Hydrometeorol.*, *2*, 193–211, doi:10.1175/1525-7541(2001)002<0193:TIOSMC>2.0.CO;2.

Beheng, K. D. (1994), A parameterization of warm cloud microphysics conversion processes, *Atmos. Res.*, *33*, 193–206, doi:10.1016/0169-8095(94)90020-5.

Bell, T. L., D. Rosenfeld, K.-M. Kim, J.-M. Yoo, M.-I. Lee, and M. Hahnenberger (2008), Midweek increase in U.S. Summer rain and storm heights suggests air pollution invigorates rainstorms, *J. Geophys. Res.*, *113*, D02209, doi:10.1029/2007JD008623.

Benjamin, T. B. (1968), Gravity currents and related phenomena, *J. Fluid Mech.*, *31*, 209–248, doi:10.1017/S0022112068000133.

Berry, E. X. (1967), Cloud droplet growth by coalescence, *J. Atmos. Sci.*, *24*, 688–701, doi:10.1175/1520-0469(1967)024<0688:CDGBC>2.0.CO;2.

Berry, E. X., and R. J. Reinhardt (1974), An analysis of cloud drop growth by collection. Part I: Double distributions, *J. Atmos. Sci.*, *31*, 1814–1824, doi:10.1175/1520-0469(1974)031<1814:AAOCDG>2.0.CO;2.

Betts, A. K., R. W. Grover, and M. W. Moncrieff (1976), Structure and motion of tropical squall-lines over Venezuela, *Q. J. R. Meteorol. Soc.*, *102*, 395–404, doi:10.1002/qj.49710243209.

Biello, J., A. J. Majda, and M. W. Moncrieff (2007), Meridional momentum flux and super-rotation in the multiscale IPESD MJO model, *J. Atmos. Sci.*, *64*, 1636–1651, doi:10.1175/JAS3908.1.

Biggerstaff, M. I., and R. A. Houze Jr. (1993), Kinematics and microphysics of the transition zone of the 10–11 June 1985 squall line, *J. Atmos. Sci.*, *50*, 3091–3110, doi:10.1175/1520-0469(1993)050<3091:KAMOTT>2.0.CO;2.

Bleck, R. (1970), A fast approximative method for integrating the stochastic coalescence equation, *J. Geophys. Res.*, *75*, 5165–5171, doi:10.1029/JC075i027p05165.

Bott, A., U. Sievers, and W. Zdunkowski (1990), A radiation fog model with detailed treatment of the interaction between radiative transfer and fog microphysics, *J. Atmos. Sci.*, *47*, 2153–2166, doi:10.1175/1520-0469(1990)047<2153:ARFMWA>2.0.CO;2.

Bradley, E. F., P. A. Coppin, and J. S. Godfrey (1991), Measurements of sensible and latent heat flux in the western tropical Pacific Ocean, *J. Geophys. Res.*, *96*, 3375–3389, doi:10.1029/90JC01933.

Browning, K. A., et al. (1993), The GEWEX Cloud System Study (GCSS), *Bull. Am. Meteorol. Soc.*, *74*, 387–400, doi:10.1175/1520-0477(1993)074<0387:TGCSS>2.0.CO;2.

Bryan, G. H., J. C. Wyngaard, and J. M. Fritsch (2003), Resolution requirements for simulation of deep moist convection, *Mon. Weather Rev.*, *131*, 2394–2416, doi:10.1175/1520-0493(2003)131<2394:RRFTSO>2.0.CO;2.

Carbone, R. E. (1982), A severe winter squall line: Stormwide hydrodynamic structure, *J. Atmos. Sci.*, *39*, 258–279, doi:10.1175/1520-0469(1982)039<0258:ASFRPI>2.0.CO;2.

Carbone, R. E., J. D. Tuttle, D. Ahijevych, and S. B. Trier (2002), Inferences of predictability associated with warm season precipitation episodes, *J. Atmos. Sci.*, *59*, 2033–2056, doi:10.1175/1520-0469(2002)059<2033:IOPAWW>2.0.CO;2.

Carrió, G. G., S. C. van den Heever, and W. R. Cotton (2007), Impacts of nucleating aerosol on anvil-cirrus clouds: A modeling study, *Atmos. Res.*, *84*, 111–131, doi:10.1016/j.atmosres.2006.06.002.

Chen, C.-S. (1991), A numerical study of a squall line over the Taiwan Strait during TAMEX IOP 2, *Mon. Weather Rev.*, *119*, 2677–2698, doi:10.1175/1520-0493(1991)119<2677:ANSOAS>2.0.CO;2.

Chen, J.-P., and D. Lamb (1994), Simulation of cloud microphysical and chemical processes using a multicomponent framework. Part I: Description of the microphysical model, *J. Atmos. Sci.*, *51*, 2613–2630, doi:10.1175/1520-0469(1994)051<2613:SOCMAC>2.0.CO;2.

Chen, S., and W. R. Cotton (1988), The sensitivity of a simulated extra-tropical mesoscale convective system to long-wave radiation and ice-phase microphysics, *J. Atmos. Sci.*, *45*, 3897–3910, doi:10.1175/1520-0469(1988)045<3897:TSOASE>2.0.CO;2.

Chen, Y., A. D. del Genio, and J. Chen (2007), The tropical atmospheric El Niño signal in satellite precipitation data and a global climate model, *J. Clim.*, *20*, 3580–3601, doi:10.1175/JCLI4208.1.

Cheng, A., and K.-M. Xu (2006), Simulation of shallow cumuli and their transition to deep convective clouds by cloud-resolving models with different third-order turbulence closures, *Q. J. R. Meteorol. Soc.*, *132*, 359–382, doi:10.1256/qj.05.29.

Cheng, A., K.-M. Xu, and J.-C. Golaz (2004), The liquid water oscillation in modeling boundary layer cumuli with third-order turbulence closure models, *J. Atmos. Sci.*, *61*, 1621–1629, doi:10.1175/1520-0469(2004)061<1621:TLWOIM>2.0.CO;2.

Cheng, C.-T., W.-C. Wang, and J.-P. Chen (2007), A modeling study of aerosol impacts on cloud microphysics and radiative properties, *Q. J. R. Meteorol. Soc.*, *133*, 283–297, doi:10.1002/qj.25.

Cheng, W. Y. Y., T. Wu, and W. R. Cotton (2001), Large-eddy simulations of the 26 November 1991 FIRE II cirrus case, *J. Atmos. Sci.*, *58*, 1017–1034, doi:10.1175/1520-0469(2001)058<1017:LESOTN>2.0.CO;2.

Chevallier, F., and P. Bauer (2003), Model rain and clouds over oceans: Comparison with SSM/I observations, *Mon. Weather Rev.*, *131*, 1240–1255, doi:10.1175/1520-0493(2003)131<1240:MRACOO>2.0.CO;2.

Chin, H.-N. S. (1994), The impact of the ice phase and radiation on a mid-latitude squall line system, *J. Atmos. Sci.*, *51*, 3320–3343, doi:10.1175/1520-0469(1994)051<3320:TIOTIP>2.0.CO;2.

Chin, H.-N. S., Q. Fu, M. M. Bradley, and C. R. Molenkamp (1995), Modeling of a tropical squall line in two dimensions and its sensitivity to environmental winds and radiation, *J. Atmos. Sci.*, *52*, 3172–3193, doi:10.1175/1520-0469(1995)052<3172:MOATSL>2.0.CO;2.

Churchill, D. D., and R. A. Houze Jr. (1991), Effects of radiation and turbulence on the diabatic heating and water budget of the stratiform region of a tropical cloud cluster, *J. Atmos. Sci.*, *48*, 903–922, doi:10.1175/1520-0469(1991)048<0903:EORATO>2.0.CO;2.

Clark, T. L. (1973), Numerical modeling of the dynamics and microphysics of warm cumulus convection, *J. Atmos. Sci.*, *30*, 857–878, doi:10.1175/1520-0469(1973)030<0857:NMOTDA2.0.CO;2.

Clark, T. L. (1974), On modeling nucleation and condensation theory in Eulerian spatial domain, *J. Atmos. Sci.*, *31*, 2099–2117, doi:10.1175/1520-0469(1974)031<2099:OMNACT>2.0.CO;2.

Clark, T. L. (1976), Use of log-normal distributions for numerical calculations of condensation and collection, *J. Atmos. Sci.*, *33*, 810–821, doi:10.1175/1520-0469(1976)033<0810:UOLNDF>2.0.CO;2.

Clark, T. L. (1979), Numerical simulations with a three-dimensional cloud model: Lateral boundary condition experiments and multicellular severe storm simulations, *J. Atmos. Sci.*, *36*, 2191–2215, doi:10.1175/1520-0469(1979)036<2191:NSWATD>2.0.CO;2.

Clark, T. L., and R. D. Farley (1984), Severe downslope windstorm calculations in two and three spatial dimensions using anelastic interactive grid nesting: A possible mechanism for gustiness, *J. Atmos. Sci.*, *41*, 329–350, doi:10.1175/1520-0469(1984)041<0329:SDWCIT>2.0.CO;2.

Clark, T. L., and W. D. Hall (1983), A cloud physical parameterization method using movable basis functions: Stochastic coalescence parcel calculations, *J. Atmos. Sci.*, *40*, 1709–1728, doi:10.1175/1520-0469(1983)040<1709:ACPPMU>2.0.CO;2.

Clark, T. L., T. Hauf, and J. P. Kuettner (1986), Convectively forced internal gravity waves: Results from two-dimensional numerical experiments, *Q. J. R. Meteorol. Soc.*, *112*, 899–925, doi:10.1002/qj.49711247402.

Cotton, W. R. (2003), Cloud modeling from days of EML to the present—Have we made progress?, in *Symposium on Cloud Systems, Hurricanes and TRMM*, *Meteorol. Monogr.*, *29*(51), 95–106.

Cotton, W. R., and R. A. Anthes (1989), *Storm and Cloud Dynamics*, 881 pp., Academic, San Diego, Calif.

Cotton, W. R., and G. J. Tripoli (1978), Cumulus convection in shear flow - three-dimensional numerical experiments, *J. Atmos. Sci.*, *35*, 1503–1521, doi:10.1175/1520-0469(1978)035<1503:CCISFD>2.0.CO;2.

Cotton, W. R., M. A. Stephens, T. Nehrkorn, and G. J. Tripoli (1982), The Colorado State University three-dimensional cloud-mesoscale model-1982. Part II: An ice-phase parameterization, *J. Rech. Atmos.*, *16*, 295–320.

Cotton, W. R., G. J. Tripoli, R. M. Rauber, and E. A. Mulville (1986), Numerical simulation of the effects of varying ice crystal nucleation rates and aggregation processes on orographic snowfall, *J. Clim. Appl. Meteorol.*, *25*, 1658–1680, doi:10.1175/1520-0450(1986)025<1658:NSOTEO>2.0.CO;2.

Cotton, W. R., G. D. Alexander, R. Hertenstein, R. L. Walko, R. L. McAnelly, and M. Nicholls (1995), Cloud venting—A review and some new global annual estimates, *Earth Sci. Rev.*, *39*, 169–206, doi:10.1016/0012-8252(95)00007-0.

Cotton, W. R., et al. (2003), RAMS 2001: Current status and future directions, *Meteorol. Atmos. Phys.*, *82*, 5–29, doi:10.1007/s00703-001-0584-9.

Cox, S. K., and K. T. Griffith (1979), Estimates of radiative divergence during Phase III of the GARP Atlantic Tropical Experiment: Part II. Analysis of Phase III results, *J. Atmos. Sci.*, *36*, 586–601, doi:10.1175/1520-0469(1979)036<0586:EORDDP>2.0.CO;2.

Craig, G. C., B. G. Cohen, and R. S. Plant (2005), Statistical mechanics and stochastic convective parameterization, paper presented at the Workshop on Representation of Sub-Grid Processes Using Stochastic-Dynamic Models, Eur. Cent. for Med.-Range Weather Forecasts, Reading, U. K., 6–8 June.

Cunning, J. B. (1986), The Oklahoma-Kansas Preliminary Regional Experiment for STORM-Central, *Bull. Am. Meteorol. Soc.*, *67*, 1478–1486, doi:10.1175/1520-0477(1986)067<1478:TOKPRE>2.0.CO;2.

Dharssi, I., R. Kershaw, and W.-K. Tao (1997), Sensitivity of a simulated tropical squall line to longwave radiation, *Q. J. R. Meteorol. Soc.*, *123*, 187–206, doi:10.1002/qj.49712353708.

Dowell, D., F. Zhang, L. Wicker, C. Snyder, and N. A. Crook (2004), Wind and thermodynamic retrievals in the 17 May 1981 Arcadia, Oklahoma supercell: Ensemble Kalman filter experiments, *Mon. Weather Rev.*, *132*, 1982–2005, doi:10.1175/1520-0493(2004)132<1982:WATRIT>2.0.CO;2.

Dudhia, J. (1989), Numerical study of convection observed during the Winter Monsoon Experiment using a mesoscale two-dimensional model, *J. Atmos. Sci.*, *46*, 3077–3107, doi:10.1175/1520-0469(1989)046<3077:NSOCOD>2.0.CO;2.

Emanuel, K. A. (1994), *Atmospheric Convection*, 580 pp., Oxford Univ. Press, New York.

Facchini, M. C., M. Mircea, S. Fuzzi, and R. J. Charlson (1999), Cloud albedo enhancement by surface-active organic solutes in growing droplets, *Nature*, *401*, 257–259, doi:10.1038/45758.

Fairall, C., E. F. Bradley, D. P. Rogers, J. B. Edson, and G. S. Young (1996), Bulk parameterization of air-sea fluxes for TOGA COARE, *J. Geophys. Res.*, *101*, 3747–3764, doi:10.1029/95JC03205.

Feingold, C., and P. Y. Chuang (2002), Analysis of the influence of film-forming compounds on droplet growth: Implications for cloud microphysical processes and climate, *J. Atmos. Sci.*, *59*, 2006–2018, doi:10.1175/1520-0469(2002)059<2006:AOTIOF>2.0.CO;2.

Feingold, G., and S. M. Kreidenweis (2000), Does heterogeneous processing of aerosol increase the number of cloud droplets?, *J. Geophys. Res.*, *105*, 24,351–24,361, doi:10.1029/2000JD900369.

Feingold, G., B. Stevens, W. R. Cotton, and A. S. Frisch (1996), The relationship between drop in-cloud residence time and drizzle production in numerically simulated stratocumulus clouds, *J. Atmos. Sci.*, *53*, 1108–1122, doi:10.1175/1520-0469(1996)053<1108:TRBDIC>2.0.CO;2.

Feingold, G., R. L. Walko, B. Stevens, and W. R. Cotton (1998), Simulations of marine stratocumulus using a new microphysical parameterization scheme, *Atmos. Res.*, *47–48*, 505–528, doi:10.1016/S0169-8095(98)00058-1.

Ferrier, B. S. (1994), A double-moment multiple-phase four-class bulk ice scheme. Part I: Description, *J. Atmos. Sci.*, *51*, 249–280, doi:10.1175/1520-0469(1994)051<0249:ADMMPF>2.0.CO;2.

Ferrier, B. S., W.-K. Tao, and J. Simpson (1995), A double-moment multiple-phase four-class bulk ice scheme. Part II: Simulations of convective storms in different large-scale environments and comparisons with other bulk parameterizations, *J. Atmos. Sci.*, *52*, 1001–1033, doi:10.1175/1520-0469(1995)052<1001:ADMMPF>2.0.CO;2.

Fitzgerald, J. W. (1974), Effect of aerosol composition on cloud droplet size distribution: A numerical study, *J. Atmos. Sci.*, *31*, 1358–1367, doi:10.1175/1520-0469(1974)031<1358:EOACOC>2.0.CO;2.

Flossmann, A. I., W. D. Hall, and H. R. Pruppacher (1985), A theoretical study of the wet removal of atmospheric pollutants. Part I: The redistribution of aerosol particles captured through nucleation and impaction scavenging by cloud droplets, *J. Atmos. Sci.*, *42*, 583–606, doi:10.1175/1520-0469(1985)042<0583:ATSOTW>2.0.CO;2.

Fovell, R. G., and Y. Ogura (1988), Numerical simulation of a midlatitude squall line in two dimensions, *J. Atmos. Sci.*, *45*, 3846–3879, doi:10.1175/1520-0469(1988)045<3846:NSOAMS>2.0.CO;2.

Fritsch, J. M., and R. E. Carbone (2002), Research and development to improve quantitative precipitation forecasts in the warm season: A synopsis of the March 2002 USWRP Workshop and statement of priority recommendations, technical report, 134 pp., Sci. Steer. Comm., U.S. Weather Res. Program, Boulder, Colo.

Fu, Q., S. K. Krueger, and K. N. Liou (1995), Interactions of radiation and convection in simulated tropical cloud clusters, *J. Atmos. Sci.*, *52*, 1310–1328, doi:10.1175/1520-0469(1995)052<1310:IORACI>2.0.CO;2.

Gao, S., and X. Li (2008), *Cloud-Resolving Modeling of Convective Processes*, 206 pp., Springer, Dordrecht, Netherlands.

Golaz, J.-C., H. Jiang, and W. R. Cotton (2001), A large-eddy simulation study of cumulus clouds over land and sensitivity to soil moisture, *Atmos. Res.*, *59–60*, 373–392, doi:10.1016/S0169-8095(01)00113-2.

Grabowski, W. W. (2001), Coupling cloud processes with the large-scale dynamics using the Cloud-resolving Convection parameterization (CRCP), *J. Atmos. Sci.*, *58*, 978–997, doi:10.1175/1520-0469(2001)058<0978:CCPWTL>2.0.CO;2.

Grabowski, W. W. (2004), An improved framework for superparameterization, *J. Atmos. Sci.*, *61*, 1940–1952, doi:10.1175/1520-0469(2004)061<1940:AIFFS>2.0.CO;2.

Grabowski, W. W., and T. L. Clark (1991), Cloud–environment interface instability: Rising thermal calculations in two spatial dimensions, *J. Atmos. Sci.*, *48*, 527–546, doi:10.1175/1520-0469(1991)048<0527:CIIRTC>2.0.CO;2.

Grabowski, W. W., and M. W. Moncrieff (2001), Large-scale organization of tropical convection in two-dimensional explicit numerical simulations, *Q. J. R. Meteorol. Soc.*, *127*, 445–468, doi:10.1002/qj.49712757211.

Grabowski, W. W., and M. W. Moncrieff (2002), Large-scale organization of tropical convection in two-dimensional explicit numerical simulations: Effects of interactive radiation, *Q. J. R. Meteorol. Soc.*, *128*, 2349–2375, doi:10.1256/qj.01.104.

Grabowski, W. W., and P. K. Smolarkiewicz (1999), CRCP: A cloud resolving convection parameterization for modeling the tropical convective atmosphere, *Physica*, *133*, 171–178.

Grabowski, W. W., X. Wu, M. W. Moncrieff, and W. D. Hall (1998), Cloud-resolving modeling of cloud systems during Phase III of GATE. Part II: Effects of resolution and the third spatial dimension, *J. Atmos. Sci.*, *55*, 3264–3282, doi:10.1175/1520-0469(1998)055<3264:CRMOCS>2.0.CO;2.

Gray, W. M., and R. W. Jacobson Jr. (1977), Diurnal variation of deep cumulus convection, *Mon. Weather Rev.*, *105*, 1171–1188, doi:10.1175/1520-0493(1977)105<1171:DVODCC>2.0.CO;2.

Grecu, M., and W. S. Olson (2006), Bayesian estimation of precipitation from satellite passive microwave observations using combined radar–radiometer retrievals, *J. Appl. Meteorol. Climatol.*, *45*, 416–433, doi:10.1175/JAM2360.1.

Haertel, P. T., and G. N. Kiladis (2004), Dynamics of 2-day equatorial waves, *J. Atmos. Sci.*, *61*, 2707–2721, doi:10.1175/JAS3352.1.

Hansen, M. C., R. S. DeFries, J. R. G. Townshend, and R. Sohlberg (2000), Global land cover classification at 1km spatial resolution using a classification tree approach, *Int. J. Remote Sens.*, *21*, 1331–1364, doi:10.1080/014311600210209.

Hartmann, D. L., H. H. Hendon, and R. A. Houze Jr. (1984), Some implications of mesoscale circulations in tropical cloud clusters for large-scale dynamics and climate, *J. Atmos. Sci.*, *41*, 113–121, doi:10.1175/1520-0469(1984)041<0113:SIOTMC>2.0.CO;2.

Hartmann, D. L., L. A. Moy, and Q. Fu (2001), Tropical convection and the energy balance at the top if the atmosphere, *J. Clim.*, *14*, 4495–4511, doi:10.1175/1520-0442(2001)014<4495:TCATEB>2.0.CO;2.

Held, I. M., R. S. Hemler, and V. Ramaswamy (1993), Radiative-convective equilibrium with explicit two-dimensional moist convection, *J. Atmos. Sci.*, *50*, 3909–3927, doi:10.1175/1520-0469(1993)050<3909:RCEWET>2.0.CO;2.

Hoskins, B. J., and D. J. Karoly (1981), The steady linear response of a spherical atmosphere to thermal and orographic forcing, *J. Atmos. Sci.*, *38*, 1179–1196, doi:10.1175/1520-0469(1981)038<1179:TSLROA>2.0.CO;2.

Hou, A. Y., and S. Q. Zhang (2007), Assimilation of precipitation information using column model physics as a weak constraint, *J. Atmos. Sci.*, *64*, 3865–3878, doi:10.1175/2006JAS2028.1.

Hounslow, M. J., R. L. Ryall, and V. R. Marshall (1988), A discretized population balance for nucleation growth and aggregation, *AIChE J.*, *34*, 1821–1832, doi:10.1002/aic.690341108.

Houze, R. A., Jr. (1977), Structure and dynamics of a tropical squall-line system, *Mon. Weather Rev.*, *105*, 1540–1567, doi:10.1175/1520-0493(1977)105<1540:SADOAT>2.0.CO;2.

Houze, R. A., Jr. (1982), Cloud clusters and large-scale vertical motions in the tropics, *J. Meteorol. Soc. Jpn.*, *60*, 396–409.

Houze, R. A., Jr. (1989), Observed structure of mesoscale convective systems and implications for large-scale heating, *Q. J. R. Meteorol. Soc.*, *115*, 425–461, doi:10.1002/qj.49711548702.

Houze, R. A., Jr. (1993), *Cloud Dynamics*, 573 pp., Academic, San Diego, Calif.

Houze, R. A., Jr. (2004), Mesoscale convective systems, *Rev. Geophys.*, *42*, RG4003, doi:10.1029/2004RG000150.

Houze, R. A., Jr., C.-C. Cheng, C. A. Leary, and J. F. Gamache (1980), Diagnosis of cloud mass and heat fluxes from radar and synoptic data, *J. Atmos. Sci.*, *37*, 754–773.

Hu, M., and M. Xue (2007), Impact of configurations of rapid intermittent assimilation of WSR-88D radar data for the 8 May 2003 Oklahoma City tornadic thunderstorm case, *Mon. Weather Rev.*, *135*, 507–525, doi:10.1175/MWR3313.1.

Iguchi, T., T. Kozu, R. Meneghini, J. Awaka, and K. Okamoto (2000), Rain profiling algorithm for the TRMM precipitation radar, *J. Appl. Meteorol.*, *39*, 2038–2052, doi:10.1175/1520-0450(2001)040<2038:RPAFTT>2.0.CO;2.

Ikawa, M. (1988), Comparison of some schemes for nonhydrostatic models with orography, *J. Meteorol. Soc. Jpn.*, *66*, 753–776.

Ikawa, M., H. Mizuno, T. Matsuo, M. Murakami, Y. Yamada, and K. Sait (1991), Numerical modeling of the convective snow cloud over the Sea of Japan, *J. Meteorol. Soc. Jpn.*, *69*, 641–667.

Johnson, D. E., W.-K. Tao, J. Simpson, and C.-H. Sui (2002), A study of the response of deep tropical clouds to large-scale thermodynamic forcing. Part I: Modeling strategies and simulations of TOGA COARE convective systems, *J. Atmos. Sci.*, *59*, 3492–3518, doi:10.1175/1520-0469(2002)059<3492:ASOTRO>2.0.CO;2.

Johnson, R. H., T. M. Rickenbach, S. A. Rutledge, P. E. Ciesielski, and W. H. Schubert (1999), Trimodal characteristics of tropical convection, *J. Clim.*, *12*, 2397–2418, doi:10.1175/1520-0442(1999)012<2397:TCOTC>2.0.CO;2.

Jorgensen, D. P., M. A. LeMone, and S. B. Trier (1997), Structure and evolution of the 22 February 1993 TOGA COARE squall line: Aircraft observations of precipitation, circulation, and surface fluxes, *J. Atmos. Sci.*, *54*, 1961–1985, doi:10.1175/1520-0469(1997)054<1961:SAEOTF>2.0.CO;2.

Juang, H. M., W.-K. Tao, X. Zeng, C.-L. Shie, and J. Simpson (2007), Parallelization of a cloud-resolving model for massively parallel computing by using message passing interface, *Terr. Atmos. Oceanic Sci.*, *18*, 593–622.

Kerkweg, A., S. Wurzler, T. Reisin, and A. Bott (2003), On the cloud processing of aerosol particles: A entraining air-parcel model with two dimensional spectral cloud microphysics and a new formation of the collection kernel, *Q. J. R. Meteorol. Soc.*, *129*, 1–18, doi:10.1256/qj.02.52.

Kessler, E., III (1969), *On the Distribution and Continuity of Water Substance in Atmospheric Circulation*, *Meteorol. Monogr.*, *32*, 84 pp.

Khain, A., M. Ovtchinnikov, M. Pinsky, A. Pokrovsky, and H. Krugliak (2000), Notes on the state-of-the-art numerical modeling of cloud microphysics, *Atmos. Res.*, *55*, 159–224, doi:10.1016/S0169-8095(00)00064-8.

Khain, A., A. Pokrovsky, M. Pinsky, A. Seigert, and V. Phillips (2004), Simulation of effects of atmospheric aerosols on deep turbulent convective clouds using a spectral microphysics mixed-phase cumulus cloud model. Part I: Model description and possible applications, *J. Atmos. Sci.*, *61*, 2983–3001, doi:10.1175/JAS-3281.1.

Khain, A., D. Rosenfeld, and A. Pokrovsky (2005), Aerosol impact on the dynamics and microphysics of deep convective clouds, *Q. J. R. Meteorol. Soc.*, *131*, 2639–2663, doi:10.1256/qj.04.62.

Khain, A. P., N. BenMoshe, and A. Pokrovsky (2008), Factors determining the impact of aerosols on surface precipitation from clouds: An attempt at classification, *J. Atmos. Sci.*, *65*, 1721–1748, doi:10.1175/2007JAS2515.1.

Khairoutdinov, M. F., and D. A. Randall (2001), A cloud resolving model as a cloud parameterization in the NCAR community climate system model: Preliminary results, *Geophys. Res. Lett.*, *28*, 3617–3620, doi:10.1029/2001GL013552.

Khairoutdinov, M. F., and D. A. Randall (2006), High-resolution simulation of shallow-to-deep convection transition over land, *J. Atmos. Sci.*, *63*, 3421–3436, doi:10.1175/JAS3810.1.

Khairoutdinov, M., D. A. Randall, and C. DeMott (2005), Simulations of the atmospheric general circulation using a cloud-resolving model as a superparameterization of physical processes, *J. Atmos. Sci.*, *62*, 2136–2154, doi:10.1175/JAS3453.1.

Khouider, B., and A. J. Majda (2007), A simple multicloud parameterization for convectively coupled tropical waves. Part II: Nonlinear simulations, *J. Atmos. Sci.*, *64*, 381–400, doi:10.1175/JAS3833.1.

Kiladis, G. N., M. C. Wheeler, P. T. Haertel, K. H. Straub, and P. E. Roundy (2009), Convectively coupled equatorial waves, *Rev. Geophys.*, *47*, RG2003, doi:10.1029/2008RG000266.

Klemp, J. B., and R. Wilhelmson (1978a), The simulation of three-dimensional convective storm dynamics, *J. Atmos. Sci.*, *35*, 1070–1096, doi:10.1175/1520-0469(1978)035<1070:TSOTDC>2.0.CO;2.

Klemp, J. B., and R. Wilhelmson (1978b), Simulations of right and left moving storms through storm splitting, *J. Atmos. Sci.*, *35*, 1097–1110, doi:10.1175/1520-0469(1978)035<1097:SORALM>2.0.CO;2.

Koren, I., Y. J. Kaufman, D. Rosenfeld, L. A. Remer, and Y. Rudich (2005), Aerosol invigoration and restructuring of Atlantic convective clouds, *Geophys. Res. Lett.*, *32*, L14828, doi:10.1029/2005GL023187.

Kraus, E. B. (1963), The diurnal precipitation change over the sea, *J. Atmos. Sci.*, *20*, 551–556, doi:10.1175/1520-0469(1963)020<0551:TDPCOT>2.0.CO;2.

Krueger, S. K. (1988), Numerical simulation of tropical cumulus clouds and their interaction with the subcloud layer, *J. Atmos. Sci.*, *45*, 2221–2250, doi:10.1175/1520-0469(1988)045<2221:NSOTCC>2.0.CO;2.

Kubar, T. L., D. L. Hartmann, and R. Wood (2007), Radiative and convective driving of tropical high clouds, *J. Clim.*, *20*, 5510–5526, doi:10.1175/2007JCLI1628.1.

Kuell, V., A. Gassmann, and A. Bott (2007), Towards a new hybrid cumulus parametrization scheme for use in non-hydrostatic weather prediction models, *Q. J. R. Meteorol. Soc.*, *133*, 479–490, doi:10.1002/qj.28.

Kumar, S. V., et al. (2006), LIS—An interoperable framework for high resolution land surface modeling, *Environ. Model. Softw.*, *21*, 1402–1415, doi:10.1016/j.envsoft.2005.07.004.

Kummerow, C., R. A. Mack, and I. M. Hakkarinen (1989), A self-consistency approach to improve microwave rainfall rate estimation from space, *J. Appl. Meteorol.*, *28*, 869–884, doi:10.1175/1520-0450(1989)028<0869:ASCATI>2.0.CO;2.

Kummerow, C., W. S. Olson, and L. Giglio (1996), A simplified scheme for obtaining precipitation and vertical hydrometeor profiles from passive microwave sensors, *IEEE Trans. Geosci. Remote Sens.*, *34*, 1213–1232, doi:10.1109/36.536538.

Lafore, J.-P., and M. W. Moncrieff (1989), A numerical investigation of the scale interaction between a tropical squall line and its environment, *J. Atmos. Sci.*, *46*, 521–544.

Lafore, J.-P., J.-L. Redelsperger, and G. Jaubert (1988), Comparison between a three-dimensional simulation and Doppler radar data of a tropical squall line: Transports of mass, momentum,

heat, and moisture, *J. Atmos. Sci.*, *45*, 3483–3500, doi:10.1175/1520-0469(1988)045<3483:CBATDS>2.0.CO;2.

Laing, A. G., and J. M. Fritsch (1997), The global population of mesoscale convective complexes, *Q. J. R. Meteorol. Soc.*, *123*, 389–405, doi:10.1002/qj.49712353807.

Lane, T. P., and M. J. Reeder (2001), Convectively generated gravity waves and their effect on the cloud environment, *J. Atmos. Sci.*, *58*, 2427–2440, doi:10.1175/1520-0469(2001)058<2427:CGGWAT>2.0.CO;2.

Lang, S., W.-K. Tao, J. Simpson, and B. Ferrier (2003), Modeling of convective-stratiform precipitation processes: Sensitivity to partitioning methods, *J. Appl. Meteorol.*, *42*, 505–527, doi:10.1175/1520-0450(2003)042<0505:MOCSPP>2.0.CO;2.

Lau, K. M., C. H. Sui, and W.-K. Tao (1993), A preliminary study of the tropical water cycle and its sensitivity to surface warming, *Bull. Am. Meteorol. Soc.*, *74*, 1313–1321, doi:10.1175/1520-0477(1993)074<1313:APSOTT>2.0.CO;2.

Lau, K. M., C.-H. Sui, M.-D. Chou, and W.-K. Tao (1994), An inquiry into the cirrus-cloud thermostat effect for tropical sea Surface temperature, *Geophys. Res. Lett.*, *21*, 1157–1160, doi:10.1029/94GL00222.

LeMone, M. A., and M. W. Moncrieff (1994), Momentum and mass transport by convective bands: Comparisons of highly idealized dynamical models to observations, *J. Atmos. Sci.*, *51*, 281–305, doi:10.1175/1520-0469(1994)051<0281:MAMTBC>2.0.CO;2.

LeMone, M. A., D. P. Jorgenson, S. Lewis, B. Smull, and T. Matejka (1995), Boundary layer recovery in the stratiform region of mesoscale convective system in TOGA COARE, paper presented at the 21st Conference on Hurricanes and Tropical Meteorology, Am. Meteorol. Soc., Miami, Fla.

Leroy, D., M. Monier, W. Wobrock, and A. I. Flossmann (2006), A numerical study of the effects of the aerosol particle spectrum on the development of the ice phase and precipitation formation, *Atmos. Res.*, *80*, 15–45, doi:10.1016/j.atmosres.2005.06.007.

Levin, Z., and W. R. Cotton (Eds.) (2008), *Aerosol Pollution Impact on Precipitation: A Scientific Review*, 382 pp., Springer, New York.

Li, X., W.-K. Tao, A. Khain, J. Simpson, and D. Johnson (2009), Sensitivity of a cloud-resolving model to bulk and explicit-bin microphysics schemes. Part I: Comparisons, *J. Atmos. Sci.*, *66*, 3–21, doi:10.1175/2008JAS2646.1.

Lin, J. C., T. Matsui, R. A. Pielke Sr., and C. Kummerow (2006), Effects of biomass burning-derived aerosols on precipitation and clouds in the Amazon Basin: A satellite-based empirical study, *J. Geophys. Res.*, *111*, D19204, doi:10.1029/2005JD006884.

Lin, J.-L., et al. (2006), Tropical intraseasonal variability in 14 IPCC AR4 climate models. Part I: Convective signals, *J. Clim.*, *19, 2665–2690, doi:10.1175/JCLI3735.1.*

Lin, Y.-L., R. D. Farley, and H. D. Orville (1983), Bulk parameterization of the snow field in a cloud model, *J. Clim. Appl. Meteorol.*, *22*, 1065–1092, doi:10.1175/1520-0450(1983)022<1065:BPOTSF>2.0.CO;2.

Lipps, F. B., and R. S. Helmer (1986), Numerical simulation of deep tropical convection associated with large-scale convergence, *J. Atmos. Sci.*, *43*, 1796–1816, doi:10.1175/1520-0469(1986)043<1796:NSODTC>2.0.CO;2.

Liu, C., and M. W. Moncrieff (1998), A numerical study of the diurnal cycle of tropical oceanic convection, *J. Atmos. Sci.*, *55*, 2329–2344, doi:10.1175/1520-0469(1998)055<2329:ANSOTD>2.0.CO;2.

Liu, C., and M. W. Moncrieff (2004), Effects of convectively generated gravity waves and rotation on the organization of convection, *J. Atmos. Sci.*, *61*, 2218–2227, doi:10.1175/1520-0469(2004)061<2218:EOCGGW>2.0.CO;2.

Lohmann, U., K. Broekhuizen, R. Leatich, N. Shantz, and J. Abbatt (2004), How efficient is cloud droplet formation of organic aerosols?, *Geophys. Res. Lett.*, *31*, L05108, doi:10.1029/2003GL018999.

Ludlam, F. H. (1980), *Clouds and Storms: The Behavior and Effect of Water in the Atmosphere*, 405 pp., Pa. State Univ. Press, University Park.

Lynn, B. H., W.-K. Tao, and P. Wetzel (1998), A study of landscape generated deep moist convection, *Mon. Weather Rev.*, *126*, 928–942, doi:10.1175/1520-0493(1998)126<0928:ASOLGD>2.0.CO;2.

Lynn, B. H., W.-K. Tao, and F. Abramopoulos (2001), A parameterization for the triggering of landscape-generated moist convection. Part I: Analyses of high-resolution model results, *J. Atmos. Sci.*, *58*, 575–592, doi:10.1175/1520-0469(2001)058<0575:APFTTO>2.0.CO;2.

Lynn, B. H., A. Khain, J. Dudhia, D. Rosenfeld, A. Pokrovsky, and A. Seifert (2005), Spectral (bin) microphysics coupled with a mesoscale model (MM5). Part II: Simulation of a CaPE rain event with a squall line, *Mon. Weather Rev.*, *133*, 59–71, doi:10.1175/MWR-2841.1.

Madden, R., and P. Julian (1972), Description of global-scale circulation cells n the tropics with a 40–50 day period, *J. Atmos. Sci.*, *29*, 1109–1123, doi:10.1175/1520-0469(1972)029<1109:DOGSCC>2.0.CO;2.

Manton, M., and W. R. Cotton (1977), Formulation of approximate equations for modeling moist convection on the mesoscale, *Tech. Rep. 266*, Colo. State Univ., Fort Collins.

Mapes, B. E. (1993), Gregarious tropical convection, *J. Atmos. Sci.*, *50*, 2026–2037, doi:10.1175/1520-0469(1993)050<2026:GTC>2.0.CO;2.

McCumber, M., W.-K. Tao, J. Simpson, R. Penc, and S.-T. Soong (1991), Comparison of ice-phase microphysical parameterization schemes using numerical simulations of convection, *J. Appl. Meteorol.*, *30*, 987–1004.

Meneghini, R., J. A. Jones, T. Iguchi, K. Okamoto, and J. Kwiatkowski (2004), A hybrid surface reference technique and its application to the TRMM precipitation radar, *J. Atmos. Oceanic Technol.*, *21*, 1645–1658, doi:10.1175/JTECH1664.1.

Meyers, M. P., R. L. Walko, J. Y. Harrington, and W. R. Cotton (1997), New RAMS cloud microphysics. Part II: The two-moment scheme, *Atmos. Res.*, *45*, 3–39, doi:10.1016/S0169-8095(97)00018-5.

Milbrandt, J. A., and M. K. Yau (2005), A multimoment bulk microphysics parameterization. Part II: A proposed three-moment closure and scheme description, *J. Atmos. Sci.*, *62*, 3065–3081, doi:10.1175/JAS3535.1.

Miller, M. J., and R. P. Pearce (1974), A three-dimensional primitive equation model of cumulonimbus and squall lines, *Q. J. R. Meteorol. Soc.*, *100*, 133–154, doi:10.1002/qj.49710042402.

Miller, R. A., and W. M. Frank (1993), Radiative forcing of simulated tropical cloud clusters, *Mon. Weather Rev.*, *121*, 482–498, doi:10.1175/1520-0493(1993)121<0482:RFOSTC>2.0.CO;2.

Miura, H., H. Tomita, T. Nasuno, S. Iga, M. Satoh, and T. Matsuno (2005), A climate sensitivity test using a global cloud resolving model under an aqua planet condition, *Geophys. Res. Lett.*, *32*, L19717, doi:10.1029/2005GL023672.

Moeng, C.-H., J. C. McWilliams, R. Rotunno, P. P. Sullivan, and J. Weil (2004), Investigating 2D modeling of atmospheric convection in the PBL, *J. Atmos. Sci.*, *61*, 889–903, doi:10.1175/1520-0469(2004)061<0889:IDMOAC>2.0.CO;2.

Mohr, K. I., R. D. Baker, W.-K. Tao, and J. S. Famiglietti (2003), The sensitivity of West African convective lines water budgets to land cover, *J. Hydrometeorol.*, *4*, 62–76, doi:10.1175/1525-7541(2003)004<0062:TSOWAC>2.0.CO;2.

Moncrieff, M. W. (1978), The dynamical structure of two-dimensional steady convection in constant vertical shear, *Q. J. R. Meteorol. Soc.*, *104*, 543–567, doi:10.1002/qj.49710444102.

Moncrieff, M. W. (1981), A theory of organized steady convection and its transport properties, *Q. J. R. Meteorol. Soc.*, *107*, 29–50, doi:10.1256/smsqj.45102.

Moncrieff, M. W. (1989), Dynamical models of narrow-cold-frontal rainbands and related phenomena, *J. Atmos. Sci.*, *46*, 150–162, doi:10.1175/1520-0469(1989)046<0150:AMONCF>2.0.CO;2.

Moncrieff, M. W. (1992), Organized convective systems: Archetypal dynamical models, mass and momentum flux theory, and

parameterization, *Q. J. R. Meteorol. Soc.*, *118*, 819–850, doi:10.1002/qj.49711850703.

Moncrieff, M. W. (1997), Momentum transport by organized convection, in *NATO Advanced Study Series: C. The Physics and Parameterization of Moist Atmospheric Convection*, *NATO ASI Ser., Ser. C.*, vol. 505, edited by R. Smith, pp. 231–253, Kluwer Acad., Dordrecht, Netherlands.

Moncrieff, M. W. (2004), Analytic representation of the large-scale organization of tropical convection, *J. Atmos. Sci.*, *61*, 1521–1538, doi:10.1175/1520-0469(2004)061<1521:AROTLO>2.0.CO;2.

Moncrieff, M. W., and J. S. A. Green (1972), The propagation and transfer properties of steady convective overturning in shear, *Q. J. R. Meteorol. Soc.*, *98*, 336–352, doi:10.1002/qj.49709841607.

Moncrieff, M. W., and E. Klinker (1997), Mesoscale cloud systems in the tropical western Pacific as a process in general circulation models, *Q. J. R. Meteorol. Soc.*, *123*, 805–827, doi:10.1002/qj.49712354002.

Moncrieff, M. W., and C. Liu (1999), Convection initiation by density currents: Role of convergence, shear and dynamical organization, *Mon. Weather Rev.*, *127*, 2455–2464, doi:10.1175/1520-0493(1999)127<2455:CIBDCR>2.0.CO;2.

Moncrieff, M. W., and C. Liu (2006), Representing convective organization in prediction models by a hybrid strategy, *J. Atmos. Sci.*, *63*, 3404–3420, doi:10.1175/JAS3812.1.

Moncrieff, M. W., and M. J. Miller (1976), The dynamics and simulation of tropical cumulonimbus and squall-lines, *Q. J. R. Meteorol. Soc.*, *102*, 373–394, doi:10.1002/qj.49710243208.

Moncrieff, M. W., and D. W. K. So (1989), A hydrodynamical theory of conservative bounded density currents, *J. Fluid Mech.*, *198, 177–197, doi:10.1017/S0022112089000091.*

Moncrieff, M. W., S. K. Krueger, D. Gregory, J.-L. Redelsperger, and W.-K. Tao (1997), GEWEX Cloud System Study (GCSS) Working Group 4: Precipitating convective cloud systems, *Bull. Am. Meteorol. Soc.*, *78*, 831–845, doi:10.1175/1520-0477(1997)078<0831:GCSSGW>2.0.CO;2.

Moncrieff, M. W., M. Shapiro, J. Slingo, and F. Molteni (2007), Collaborative research at the intersection of weather and climate, *WMO Bull.*, *56*, 204–211.

Mordy, W. A. (1959), Computations of the growth by condensation of a population of cloud droplets, *Tellus*, *11*, 16–44.

Morita, J., Y. N. Takayabu, S. Shige, and Y. Kodama (2006), Analysis of rainfall characteristics of the Madden-Julian Oscillation using TRMM satellite data, *Dyn. Atmos. Oceans*, *42*, 107–126, doi:10.1016/j.dynatmoce.2006.02.002.

Morrison, H., J. A. Curry, and V. I. Khvorostyanov (2005), A new double-moment microphysics parameterization for application in cloud and climate models. Part I: Description, *J. Atmos. Sci.*, *62*, 1665–1677, doi:10.1175/JAS3446.1.

Murakami, M. (1990), Numerical modeling of dynamical and microphysical evolution of an isolated convective cloud—The 19 July 1981 CCOPE cloud, *J. Meteorol. Soc. Jpn.*, *68*, 107–128.

Nakajima, K., and T. Matsuno (1988), Numerical experiments concerning the origin of cloud cluster in tropical atmosphere, *J. Meteorol. Soc. Jpn.*, *66*, 309–329.

Nakazawa, T. (1988), Tropical superclusters within intraseasonal variations over the western Pacific, *J. Meteorol. Soc. Jpn.*, *66*, 823–839.

Nasuno, T., H. Tomita, S. Iga, H. Miura, and M. Satoh (2008), Multi-scale organization of convection simulated with explicit cloud processes on an aquaplanet, *J. Atmos. Sci.*, *65*, 1246–1265, doi:10.1175/2007JAS2395.1.

National Research Council (2005), *Radiative Forcing of Climate Change: Expanding the Concept and Addressing Uncertainties*, Natl. Acad., Washington, D. C.

Nesbitt, S. W., R. Cifelli, and S. A. Rutledge (2006), Storm morphology and rainfall characteristics of TRMM precipitation features, *Mon. Weather Rev.*, *134*, 2702–2721, doi:10.1175/MWR3200.1.

Nicholls, M. E. (1987), A comparison of the results of a two-dimensional numerical simulation of a tropical squall line with observations, *Mon. Weather Rev.*, *115*, 3055–3077, doi:10.1175/1520-0493(1987)115<3055:ACOTRO>2.0.CO;2.

Nicholls, M. E., R. A. Pielke, and W. R. Cotton (1991), Thermally forced gravity waves in an atmosphere at rest, *J. Atmos. Sci.*, *48*, 1869–1884, doi:10.1175/1520-0469(1991)048<1869:TFGWIA>2.0.CO;2.

Nickerson, E. C., E. Richard, R. Rosset, and D. R. Smith (1986), The numerical simulation of clouds, rain, and airflow over the Vosgas and Black Forest Mountain: A meso-beta model with parameterized microphysics, *Mon. Weather Rev.*, *114*, 398–414, doi:10.1175/1520-0493(1986)114<0398:TNSOCR>2.0.CO;2.

Ogura, Y., and N. A. Phillips (1962), Scale analysis of deep and shallow convection in the atmosphere, *J. Atmos. Sci.*, *19*, 173–179, doi:10.1175/1520-0469(1962)019<0173:SAODAS>2.0.CO;2.

Olson, W. S., et al. (2006), Precipitation and latent heating distributions from satellite passive microwave radiometry. Part I: Method and uncertainties, *J. Appl. Meteorol.*, *45*, 702–720, doi:10.1175/JAM2369.1.

Orville, R. E., R. Zhang, J. N. Gammon, D. Collins, B. Ely, and S. Steiger (2001), Enhancement of cloud-to-ground lightening over Houston, Texas, *Geophys. Res. Lett.*, *28*, 2597–2600, doi:10.1029/2001GL012990.

Panegrossi, G., S. Dietrich, F. S. Marzano, A. Mugnai, E. A. Smith, X. Xiang, G. J. Tripoli, P. K. Wang, and J. P. V. Poiares Baptista (1998), Use of cloud model microphysics for passive microwave-based precipitation retrieval: Significance of consistency between model and measurement manifolds, *J. Atmos. Sci.*, *55*, 1644–1673, doi:10.1175/1520-0469(1998)055<1644:UOCMMF>2.0.CO;2.

Peng, L., C.-H. Sui, K.-M. Lau, and W.-K. Tao (2001), Genesis and evolution of hierarchical cloud clusters in a two-dimensional cumulus-resolving model, *J. Atmos. Sci.*, *58*, 877–895, doi:10.1175/1520-0469(2001)058<0877:GAEOHC>2.0.CO;2.

Pielke, R. A., Sr., et al. (1992), A comprehensive meteorological modeling system—RAMS, *Meteorol. Atmos. Phys.*, *49*, 69–91, doi:10.1007/BF01025401.

Rajendran, R., T. N. Krishnamurti, V. Misra, and W.-K. Tao (2004), An empirical cumulus parameterization scheme based on TRMM latent heating profiles, *J. Meteorol. Soc. Jpn.*, *82*, 989–1006, doi:10.2151/jmsj.2004.989.

Ramanathan, V., and W. Collins (1991), Thermodynamic regulation of ocean warming by cirrus clouds deduced from observations of the 1987 El Niño, *Nature*, *351*, 27–32, doi:10.1038/351027a0.

Ramanathan, V., R. D. Cess, E. F. Harrison, P. Minnis, B. R. Barkstrom, E. Ahmad, and D. Hartmann (1989), Cloud-radiative forcing and climate: Results from the Earth radiation budget experiment, *Science*, *243*, 57–63, doi:10.1126/science.243.4887.57.

Ramanathan, V., P. J. Crutzen, J. T. Kiehl, and D. Rosenfeld (2001), Aerosols, climate, and the hydrological cycle, *Science*, *294*, 2119–2124, doi:10.1126/science.1064034.

Randall, D. A., Harshvardhan, and D. A. Dazlich (1991), Diurnal variability of the hydrologic cycle in a general circulation model, *J. Atmos. Sci.*, *48*, 40–62, doi:10.1175/1520-0469(1991)048<0040:DVOTHC>2.0.CO;2.

Randall, D. A., et al. (2003a), Confronting models with data: The GEWEX cloud system study, *Bull. Am. Meteorol. Soc.*, *84*, 455–469, doi:10.1175/BAMS-84-4-455.

Randall, D. A., M. Khairoutdinov, A. Arakawa, and W. W. Grabowski (2003b), Breaking the cloud parameterization deadlock, *Bull. Am. Meteorol. Soc.*, *84*, 1547–1564, doi:10.1175/BAMS-84-11-1547.

Ray, P., C. Zhang, J. Dudhia, and S. S. Chen (2009), A numerical case study on the initiation of the Madden-Julian Oscillation, *J. Atmos. Sci.*, *66*, 310–331.

Redelsperger, J.-L., and T. L. Clark (1990), The initiation and horizontal scale selection of convection over gently sloping terrain, *J. Atmos. Sci.*, *47*, 516–541, doi:10.1175/1520-0469(1990)047<0516:TIAHSS>2.0.CO;2.

Redelsperger, J.-L., and J.-P. Lafore (1988), A three-dimensional simulation of a tropical squall line: Convective organization and thermodynamic vertical transport, *J. Atmos. Sci.*, *45*, 1334–1356, doi:10.1175/1520-0469(1988)045<1334:ATDSOA>2.0.CO;2.

Redelsperger, J.-L., and G. Sommeria (1986), A three-dimensional simulation of a convective storm: Sensitivity studies on subgrid parameterization and spatial resolution, *J. Atmos. Sci.*, *43*, 2619–2635, doi:10.1175/1520-0469(1986)043<2619:TDSOAC>2.0.CO;2.

Reisner, J., R. M. Rasmussen, and R. T. Bruintjes (1998), Explicit forecasting of supercooled liquid water in winter storms using the MM5 mesoscale model, *Q. J. R. Meteorol. Soc.*, *124*, 1071–1108, doi:10.1002/qj.49712454804.

Respondek, P. S., A. I. Flossmann, R. R. Alheit, and H. R. Pruppacher (1995), A theoretical study of the wet removal of atmospheric pollutants. Part V: The uptake, redistribution and deposition of $(NH_4)_2SO_4$ by a convective cloud containing ice, *J. Atmos. Sci.*, *52*, 2121–2132, doi:10.1175/1520-0469(1995)052<2121:ATSOTW>2.0.CO;2.

Rickenbach, T. M., and S. A. Rutledge (1998), Convection in TOGA COARE: Horizontal scale, morphology, and rainfall production, *J. Atmos. Sci.*, *55*, 2715–2729, doi:10.1175/1520-0469(1998)055<2715:CITCHS>2.0.CO;2.

Riehl, H., and J. Simpson (1979), The heat balance of the equatorial trough zone, revisited, *Beitr. Phys. Atmos.*, *52*, 287–305.

Rosenfeld, D. (1999), TRMM observed first direct evidence of smoke from forest fires inhibiting rainfall, *Geophys. Res. Lett.*, *26*(20), 3105–3108, doi:10.1029/1999GL006066.

Rosenfeld, D. (2000), Suppression of rain and snow by urban and industrial air pollution, *Science*, *287*, 1793–1796, doi:10.1126/science.287.5459.1793.

Rosenfeld, D., and I. Lensky (1998), Satellite-based insights into precipitation formation processes in continental and maritime convective clouds, *Bull. Am. Meteorol. Soc.*, *79*, 2457–2476, doi:10.1175/1520-0477(1998)079<2457:SBIIPF>2.0.CO;2.

Rosenfeld, D., and C. W. Ulbrich (2003), Cloud microphysical properties, processes, and rainfall estimation opportunities, in *Radar and Atmospheric Science: A Collection of Essays in Honor of David Atlas*, edited by R. M. Wakimoto and R. Srivastava, *Meteorol. Monogr.*, *52*, chap. 10, 237–258.

Rosenfeld, D., and W. L. Woodley (2000), Convective clouds with sustained highly supercooled liquid water down to −37°C, *Nature*, *405*, 440–442, doi:10.1038/35013030.

Rosenfeld, D., Y. Rudich, and R. Lahav (2001), Desert dust suppressing: A possible desertification feedback loop, *Proc. Natl. Acad. Sci. U. S. A.*, *98*, 5975–5980, doi:10.1073/pnas.101122798.

Rossow, W. B., and E. Duenas (2004), The International Satellite Cloud Climatology Project (ISCCP) Web site: An online resource for research, *Bull. Am. Meteorol. Soc.*, *85*, 167–172, doi:10.1175/BAMS-85-2-167.

Rotunno, R., J. B. Klemp, and M. L. Weisman (1988), A theory for strong, long-lived squall lines, *J. Atmos. Sci.*, *45*, 463–485, doi:10.1175/1520-0469(1988)045<0463:ATFSLL>2.0.CO;2.

Rutledge, S. A., and P. V. Hobbs (1984), The mesoscale and m croscale structure and organization of clouds and precipitation in mid-latitude clouds. Part XII: A diagnostic modeling study of precipitation development in narrow cold frontal rainbands, *J. Atmos. Sci.*, *41*, 2949–2972, doi:10.1175/1520-0469(1984)041<2949:TMAMSA>2.0.CO;2.

Rutledge, S. A., and D. R. MacGorman (1988), Cloud-to ground lightening activity in the 10–11 June 1985 mesoscale convective system observed during the Oklahoma–Kansas PRE-STORM project, *Mon. Weather Rev.*, *116*, 1393–1408, doi:10.1175/1520-0493(1988)116<1393:CTGLAI>2.0.CO;2.

Rutledge, S. A., R. A. Houze Jr., and M. I. Biggerstaff (1988), The Oklahoma-Kansas mesoscale convective system of 10–11 June 1985: Precipitation structure and single-Doppler radar analysis, *Mon. Weather Rev.*, *116*, 1409–1430, doi:10.1175/1520-0493(1988)116<1409:TOMCSO>2.0.CO;2.

Saito, K., M. Murakami, T. Matsuo, and H. Mizuno (1996), Sensitivity experiments on the orographic snowfall over the mountainous region of northern Japan, *J. Meteorol. Soc. Jpn.*, *74*, 797–813.

Saito, K., et al. (2006), The operational JMA nonhydrostatic mesoscale model, *Mon. Weather Rev.*, *134*, 1266–1297.

Saleeby, S. M., and W. R. Cotton (2004), A large droplet mode and prognostic number concentration of cloud droplets in the Colorado State University Regional Atmospheric Modeling System (RAMS). Part I: Module descriptions and supercell test simulations, *J. Appl. Meteorol.*, *43*, 182–195, doi:10.1175/1520-0450(2004)043<0182:ALMAPN>2.0.CO;2.

Saleeby, S. M., and W. R. Cotton (2008), A binned approach to cloud-droplet riming implemented in a bulk microphysics model, *J. Appl. Meteorol. Climatol.*, *47*, 694–703, doi:10.1175/2007JAMC1664.1.

Satoh, S., and A. Noda (2001), Retrieval of latent heating profiles from TRMM radar data, paper presented at the 30th International Conference on Radar Meteorology, Am. Meteorol. Soc., Munich, Germany, 19–24 July.

Satoh, M., H. Tomita, H. Miura, S. Iga, and T. Nasuno (2005), Development of a global cloud resolving model—A multi-scale structure of tropical convections, *J. Earth Simulator*, *3*, 1–9.

Satoh, M., T. Matsuno, H. Tomita, H. Miura, T. Nasuno, and S. Iga (2008), Nonhydrostatic icosahedral atmospheric model (NICAM) for global cloud resolving simulations, *J. Comput. Phys.*, *227*, 3486–3514, doi:10.1016/j.jcp.2007.02.006.

Schlesinger, R. E. (1978), A three-dimensional numerical model of an isolated thunderstorm: Part I. Comparative experiments for variable ambient wind shear, *J. Atmos. Sci.*, *35*, 690–713, doi:10.1175/1520-0469(1978)035<0690:ATDNMO>2.0.CO;2.

Schumacher, C., R. A. Houze Jr., and I. Kraucunas (2004), The tropical dynamical response to latent heating estimates derived from the TRMM precipitation radar, *J. Atmos. Sci.*, *61*, 1341–1358, doi:10.1175/1520-0469(2004)061<1341:TTDRTL>2.0.CO;2.

Seifert, A., and K. D. Beheng (2001), A double-moment parameterization for simulating autoconversion, accretion and selfcollection, *Atmos. Res.*, *59–60*, 265–281, doi:10.1016/S0169-8095(01)00126-0.

Seifert, A., and K. D. Beheng (2006a), A two-moment cloud microphysics parameterization for mixed-phase clouds. Part I: Model description, *Meteorol. Atmos. Phys.*, *92*, 45–66, doi:10.1007/s00703-005-0112-4.

Seifert, A., and K. D. Beheng (2006b), A two-moment cloud microphysics parameterization for mixed-phase clouds. Part II: Maritime vs. continental deep convective storms, *Meteorol. Atmos. Phys.*, *92*, 67–82, doi:10.1007/s00703-005-0113-3.

Shepherd, J. M. (2005), A review of current investigations of urban-induced rainfall and recommendations for the future, *Earth Interact.*, *9*, paper 12, doi:10.1175/EI156.1.

Shige, S., Y. N. Takayabu, W.-K. Tao, and D. E. Johnson (2004), Spectral retrieval of latent heating profiles from TRMM PR data. Part I: Development of a model-based algorithm, *J. Appl. Meteorol.*, *43*, 1095–1113, doi:10.1175/1520-0450(2004)043<1095:SROLHP>2.0.CO;2.

Shige, S., Y. N. Takayabu, W.-K. Tao, and C.-L. Shie (2007), Spectral retrieved of latent heating profiles from TRMM PR data. Part II: Algorithm improvement and its estimates over the tropical ocean regions, *J. Appl. Meteorol.*, *46*, 1098–1124, doi:10.1175/JAM2510.1.

Shutts, G. J., and T. N. Palmer (2007), Convective forcing fluctuations in a cloud-resolving model: Relevance to the stochastic parameterization problem, *J. Clim.*, *20*, 187–202, doi:10.1175/JCLI3954.1.

Simpson, J., R. H. Simpson, D. A. Andrews, and M. A. Eaton (1965), Experimental cumulus dynamics, *Rev. Geophys.*, *3*, 387–431, doi:10.1029/RG003i003p00387.

Simpson, J., G. W. Brier, and R. H. Simpson (1967), Stormfury cumulus seeding experiment 1965: Statistical analysis and main results, *J. Atmos. Sci.*, *24*, 508–521, doi:10.1175/1520-0469(1967)024<0508:SCSESA>2.0.CO;2.

Simpson, J., R. F. Adler, and G. R. North (1988), A proposed tropical rainfall measuring mission (TRMM) satellite, *Bull. Am. Meteorol. Soc.*, *69*, 278–295, doi:10.1175/1520-0477(1988)069<0278:APTRMM>2.0.CO;2.

Simpson, J., C. Kummerow, W.-K. Tao, and R. Adler (1996), On the Tropical Rainfall Measuring Mission (TRMM), *Meteorol. Atmos. Phys.*, *60*, 19–36, doi:10.1007/BF01029783.

Skamarock, W. C. (2004), Evaluating mesoscale NWP models using kinetic energy spectra, *Mon. Weather Rev.*, *132*, 3019–3032, doi:10.1175/MWR2830.1.

Smith, E. A., X. Xiang, A. Mugnai, and G. J. Tripoli (1992), A cloud radiation model for spaceborne precipitation retrieval, paper presented at the International TRMM Workshop on the Processing and Utilization of the Rainfall Data Measured From Space, Commun. Res. Lab., Tokyo.

Smith, E. A., X. Xiang, A. Mugnai, and G. J. Tripoli (1994), Design of an inversion-based precipitation profile retrieval algorithm using an explicit cloud model for initial guess microphysics, *Meteorol. Atmos. Phys.*, *54*, 53–78, doi:10.1007/BF01030052.

Smith, R. K. (Ed.) (1997), *The Physics and Parameterization of Moist Atmospheric Convection*, 498 pp., *NATO ASI Ser., Ser. C*, vol. 505, Kluwer Acad., Dordrecht, Netherlands.

Smull, B. F., and R. A. Houze Jr. (1987a), Dual-Doppler radar analysis of a midlatitude squall line with a trailing region of stratiform rain, *J. Atmos. Sci.*, *44*, 2128–2147, doi:10.1175/1520-0469(1987)044<2128:DDRAOA>2.0.CO;2.

Smull, B. F., and R. A. Houze Jr. (1987b), Rear inflow in squall lines with trailing stratiform precipitation, *Mon. Weather Rev.*, *115*, 2869–2889, doi:10.1175/1520-0493(1987)115<2869:RIISLW>2.0.CO;2.

Sommeria, G. (1976), Three-dimensional simulation of turbulent processes in an undisturbed trade wind boundary layer, *J. Atmos. Sci.*, *33*, 216–241, doi:10.1175/1520-0469(1976)033<0216:TDSOTP>2.0.CO;2.

Soong, S.-T. (1974), Numerical simulation of warm rain development in an axisymmetric cloud model, *J. Atmos. Sci.*, *31*, 1262–1285, doi:10.1175/1520-0469(1974)031<1262:NSOWRD>2.0.CO;2.

Soong, S.-T., and Y. Ogura (1973), A comparison between axisymmetric and slab-symmetric cumulus cloud models, *J. Atmos. Sci.*, *30*, 879–893, doi:10.1175/1520-0469(1973)030<0879:ACBAAS>2.0.CO;2.

Soong, S.-T., and Y. Ogura (1980), Response of trade wind cumuli to large-scale processes, *J. Atmos. Sci.*, *37*, 2035–2050, doi:10.1175/1520-0469(1980)037<2035:ROTCTL>2.0.CO;2.

Soong, S.-T., and W.-K. Tao (1980), Response of deep tropical clouds to mesoscale processes, *J. Atmos. Sci.*, *37*, 2016–2036, doi:10.1175/1520-0469(1980)037<2016:RODTCC>2.0.CO;2.

Sperber, K. R., J. M. Slingo, D. E. Waliser, and P. M. Inness (2008), Coarse-resolution models only partly cloudy, *Science*, *320*, 612–613, doi:10.1126/science.320.5876.612a.

Squires, P., and T. Twomey (1961), The relation between cloud drop numbers and the spectrum of cloud nuclei, in *Physics of Precipitation*, *Geophys. Monogr. Ser.*, vol. 5, edited by H. Weickmann, pp. 211–219, AGU, Washington, D. C.

Steiner, J. T. (1973), A three-dimensional model of cumulus cloud development, *J. Atmos. Sci.*, *30*, 414–435, doi:10.1175/1520-0469(1973)030<0414:ATDMOC>2.0.CO;2.

Stephens, G. L. (1983), The influence of radiative transfer on the mass and heat budget of ice crystals falling in the atmosphere, *J. Atmos. Sci.*, *40*, 1729–1739, doi:10.1175/1520-0469(1983)040<1729:TIORTO>2.0.CO;2.

Straub, K. H., and G. N. Kiladis (2002), Observations of a convectively coupled Kelvin wave in the eastern Pacific ITCZ, *J. Atmos. Sci.*, *59*, 30–53, doi:10.1175/1520-0469(2002)059<0030:OOACCK>2.0.CO;2.

Sui, C.-H., and K.-M. Lau (1989), Origin of low-frequency (Intraseasonal) oscillations in the tropical atmosphere. Part II: Structure and propagation of mobile wave-CISK modes and their modification by lower boundary forcing, *J. Atmos. Sci.*, *46*, 37–56, doi:10.1175/1520-0469(1989)046<0037:OOLFOI>2.0.CO;2.

Sui, C.-H., K.-M. Lau, W.-K. Tao, and J. Simpson (1994), The tropical water and energy cycles in a cumulus ensemble model. Part I: Equilibrium climate, *J. Atmos. Sci.*, *51*, 711–728, doi:10.1175/1520-0469(1994)051<0711:TTWAEC>2.0.CO;2.

Sui, C.-H., X. Li, and K.-M. Lau (1998), Radiative-convective processes in simulated diurnal variations of tropical oceanic convection, *J. Atmos. Sci.*, *55*, 2345–2359, doi:10.1175/1520-0469(1998)055<2345:RCPISD>2.0.CO;2.

Sui, C.-H., X. Li, K.-M. Lau, W.-K. Tao, M.-D. Chou, and M.-J. Yang (2008), Convective-radiative-mixing processes in the tropical ocean-atmosphere, in *Recent Progress in Atmospheric Sciences With Applications to the Asia-Pacific Region*, pp. 49–65, World Sci., Singapore.

Sun, J. (2005), Convective-scale assimilation of radar data: Progress and challenges, *Q. J. R. Meteorol. Soc.*, *131*, 3439–3463, doi:10.1256/qj.05.149.

Sun, J., and N. A. Crook (1998), Dynamical and microphysical retrieval from Doppler radar observations using a cloud model and its adjoint. Part II: Retrieval experiments of an observed Florida convective storm, *J. Atmos. Sci.*, *55*, 835–852, doi:10.1175/1520-0469(1998)055<0835:DAMRFD>2.0.CO;2.

Takahashi, T. (1976), Hail in an axisymmetric cloud model, *J. Atmos. Sci.*, *33*, 1579–1601, doi:10.1175/1520-0469(1976)033<1579:HIAACM>2.0.CO;2.

Tao, W.-K. (2003), Goddard Cumulus Ensemble (GCE) model: Application for understanding precipitation processes, in *Cloud Systems, Hurricanes, and the Tropical Rainfall Measuring Mission (TRMM): A Tribute to Dr. Joanne Simpson*, *Meteorol. Monogr.*, *51*, 107–138.

Tao, W.-K. (2007), Convective cloud systems modeling, *J. Meteorol. Soc. Jpn.*, *85*, 305–330.

Tao, W.-K., and M. Moncrieff (2003), Cloud modeling, in *Encyclopedia of Atmospheric Sciences*, edited by J. Holton, J. Curry, and J. Pyle, pp. 539–548, Academic, Amsterdam.

Tao, W.-K., and J. Simpson (1989), Modeling study of a tropical squall-type convective line, *J. Atmos. Sci.*, *46*, 177–202, doi:10.1175/1520-0469(1989)046<0177:MSOATS>2.0.CO;2.

Tao, W.-K., and J. Simpson (1993), The Goddard Cumulus Ensemble Model. Part I: Model description, *Terr. Atmos. Oceanic Sci.*, *4*, 19–54.

Tao, W.-K., and S.-T. Soong (1986), A study of the response of deep tropical clouds to mesoscale processes: Three-dimensional numerical experiments, *J. Atmos. Sci.*, *43*, 2653–2676, doi:10.1175/1520-0469(1986)043<2653:ASOTRO>2.0.CO;2.

Tao, W.-K., J. Simpson, and S.-T. Soong (1987), Statistical properties of a cloud ensemble: A numerical study, *J. Atmos. Sci.*, *44*, 3175–3187, doi:10.1175/1520-0469(1987)044<3175:SPOACE>2.0.CO;2.

Tao, W.-K., J. Simpson, S. Lang, M. McCumber, R. Adler, and R. Penc (1990), An algorithm to estimate the heating budget from vertical hydrometeor profiles, *J. Appl. Meteorol.*, *29*, 1232–1244, doi:10.1175/1520-0450(1990)029<1232:AATETH>2.0.CO;2.

Tao, W.-K., J. Simpson, and S.-T. Soong (1991), Numerical simulation of a sub-tropical squall line over Taiwan Strait, *Mon. Weather Rev.*, *119*, 2699–2723, doi:10.1175/1520-0493(1991)119<2699:NSOASS>2.0.CO;2.

Tao, W.-K., J. Simpson, C.-H. Sui, B. Ferrier, S. Lang, J. Scala, M.-D. Chou, and K. Pickering (1993a), Heating, moisture and water budgets of tropical and mid-latitude squall lines: Comparisons and sensitivity to longwave radiation, *J. Atmos. Sci.*, *50*,

673–690, doi:10.1175/1520-0469(1993)050<0673:HMAWBO>2.0.CO;2.

Tao, W.-K., J. Simpson, S. Lang, J. Simpson, and R. Adler (1993b), Retrieval Algorithms for estimating the vertical profiles of latent heat release: Their applications for TRMM, *J. Meteorol. Soc. Jpn.*, *71*, 685–700.

Tao, W.-K., J. Scala, and J. Simpson (1995), The effects of melting processes on the development of a tropical and a mid-latitudes squall line, *J. Atmos. Sci.*, *52*, 1934–1948, doi:10.1175/1520-0469(1995)052<1934:TEOMPO>2.0.CO;2.

Tao, W.-K., S. Lang, J. Simpson, C.-H. Sui, B. Ferrier, and M.-D. Chou (1996), Mechanisms of cloud-radiation interaction in the tropics and midlatitudes, *J. Atmos. Sci.*, *53*, 2624–2651, doi:10.1175/1520-0469(1996)053<2624:MOCRII>2.0.CO;2.

Tao, W.-K., J. Simpson, C.-H. Sui, C.-L. Shie, B. Zhou, K. M. Lau, and M. Moncrieff (1999), On equilibrium states simulated by cloud-resolving models, *J. Atmos. Sci.*, *56*, 3128–3139, doi:10.1175/1520-0469(1999)056<3128:ESSBCR>2.0.CO;2.

Tao, W.-K., S. Lang, J. Simpson, W. S. Olson, D. Johnson, B. Ferrier, C. Kummerow, and R. Adler (2000), Vertical profiles of latent heat release and their retrieval in TOGA COARE convective systems using a cloud resolving model, SSM/I and radar data, *J. Meteorol. Soc. Jpn.*, *78*, 333–355.

Tao, W.-K., S. Lang, W. S. Olson, S. Yang, R. Meneghini, J. Simpson, C. Kummerow, E. Smith, and J. Halverson (2001), Retrieved vertical profiles of latent heat release using TRMM products for February 1998, *J. Appl. Meteorol.*, *40*, 957–982, doi:10.1175/1520-0450(2001)040<0957:RVPOLH>2.0.CO;2.

Tao, W.-K., et al. (2003), Microphysics, radiation and surface processes in the Goddard Cumulus Ensemble (GCE) model, *Meteorol. Atmos. Phys.*, *82*, 97–137, doi:10.1007/s00703-001-0594-7.

Tao, W.-K., et al. (2006), Retrieval of latent heating from TRMM measurements, *Bull. Am. Meteorol. Soc.*, *87*, 1555–1572, doi:10.1175/BAMS-87-11-1555.

Tao, W.-K., X. Li, A. Khain, T. Matsui, S. Lang, and J. Simpson (2007), The role of atmospheric aerosol concentration on deep convective precipitation: Cloud-resolving model simulations, *J. Geophys. Res.*, *112*, D24S18, doi:10.1029/2007JD008728.

Tao, W.-K., et al. (2009), A multi-scale modeling system: Developments, applications and critical issues, *Bull. Am. Meteorol. Soc.*, *90*, 515–534, doi:10.1175/2008BAMS2542.1.

Telford, J. W. (1980), A new aspect of condensation theory, *Pure Appl. Geophys.*, *118*, 720–742, doi:10.1007/BF01593025.

Teller, A., and Z. Levin (2006), The effects of aerosols on precipitation and dimensions of subtropical clouds: A sensitivity study using a numerical cloud model, *Atmos. Chem. Phys.*, *6*, 67–80.

Thompson, A. M., W.-K. Tao, K. E. Pickering, J. R. Scala, and J. Simpson (1997), Tropical deep convection and ozone formation, *Bull. Am. Meteorol. Soc.*, *78*, 1043–1054, doi:10.1175/1520-0477(1997)078<1043:TDCAOF>2.0.CO;2.

Thorpe, A. J., M. J. Miller, and M. W. Moncrieff (1980), Dynamical models of two-dimensional updraughts and downdraughts, *Q. J. R. Meteorol. Soc.*, *106*, 463–484, doi:10.1002/qj.49710644906.

Thorpe, A. J., M. J. Miller, and M. W. Moncrieff (1982), Two-dimensional convection in non-constant shear: A model of mid-latitude squall lines, *Q. J. R. Meteorol. Soc.*, *108*, 739–762, doi:10.1002/qj.49710845802.

Tomita, H., H. Miura, H. Iga, T. Nasuno, and M. Satoh (2005), A global cloud-resolving simulation: Preliminary results from an aqua planet experiment, *Geophys. Res. Lett.*, *32*, L08805, doi:10.1029/2005GL022459.

Toon, O. B., R. P. Turco, D. Wesyphal, R. Malone, and M. Liu (1988), A multidimensional model for aerosols: Description of computational analogs, *J. Atmos. Sci.*, *45*, 2123–2144, doi:10.1175/1520-0469(1988)045<2123:AMMFAD>2.0.CO;2.

Trier, S. B., W. C. Skamarock, M. A. LeMone, and D. B. Parsons (1996), Structure and evolution of the 22 February 1993 TOGA COARE squall line: Numerical simulations, *J. Atmos. Sci.*, *53*, 2861–2886, doi:10.1175/1520-0469(1996)053<2861:SAEOTF>2.0.CO;2.

Trier, S. B., C. A. Davis, D. A. Ahijevych, M. L. Weisman, and G. H. Bryan (2006), Mechanisms supporting long-lived episodes of propagating nocturnal convection within a 7-day WRF model simulation, *J. Atmos. Sci.*, *63*, 2437–2461, doi:10.1175/JAS3768.1.

Tripoli, G. J., and W. R. Cotton (1989), Numerical study of an observed orogenic mesoscale convective system. Part 2: Analysis of governing dynamics, *Mon. Weather Rev.*, *117*, 305–328, doi:10.1175/1520-0493(1989)117<0305:NSOAOO>2.0.CO;2.

Tulich, S. N., D. A. Randall, and B. E. Mapes (2007), Vertical-mode and cloud decomposition of large-scale convectively coupled gravity waves in a two-dimensional cloud-resolving model, *J. Atmos. Sci.*, *64*, 1210–1229, doi:10.1175/JAS3884.1.

Twomey, S. A. (1977), The influence of pollution on the shortwave albedo of clouds, *J. Atmos. Sci.*, *34*, 1149–1152, doi:10.1175/1520-0469(1977)034<1149:TIOPOT>2.0.CO;2.

Twomey, S. A., M. Piepgrass, and T. L. Wolfe (1984), An assessment of the impact of pollution on global cloud albedo, *Tellus, Ser. B*, *36*, 356–366.

Tzivion, S., G. Feingold, and Z. Levin (1987), An efficient numerical solution to stochastic collection equation, *J. Atmos. Sci.*, *44*, 3139–3149, doi:10.1175/1520-0469(1987)044<3139:AENSTT>2.0.CO;2.

van den Heever, S. C., and W. R. Cotton (2007), Urban aerosol impacts on downwind convective storms, *J. Appl. Meteor. Climatol.*, *46*, 828–850, doi:10.1175/JAM2492.1.

van den Heever, S. C., G. G. Carrió, W. R. Cotton, P. J. DeMott, and A. J. Prenni (2006), Impact of nucleating aerosol on Florida storms. Part 1: Mesoscale simulations, *J. Atmos. Sci.*, *63*, 1752–1775, doi:10.1175/JAS3713.1.

Waliser, D. E., and M. W. Moncrieff (2007), Year of tropical convection—A joint WCRP-THORPEX activity to address the challenge of tropical convection, *GEWEX News*, *17*(2), 8–9.

Waliser, D. E., and M. W. Moncrieff (2008), Year of Tropical Convection (YOTC): The YOTC Science Plan, *WMO/TD 1452*, 26 pp., World Meteorol. Organ., Geneva, Switzerland.

Walko, R. L., W. R. Cotton, M. P. Meyers, and J. Y. Harrington (2000), Efficient computation of vapor and heat diffusion between hydrometeors in a numerical model, *Atmos. Res.*, *53*, 171–183, doi:10.1016/S0169-8095(99)00044-7.

Wang, C. (2005), A model study of the response of tropical deep convection to the increase of CCN concentration. Part 1. Dynamics and microphysics, *J. Geophys. Res.*, *110*, D21211, doi:10.1029/2004JD005720.

Wang, Y., W.-K. Tao, and J. Simpson (1996), The impact of ocean surface fluxes on a TOGA COARE convective system, *Mon. Weather Rev.*, *124*, 2753–2763, doi:10.1175/1520-0493(1996)124<2753:TIOOSF>2.0.CO;2.

Wang, Y., W.-K. Tao, J. Simpson, and S. Lang (2003), The sensitivity of tropical squall lines (GATE and TOGA COARE) to surface fluxes: 3-D cloud resolving model simulations, *Q. J. R. Meteorol. Soc.*, *129*, 987–1007, doi:10.1256/qj.00.131.

Warner, J. (1968), A reduction in rainfall associated with smoke from sugar-cane fires: An inadvertent weather modification?, *J. Appl. Meteorol.*, *7*, 247–251, doi:10.1175/1520-0450(1968)007<0247:ARIRAW>2.0.CO;2.

Warner, J., and S. Twomey (1967), The production of cloud nuclei by cane fires and the effects on cloud droplet concentration, *J. Atmos. Sci.*, *24*, 704–706, doi:10.1175/1520-0469(1967)024<0704:TPOCNB>2.0.CO;2.

Webster, P. J., and R. Lukas (1992), TOGA COARE: The Coupled Ocean-Atmosphere Response Experiment, *Bull. Am. Meteorol. Soc.*, *73*, 1377–1416, doi:10.1175/1520-0477(1992)073<1377:TCTCOR>2.0.CO;2.

Webster, P. J., and G. L. Stephens (1980), Tropical upper troposphere extended clouds: Inferences from Winter MONEX, *J. Atmos. Sci.*, *37*, 1521–1541.

Wilheit, T. T., A. T. C. Chang, and L. S. Chiu (1991), Retrieval of monthly rainfall indices from microwave radiometric measurements using probability distribution functions, *J. Atmos. Oceanic Technol.*, *8*, 118–136, doi:10.1175/1520-0426(1991)008<0118:ROMRIF>2.0.CO;2.

Wilhelmson, R. B. (1974), The life cycle of a thunderstorm in three dimensions, *J. Atmos. Sci.*, *31*, 1629–1651, doi:10.1175/1520-0469(1974)031<1629:TLCOAT>2.0.CO;2.

Wilhelmson, R. B., and J. B. Klemp (1978), A numerical study of storm splitting that leads to long-lived storms, *J. Atmos. Sci.*, *35*, 1974–1986, doi:10.1175/1520-0469(1978)035<1974:ANSOSS>2.0.CO;2.

Williams, E., et al. (2002), Contrasting convective regimes over the Amazon: Implications for cloud electrification, *J. Geophys. Res.*, *107*(D20), 8082, doi:10.1029/2001JD000380.

Wu, X., and M. W. Moncrieff (1996), Collective effects of organized convection and their approximation in general circulation models, *J. Atmos. Sci.*, *53*, 1477–1495, doi:10.1175/1520-0469(1996)053<1477:CEOOCA>2.0.CO;2.

Wu, X., and M. W. Moncrieff (2001), Long-term behavior of cloud systems in TOGA COARE and their interactions with radiative and surface processes. Part III: Effects on the energy budget and SST, *J. Atmos. Sci.*, *58*, 1155–1168, doi:10.1175/1520-0469(2001)058<1155:LTBOCS>2.0.CO;2.

Wu, X., W. W. Grabowski, and M. W. Moncrieff (1998), Long-term behavior of cloud systems in TOGA COARE and their interactions with radiative and surface processes. Part I: Two-dimensional modeling study, *J. Atmos. Sci.*, *55*, 2693–2714, doi:10.1175/1520-0469(1998)055<2693:LTBOCS>2.0.CO;2.

Xiao, Q., and J. Sun (2007), Multiple-radar data assimilation and short-range quantitative precipitation forecasting of a squall line observed during IHOP_2002, *Mon. Weather Rev.*, *135*, 3381–3404, doi:10.1175/MWR3471.1.

Xu, K.-M., and D. A. Randall (1995), Impact of interactive radiative transfer on the microscopic behavior of cumulus ensembles. Part II: Mechanisms for cloud-radiation interactions, *J. Atmos. Sci.*, *52*, 800–817, doi:10.1175/1520-0469(1995)052<0800:IOIRTO>2.0.CO;2.

Yang, S., and E. A. Smith (1999), Moisture budget analysis of TOGA-COARE area using SSM/I retrieved latent heating and large scale Q_2 estimates, *J. Atmos. Oceanic Technol.*, *16*, 633–655, doi:10.1175/1520-0426(1999)016<0633:MBAOTC>2.0.CO;2.

Yang, S., W. S. Olson, J.-J. Wang, T. L. Bell, E. A. Smith, and C. D. Kummerow (2006), Precipitation and latent heating distributions from satellite passive microwave radiometry. Part II: Evaluation of estimates using independent data, *J. Appl. Meteorol.*, *45*, 721–739, doi:10.1175/JAM2370.1.

Yano, J. I., J. C. McWilliams, M. W. Moncrieff, and K. A. Emanuel (1995), Hierarchical tropical cloud systems in an analog shallow-water model, *J. Atmos. Sci.*, *52*, 1724–1742, doi:10.1175/1520-0469(1995)052<1723:HTCSIA>2.0.CO;2.

Yin, Y., K. S. Carslaw, and G. Feingold (2005), Vertical transport and processing of aerosols in a mixed-phase convective cloud and the feedback on cloud development, *Q. J. R. Meteorol. Soc.*, *131*, 221–245, doi:10.1256/qj.03.186.

Yoshizaki, M. (1986), Numerical simulations of tropical squall-line clusters: Two-dimensional model, *J. Meteorol. Soc. Jpn.*, *64*, 469–491.

Yoshizaki, M., T. Kato, H. Eito, S. Hayashi, and W.-K. Tao (2004), An overview of the field experiment "Winter Mesoscale convective systems (MCSs) over the Japan Sea 2001," and comparisons of the cold-air outbreak case (14 January) between analysis and a non-hydrostatic cloud-resolving model, *J. Meteorol. Soc. Jpn.*, *82*, 1365–1384, doi:10.2151/jmsj.2004.1365.

Young, G. S., D. V. Ledvina, and C. W. Fairall (1992), Influence of precipitating convection on the surface energy budget observed during a tropical ocean global atmosphere pilot cruise in the tropical western Pacific Ocean, *J. Geophys. Res.*, *97*, 9595–9603, doi:10.1029/92JC00689.

Yuter, S. E., and R. A. Houze Jr. (1995), Three-dimensional kinematic and microphysical evolution of Florida cumulonimbus. Part II: Frequency distribution of vertical velocity, reflectivity, and differential reflectivity, *Mon. Weather Rev.*, *123*, 1941–1962, doi:10.1175/1520-0493(1995)123<1941:TDKAME>2.0.CO;2.

Zeng, X., et al. (2007), Evaluation of long-term cloud-resolving modeling with observational cloud data, *J. Atmos. Sci.*, *64*, 4153–4177, doi:10.1175/2007JAS2170.1.

Ziemiañski, M. Z., W. W. Grabowski, and M. W. Moncrieff (2005), Explicit convection over the Western Pacific Warm Pool in the Community Atmospheric Model, *J. Clim.*, *18*, 1482–1502, doi:10.1175/JCLI3345.1.

Zipser, E. J. (1969), The role of organized unsaturated convective downdrafts in the structure and rapid decay of an equatorial disturbance, *J. Appl. Meteorol.*, *8*, 799–814, doi:10.1175/1520-0450(1969)008<0799:TROOUC>2.0.CO;2.

Zipser, E. J. (1977), Mesoscale and convective-scale downdrafts as distinct components of squall-line structure, *Mon. Weather Rev.*, *105*, 1568–1589, doi:10.1175/1520-0493(1977)105<1568:MACDAD>2.0.CO;2.

M. W. Moncrieff, National Center for Atmospheric Research, P.O. Box 3000, Boulder, CO 80307-3000, USA.

W.-K. Tao, Mesoscale Atmospheric Processes Branch, Laboratory for Atmospheres, Code 613.1, NASA Goddard Space Flight Center, Greenbelt, MD 20771, USA. (wei-kuo.tao-1@nasa.gov)